FREE FALL EXPERIMENTS WITH NEGATIVE IONS AND ELECTRONS

by

Fred Carl Witteborn

Low Temperature Physics Group
Department of Physics

STANFORD UNIVERSITY
STANFORD, CALIFORNIA

FREE FALL EXPERIMENTS WITH NEGATIVE IONS AND ELECTRONS

Fred Carl Witteborn, Ph.D.
Stanford University, 1965

While the equivalence between inertial mass and passive gravitational mass has been demonstrated for bulk matter and for several neutral particles, the effect of gravity on free, charged, elementary particles and anti-particles has not been measured. Should a difference exist between the inertial and gravitational masses of any particle, then the equivalence principle of general relativity would be violated. In this dissertation are described measurements of the gravitational force on free, negative ions and a demonstration of the feasibility of making a similar measurement on free electrons. Motivation for making such a measurement on positrons is also discussed.

The principle difficulties of the experiment stem from the weakness of the earth's gravitational force compared to likely electrostatic and magnetic interactions. The gravitational attraction between the earth and an electron at its surface is exceeded by the electrostatic repulsion between two electrons up to five meters apart. The dissertation describes methods and apparatus used to reduce all electric and magnetic forces to values below or near the expected gravitational force on free electrons and free positrons.

In the experiment, pulses of electrons in the magnetic ground state (or in some cases negative ions) were guided by a vertical magnetic field along the axis of a 2 cm diameter vertical OFHC copper drift tube 25 cm high. The number of particles arriving in each of 400 successive time intervals after each emitting pulse was stored in a 400 channel scalar. The forces acting on the particles could be determined from the time of

flight distribution.

By applying delayed negative pulses to the detector and cathode at appropriate times, negative particles in a desired energy range could be made to traverse the drift tube several times before entering the detector. This technique was used to distinguish between low energy particles and particles emitted from potential traps.

Very weak, vertical, uniform, electric fields could be applied by passing axially directed electric current through the walls of the drift tube. The effects of a known applied field on a time of flight distribution made possible a measurement of the charge to mass ratio of the particles forming the distribution.

The measurements of charge to mass ratios made with applied weak electric fields showed that the particles observed in some of the experiments were negative ions with mass between 2 and 5 proton masses. These ions had an unusually long time of flight distribution with a pronounced cut-off near 170 milliseconds. Comparison with calculated distribution curves for light negative ions in fields of various strength showed that the gravitational constant for these ions was the same as for neutral bulk matter ($980 cm/sec^2$) with a standard deviation in the measurement of $\pm 15\%$. Furthermore, since helium was the only gas likely to be present in the drift tube (at $4.2^{\circ}K$), the mass analysis strongly suggests that the ions composing the distribution were He^-. Theoretical work indicates that such ions exist only in a metastable state whose lifetime before auto-ionization is 1.7×10^{-3} milliseconds. The experimental results suggest a lifetime of more than 170 milliseconds.

Analysis of time of flight and energy distributions from several experiments demonstrated conclusively that electrons having kinetic energies

of 10^{-10} eV for at least 2 cm of their flight had passed through the 2 cm diameter copper drift tube. Apparatus with a diameter of 5 cm and a height of 250 cm now being built should therefore be able to measure forces as small as the expected gravitational force on an electron or positron.

Approved for publication:

By _____
                    For Major Department

By _____
            Dean of the Graduate Division

FREE FALL EXPERIMENTS WITH NEGATIVE IONS AND ELECTRONS

A DISSERTATION

SUBMITTED TO THE DEPARTMENT OF PHYSICS

AND THE COMMITTEE ON GRADUATE STUDY

OF STANFORD UNIVERSITY

IN PARTIAL FULFILLMENT OF THE REQUIREMENTS

FOR THE DEGREE OF

DOCTOR OF PHILOSOPHY

By

Fred Carl Witteborn

May, 1965

I certify that I have read this thesis and that in my

opinion it is fully adequate, in scope and quality, as

a dissertation for the degree of Doctor of Philosophy.

I certify that I have read this thesis and that in my

opinion it is fully adequate, in scope and quality, as

a dissertation for the degree of Doctor of Philosophy.

I certify that I have read this thesis and that in my

opinion it is fully adequate, in scope and quality, as

a dissertation for the degree of Doctor of Philosophy.

Approved for the University Committee
on the Graduate Division:

Dean of the Graduate Division

ACKNOWLEDGMENTS

The problem of determining the gravitational properties of free, charged, elementary particles and many important ideas for its solution were suggested by Professor W.M. Fairbank. His direction of the research and considerable help throughout its performance are greatly appreciated.

The development of the free fall apparatus was a joint project with Mr. L.V. Knight. It is a pleasure to thank him for his cooperation in much of the experimental work.

Many members of the Stanford University staff have contributed useful comments and suggestions. Also greatly appreciated were the interest and comments of several visitors to the Physics Department. Special thanks are due Mr. G.E. Hahne of Ames Research Center for many useful discussions of the experiment, and to Professor H.A. Schwettman for advice in correcting the manuscript.

During the course of the research my wife, Nancy Witteborn, has contributed in many ways to its successful completion. Especially appreciated was her patience throughout the long period of graduate work.

The thin film electron emitters (tunnel cathodes) used in the experiments were provided by Mr. J.W. Hall,II of General Electric Receiving Tube Department.

This research was supported by grants from the National Aeronautics and Space Administration and from the Center for Materials Research.

TABLE OF CONTENTS

LIST OF FIGURES

CHAPTER I

INTRODUCTION

While the gravitational properties of neutral matter in bulk have
been determined to great accuracy [1], and those of neutrons [2], and
photons [3] have been measured also, the effect of gravity on free
charged elementary particles has not been demonstrated. The experi-
ments to be described in this dissertation have yielded measurements
of the gravitational force on free negative ions and have demonstrated
the feasibility of measuring the gravitational force on electrons. No
theories have been set forth which predict that small charged particles
should behave differently from matter in bulk in a gravitational field.
Such a difference would violate the equivalence principle and thus re-
quire a reappraisal of the general theory of relativity. Since the
equivalence principle has been verified to better than one part in 10^{11}
[1] for neutral matter, it is not expected that a different gravitational
force would be exerted on the separated charge constituents of neutral
matter. However, the very importance of such a behavior if it did exist,
warrants an experimental investigation. A difference between the gra-
vitational acceleration constant of a small charged particle and neutral
matter could provide an important clue for understanding the nature of
gravity.

A further incentive to study the gravitational force on charged
elementary particles is the suggestion by P. Morrison and T. Gold [4,5]
that antimatter may be repelled by ordinary matter. The assignment of
anti-gravitational properties to antimatter was suggested to explain the

apparent lack of symmetry in the universe between matter and antimatter. While the known universe is made up almost exclusively of ordinary matter, the equations of physics show no preference for matter over antimatter. Should a long range repulsive force exist between the two, we would understand the absence of antimatter. It would then be reasonable to suspect the existence of an anti-universe whose galaxies were composed predominately of antimatter. An alternative explanation for the absence of antimatter is that the known universe resulted merely from a statistical fluctuation in which real matter happens to be present in much greater quantities in our part of the universe and antimatter is more abundant elsewhere. There are many difficulties with this theory. Still another possibility is that the mechanism for creation of particles (whether continuously or at some remote time) greatly favors the formation of ordinary matter. This, however would sacrifice the symmetry between matter and antimatter.

Strong indirect evidence has been advanced against the assignment of anti-gravitational properties to antimatter. L. Schiff [6] has shown that a difference of 1% between the gravitational masses of electrons and virtual positrons present in the coulomb field of nuclei would have been detected in the Eötvös experiments [7]. This does not rule out the possibility that free charged elementary particles might behave differently. However, the existence of the "long-lived" ($\sim 10^{-7}$ second) neutral K meson and absence of its decay into two pions was shown by Good [8] to establish the equality of the gravitational masses of K^{o} and $\overline{K}^{o}$ to a few parts in 10^{10} of their inertial masses. Subsequently it was found that the two pion decay did take place [9], but with such a low probability as not to change the conclusions

-2-

drawn by Good beyond the stated limits of a few parts in 10^{10}. Although the experimental verification of the equivalence principle and the decay of the neutral K-meson provide very strong indirect evidence that the force of gravity on real anti-particles is the same as their matter counterparts, there is still no direct experimental evidence for stable, free anti-particles.

Motivation from a somewhat different standpoint is contained in the remarks of B.S. De Witt in a seminar at Duke University in 1957 which stimulated Professor W.M. Fairbank's interest in gravity. In summarizing the discussions at the just concluded conference on gravity at the University of North Carolina, De Witt pointed out that since there is so little experimental evidence, any different experiment on gravity should be done. The experiment described in this dissertation provides the first direct observations of the gravitational force on ions. It establishes the technique for making similar measurements on electrons. Positrons and antinucleons could be studied in the same way, provided sources of sufficiently slow anti-particles can be developed.

The principal difficulty in measuring the force of gravity on electrons and ions stems from the small size of the gravitational force compared with electric and magnetic forces. Professor W.M. Fairbank devised the following method for minimizing these forces: The charged particles of interest were to be emitted along the axis of a vertical metal tube and guided through this drift tube by a very uniform, time constant magnetic field maintained by a superconducting solenoid. While the magnetic field would prevent the electrons from leaving the axis of the tube, the magnetic moment resulting

from the electron's spin and orbital motion would interact with small

magnetic field gradients to produce vertical forces much larger than

gravity. This difficulty was to be alleviated by using only electrons

in the ground magnetic state where the magnetic energy due to spin is

almost cancelled by that due to transverse motion. These ideas brought

the experiment into the realm of possibility. A detailed discussion of

electrostatic and magnetic forces in the experiment and the methods used

to reduce them appears in the second chapter.

The method for determining the forces acting on the charged parti-

cles involves measuring the time of flight of each particle. Pulses of

electrons are emitted from a cold cathode at the bottom of the drift tube.

The arrival of each electron at the electron multiplier detector at the

top of the drift tube results in a signal. The time between the emission

of the cathode pulse and observation of each detector signal determines

the time of flight of each electron in the original pulse. The electrons

emitted from the cathode have a spread in energy, usually on the order of

0.1 eV. Thus some electrons will have short flight times and some long

flight times. An analysis of the expected distribution of flight times

under various conditions is given in the fifth chapter. If a constant

vertical force F acts on the particles, there will be a maximum time

of flight given by $t_{max} = \sqrt{\frac{2hm}{F}}$, where h is the height of the parti-

cles' path and m is the mass. If all other forces are reduced well

below the gravitational force mg, then $t_{max} = \sqrt{\frac{2h}{g}}$ and the gravitational

constant for the particle in question is determined directly from the cut-

off in the distribution of flight times. Refinements of this method,

discussed in the fourth chapter, enable one to make this measurement against a background of non-random noise signals and also to mass analyze the particles.

The actual measurements made so far are preliminary and were intended mainly to test the feasibility of working with electrons in the 10^{-11} eV to 10^{-8} eV energy range. This feasibility has been demonstrated. Electrons and ions have been observed with certainty having energies down to 2×10^{-10} eV. The passage of such low energy particles through a $\frac{7}{8}$ inch diameter copper drift tube provides new experimental information on the nature of the patch effect. Some data indicating the probable passage of electrons as low in energy as 10^{-11} eV has been obtained. Furthermore, the effect of gravity has been observed on negative ions. $\frac{e}{m}$ measurements of these ions indicate that they have a mass near that of helium. This is a surprising result, since the predicted short lifetime of He^- would have prevented our observing enough of them to measure a gravitational cut-off in their time of flight distribution. The unambiguous identification of these ions as He^- would represent the first experimental evidence of such long lifetimes (greater than 170 msec.). As will be shown, the data strongly suggests that this identification is correct.

CHAPTER II

DESIGN PARAMETERS

In order to measure the effect of gravity on electrons, the apparatus was designed to isolate the electrons from potential drops greater than mgh over the height h of the drift tube and within 0.5 mm of its axis. The gravitational potential drop mgh in a 20 cm drift tube is only 2×10^{-11} eV for an electron. The force due to the earth's gravity on an electron is exceeded by the electrostatic repulsion between two electrons separated by as much as 5 meters or by the image force 2.5 meters of less from an infinite conducting plane. The various sources of non-gravitational potential gradients and ways to reduce them are discussed in this chapter.

1. Electrostatic Effects

The diameter, length, and composition needed for the drift tube are determined mainly by electrostatic effects. First the attraction between an electron and the surface charge it induces will be examined to determine an adequate length to radius ratio. While the presence of an axial magnetic field prevents an electron from moving towards the drift tube wall, the electron does feel a vertical force from the ends of its cylindrical metal container. (Metal must be used to prevent the build up of charge on the surface. The presence of even one excess charge on the surface of an insulating drift tube would exert more vertical force than the earth's gravity unless the drift tube were over six meters in diameter.) The Green's function at the location of a charge q on the axis of a grounded cylindrical conductor with closed ends is found from a more general expression [10] to be

$$V_c = \frac{q}{\pi \epsilon a^2} \sum_{r=1}^{\infty} \frac{\sinh u_r(h-z)[\sinh u_r z]}{[\sinh u_r h] u_r [J_1(u_r a)]^2} \qquad (1)$$

where a is the drift tube radius, h its height, z the distance of the charge above the bottom, and $u_r a$ are the roots of the equation $J_0(u_r a) = 0$. The Green's function at the location of a charge q on the axis of an infinite grounded conducting cylinder is [10]

$$V_i = \frac{q}{2\pi \epsilon a^2} \sum_{r=1}^{\infty} \frac{1}{u_r [J_1(u_r a)]^2} \qquad (2)$$

The potential due to the presence of the closed ends is

$$V_c - V_i = V_{ci} = \frac{q}{2\pi \epsilon a^2} \sum_{r=1}^{\infty} \frac{-1}{u_r [J_1(u_r a)]^2} \left\{ 1 - \frac{[e^{u_r(h-z)} - e^{-u_r(h-z)}][e^{u_r z} - e^{-u_r z}]}{[e^{u_r h} - e^{-u_r h}]} \right\} \qquad (3)$$

The smallest value of $u_r a$ is $u_1 a = 2.405$, [11]. We will find that $h \gg a$, so $e^{-u_r h} \ll e^{u_r h}$. Thus the term in brackets becomes

$$\left\{ e^{-2u_r(h-z)} + e^{-2u_r z} - e^{-2u_r h} \right\} \qquad (4)$$

The last term is not a function of z and may be omitted. At distances greater than "a" from either end, all contributions are negligible compared with that from $r = 1$. Thus for $a < z < h-a$

$$V_{ci} = \frac{-q}{2\pi \epsilon a \, 2.4[J_1(2.4)]^2} [e^{-4.81(h-z)/a} + e^{-4.81 z/a}] \qquad (5)$$

A typical value of "a" used in the experiment was $a_0 = 1$ cm $= 10^{-2}$m. Then

$$V_{ci} \cong 4.45 \times 10^{-7} \text{volts} \times \frac{a_0}{a} [e^{-4.81(h-z)/a} + e^{-4.81 z/a}] . \qquad (6)$$

The requirement that $h \gg a$ is apparent from this expression. A plot of the potential energy, $q V_{ci}/2$ using $a = 1$ cm, $h = 23.6$ cm is shown in figure 1. The gravitational potential is also shown. A comparison of the slopes shows that the gravitational force exceeds the electrostatic force for a distance of 17 cm.

In practice the ends of the drift tube are not necessarily at the same potential as the walls. This arises partly from contact potential differences and partly from the penetration of high fields required near the source and detector into the drift tube region. The potential due to field penetration may be estimated from the potential due to charged conducting discs placed at either end of a grounded cylinder (the drift tube.) The choice of voltages and sizes for these discs appropriate for the conditions of the actual experiments is discussed in appendix A. Consider a charge q on the axis and at height z above the bottom of the tube. The additional potential it feels from a voltage V_b on a concentric disc of radius b at the bottom of the cylinder is found by solving Laplace's equation in cylindrical coordinates for the disc at one end of an otherwise grounded, closed, conducting cylinder. Assuming that the cylinder is long enough so that the grounded end at $z = h$ may be replaced by an infinite extension of the cylinder, the solution is,

$$V_e = \frac{2V_b b}{a} \sum_{r=1}^{\infty} \frac{J_1(u_r b) \, e^{-u_r z}}{u_r a [J_1(u_r a)]^2} \, . \tag{7}$$

Again $u_r a$ are the roots of $J_0(u_r a) = 0$ and for $a < z$ we may neglect all terms $r \neq 1$. Then

$$V_e = \frac{2V_b b \; J_1(2.4 \; b/a) \; e^{-2.4 \; z/a}}{a \; 2.4 [J_1(2.4)]^2} \tag{8}$$

FIGURE 1. Comparison of electrostatic potential energy to gravitational potential of an electron.

Solid curve is the electrostatic potential energy of an electron on the axis of a closed grounded conducting cylinder removed from gravitational fields. Length of cylinder is 23.6 cm. Diameter is 2 cm.

Dashed line is the corresponding change in the gravitational potential of an electron near the earth's surface using the gravitational constant of bulk neutral matter.

Both potentials are arbitrarily chosen to be zero at $z = 11.8$ cm.
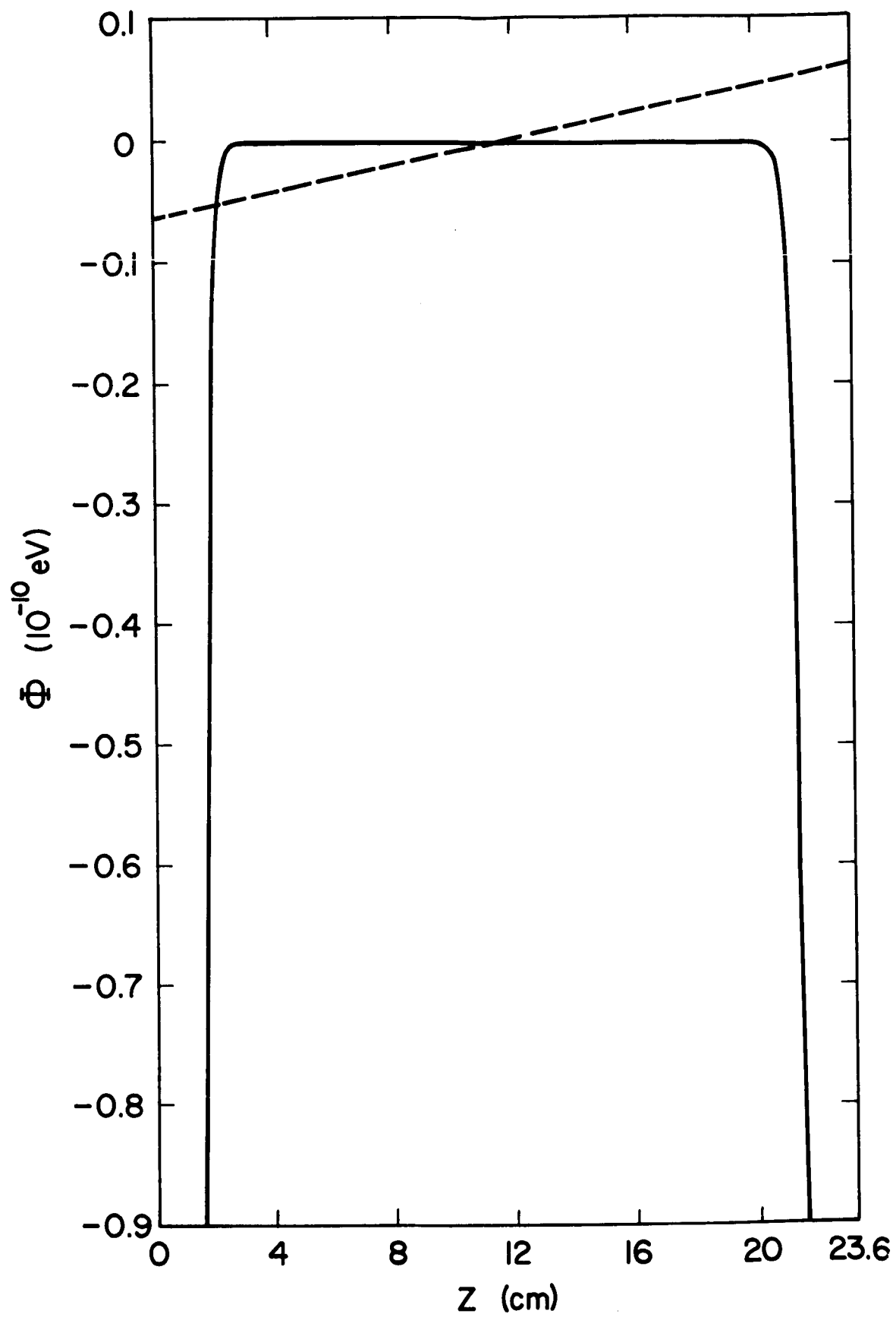
A similar expression for the potential due to stray fields from the detector is obtained by replacing z by $h-z$. Plots of V_e for values of V_b and b which approximate typical experimental conditions are shown in figure 2. The relative insensitivity of the length of field free (slope less than mg) region to V_b is fortunate, since this quantity would be hard to measure exactly.

So far it has been assumed that the electron is precisely on the axis of the drift tube. The electron may be guided away from the axis by the magnetic field lines if the guide magnet is not perfectly aligned with the drift tube. To determine the effect of such deviation from the axis it is necessary to calculate $\frac{\Delta V}{\Delta r}$ where Δr is the distance of the electron from the axis. The calculation of $\frac{\Delta V}{\Delta r}$ from the Green's function in cylindrical coordinates involves a double infinite summation over products of Bessel's functions and requires removal of a singularity resulting from the potential due to the point charge itself. An estimate may be obtained from the work W required to displace a charge a distance r from the center of a sphere of radius a. This may be treated by the method of images (Appendix B) with the result $W = \frac{qr^2}{8\pi\epsilon_0 a^3}$. If $|W| \leq mgh$ with $h = 20$ cm and $a = 1$ cm, we require $r \leq .01$ cm.

If the tube diameter varies, the electron will be attracted to the smaller diameter sections and repelled from the larger diameter ones. If the electron passed from a very long cylinder of radius "a" to a slightly larger one of radius $a + da$ the resulting change in potential energy would be approximately $\frac{q\,da}{8\pi\epsilon_0 a^2}$ (see appendix B). This is an upper limit of the expected change caused by a taper or some other diameter change of macroscopic extent in the drift tube. The best tube used in the experiment

FIGURE 2. Electrostatic potential in drift tube of radius 1.0 cm, length 23.5 cm. Solid curve is for + 100 volts on extraction aperture, + 10 volts on detector entrance grid. Dashed curve is for + 10 volts on extraction aperture, + 10 volts on detector entrance grid.
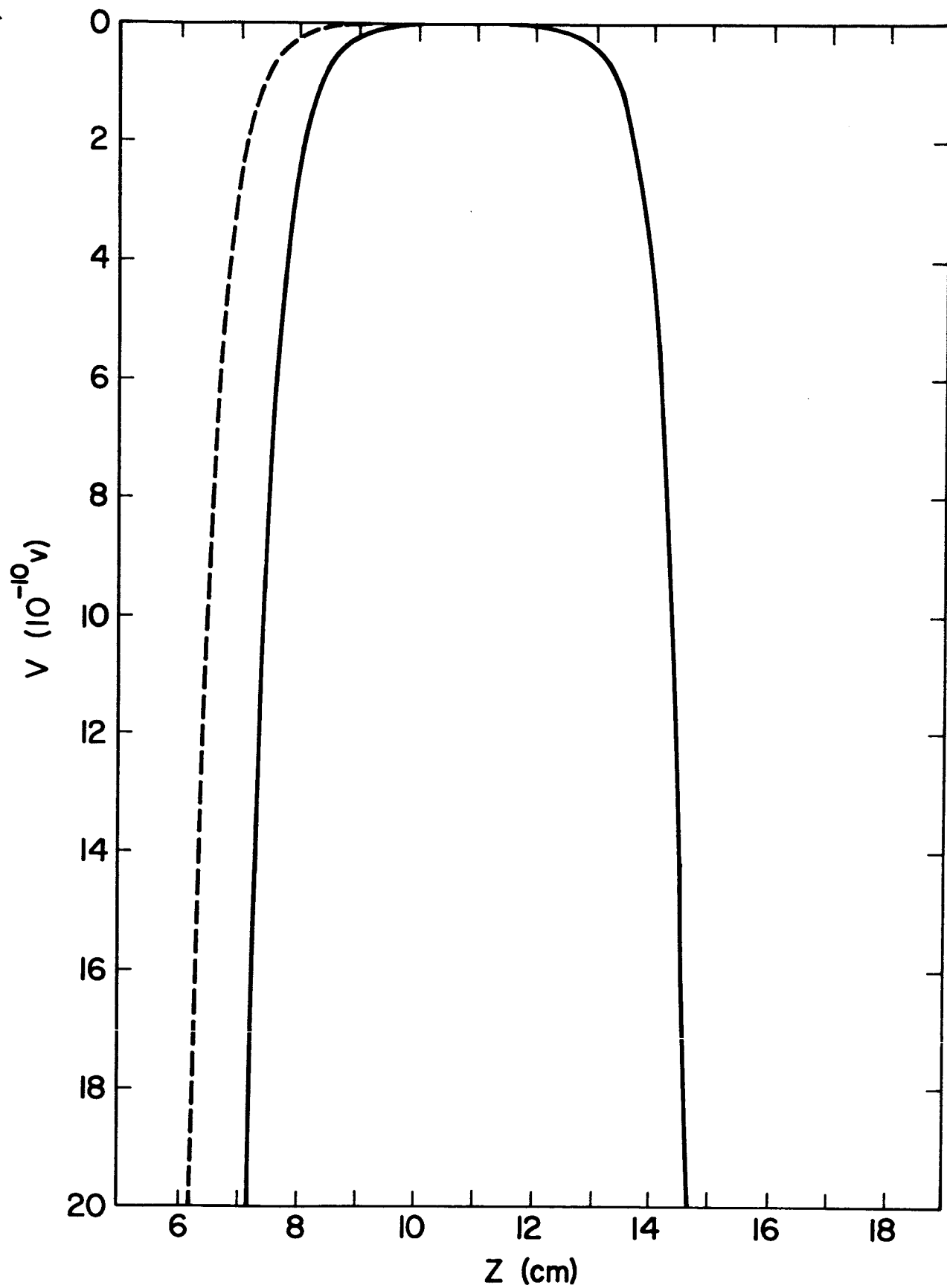
had da $\leq$ 1.0 x 10^{-4} cm, so the resulting upper limit on the potential

variation was .7 x 10^{-11} V, which would be near the expected electron

gravitational potential change, but would be less than 0.1% of that of

ions.

While the drift tube is a grounded conductor, its surface is not

really all at the same potential as assumed in the analysis so far.

The surface is composed of crystal faces or "patches" which have con-

tact potential differences on the order of 10^{-1} eV [12]. These differences

may be interpreted in terms of a dipole double layer of charge according

to the theory of Bardeen [13]. The change in potential caused by random

variations in the relative number of patches having different contact

potentials is calculated in Chapter 5. The anticipated adsorption of

many layers of gas atoms onto the drift tube surface makes even more un-

certain the potentials resulting from the patches. The passing of 10^{-10} eV

electrons through any practical drift tube appeared to be ruled out by the

measurements of Parker and Warren [14] on contact potential differences

between large areas of metal surfaces. Even after bake-out they found

potential differences greater than 10^{-3} eV. The apparatus discussed in

this dissertation was actually a pilot model for determining the size of

drift tube necessary to work at energies near 10^{-10} eV. It was expected

that many materials and surface treatments would have to be tried to min-

imize contact potential differences.

An electrostatic effect of a different nature arises from the mutual

repulsion between electrons emitted from the cathode. This problem is

discussed further in the section on the source and in Chapter 5. It suf-

fices to say that the electron interactions limit the number of 10^{-10} eV

electrons to a linear number density of $\dfrac{1 \text{ electron}}{2.5 \text{ a}}$ where a is the radius

of the tube. This limitation is obtained from the following expression [10]

for the potential V_p at distance z_1 from a point charge on the axis of

a cylinder:

$$V_p = \frac{q}{2\pi\epsilon_o a} \sum_{r=1}^{\infty} \frac{e^{-u_r z_1}}{a u_r [J_1(u_r a)]^2} \simeq \frac{q}{2\pi\epsilon_o a} \frac{e^{-2.4\, z_1/a}}{.648} \quad \text{for } z_1 > a . \tag{9}$$

If $V_p < 10^{-10} V$ then $z_1 > 2.5$ a, unless a is so large that the formula

for a point charge in space is more applicable in which case z_1 would

have to be even larger. The latter would imply a drift tube diameter of

several meters which was not considered to be practical.

All of the electrostatic effects discussed apply also to ions. Since

the expected gravitational potential of an ion is at least 1836 times more

than that of an electron, the requirements for measuring the gravitational

masses of ions are much less stringent than for the electron experiment.

2. Magnetic Effects

In order to assure that for at least a few centimeters the electron

path stayed close to the axis within the limits $r \leq .01$ cm set by electro-

static considerations mentioned previously, an axial B field of at least

40 gauss was necessary because of transverse external fields on the order

of tenths of a gauss. This amount could be lowered if elaborate external

shielding were used.

The energy of a non-relativistic electron in a uniform magnetic field

is found [15] to be $E = p_z{}^2/2m + 2\mu_\beta B(n + \frac{1}{2} + \frac{s}{2} g_s)$ where $\mu_\beta = .93 \times 10^{-20}$

ergs/gauss is the Bohr magneton, B the magnetic field strength, p_z the

momentum in the direction of B, g_s the spin gyromagnetic ratio of the

electron, $s = \pm \frac{1}{2}$ is the spin quantum number, and n is a positive integer. The $n + \frac{1}{2}$ arises from the harmonic oscillator-like solutions to the Schroedinger equation for motion perpendicular to the magnetic field. The axial motion is independent of B and has continuous eigenvalues provided the drift tube may be considered essentially infinite in length. The $sg_s/2$ term is the magnetic energy due to the electron spin.

Variations in the magnetic energy along the length of the tube must be either accurately known or made small with respect to mgh so that magnetic field gradients will not be confused with the gravitational force. The change in magnetic energy due to a change in B of 0.1 gauss would be more than 10^{-8} eV, unless $n = 0$ and $s = -\frac{1}{2}$. The latter condition is called the magnetic ground state and has about 2000 times less energy than the lowest state above it, since $g_s \cong 2.0023$. To separate electrons in higher magnetic states from those in the ground state, the cathode was located in a field as much as 4000 gauss stronger than that in the drift tube. Electrons not in the ground state accelerated as they left the high field region and traveled to the detector in less than 0.1 millisecond. Ground state electrons slowed down slightly as they left the high field, since their anomalous magnetic moments gave them a small negative potential in the magnetic field. By using electrons in the ground state, it was not only possible to reduce interactions with field gradients, but also corrections could be applied for known field gradients, because there was no uncertainty in their n value. A plot of the magnetic field profile most commonly used in the experiment is shown in figure 3. A plot of the combined electrostatic and magnetic

potential energy profiles appears in figure 4.

To prevent variations in B with time the magnet should be persistent and superconducting. This keeps the average vertical flux constant in time.

The magnetic energy of ions in a uniform field is $2\mu_M B(n + \frac{1}{2})$ plus a term $sg_s\mu_\beta B$ if there is an unpaired electron spin. μ_M is 5.05 Mp/M x 10^{-24} ergs/gauss, where M is the mass of the ion and M_p is the proton mass. The ions are formed from gas near thermal equilibrium with the drift tube so that $kT = 2\mu_M B(n_{ave} + \frac{1}{2})$. $kT = 3.6$ x 10^{-4}eV at 4.2°K, so the average magnetic energy is considerably larger than the expected 10^{-7} to 10^{-8} eV gravitational potential drop. By forming the ions in a field of 3000 gauss, decelerating them electrostatically as they leave this field, and then keeping variations in B below 0.3 gauss through a considerable part of the drift tube, the magnetic energy change is made smaller than the gravitational energy change for most of the ions formed. A more sophisticated technique, not used in these experiments, is made possible by the fact that the spin energy is larger than the orbital contribution for the first 1000 n values in the case of the $\tilde{H}$. It is therefore possible to separate those ions with n < 1000 and $s = -\frac{1}{2}$ from the remaining ions by using a field gradient to slow down the ions in the negative magnetic energy states and speed up the others. The ions in the first 1000 states thus form the major part of the "slow" ion distribution. Their interaction with magnetic field gradients relative to their gravitational interaction would be comparable to that of ground state electrons.

An additional vertical force resulting from the presence of a magnetic

FIGURE 3. Magnetic field in the drift tube. This field was used in most of the experiments. In the data of figure 21, however, a superconducting shield kept B constant to within a few gauss beyond z = 7 cm.
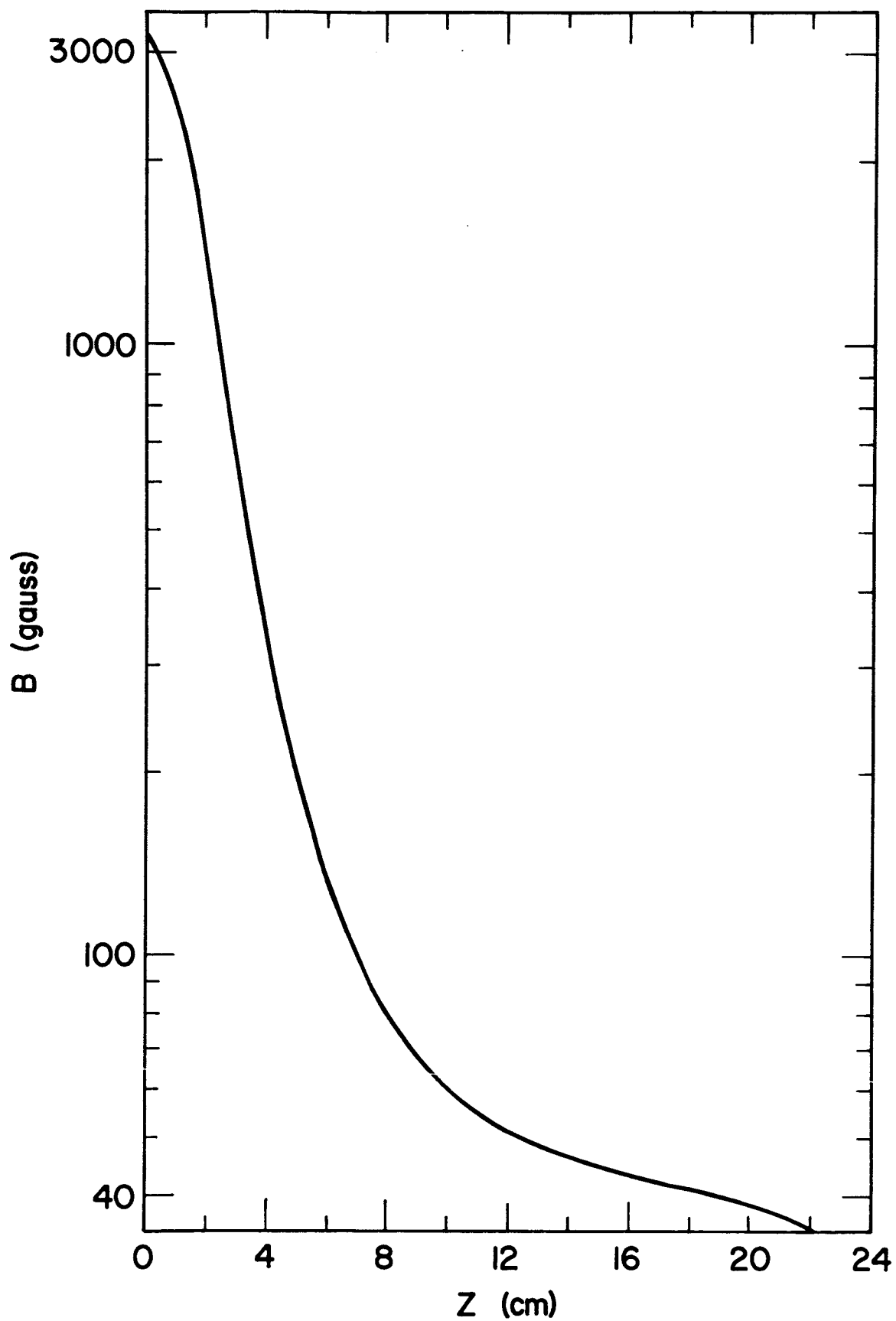
FIGURE 4. Potential energy of a ground state electron in the combined

electrostatic and magnetic fields of figures 2 and 3. The straight line

across the top (T.E.) represents the total energy of an electron that

passes through the drift tube with a minimum kinetic energy (K.E.) of

about 1.9 x 10^{-10} eV. The potential energy (P.E.) and total energy have

an arbitrary zero in this figure.

20

18

T.E.

K.E.

16

$\Phi \ (10^{-10} \ eV)$

14

12

10

8

P.E.

6

4

2

0

6   8   10   12   14   16

Z (cm)

-21-
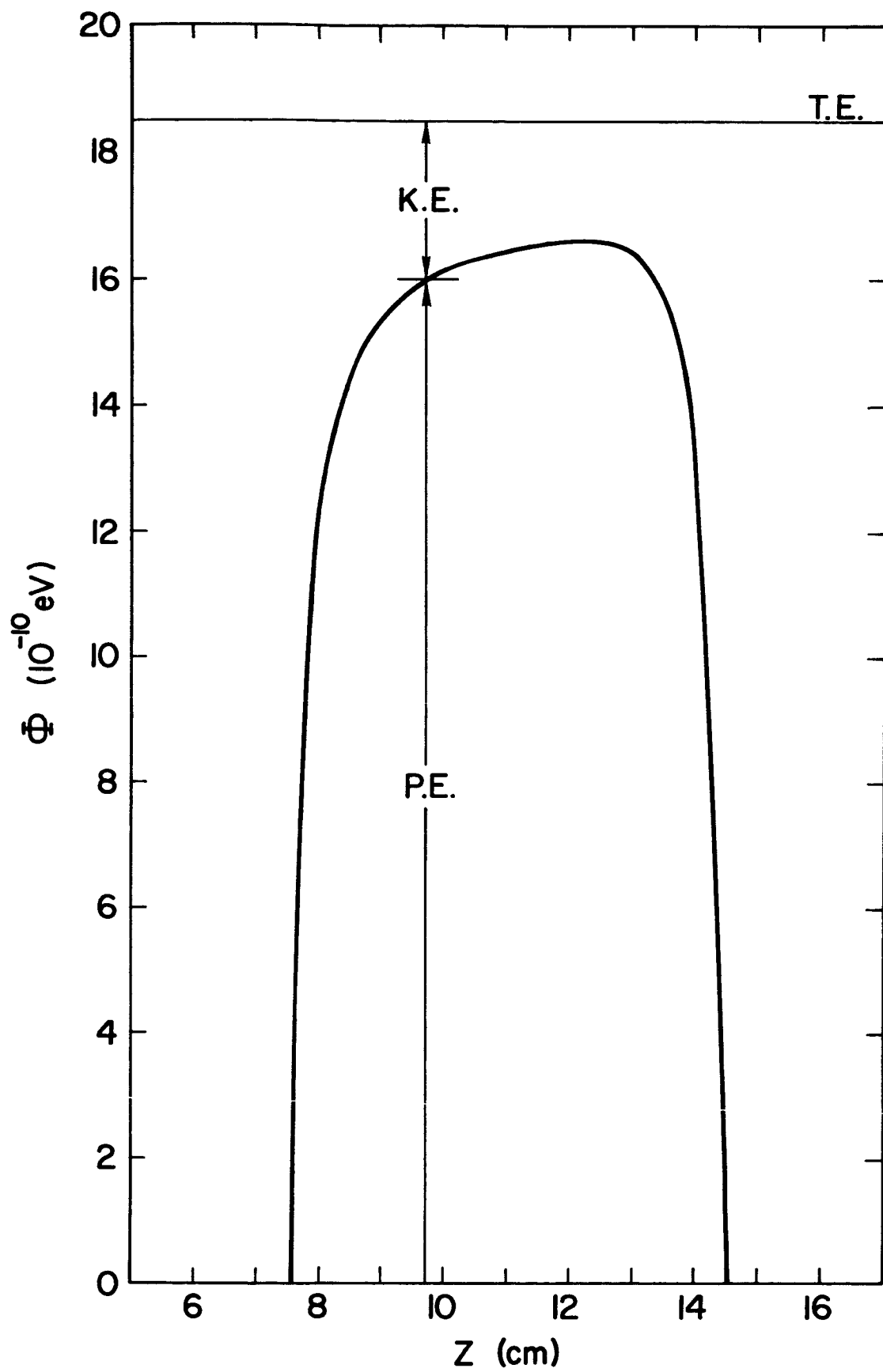
field affects charged particles that are not precisely on the axis of the drift tube. As shown in appendix B, charged particles at a distance r from the axis experience a radial electric force $q\vec{E}$, where $\vec{E} = \dfrac{q\vec{r}}{4\pi\epsilon_o a^3}$. Charges in crossed electric and magnetic fields drift with velocity $\vec{v} = \vec{E} \times \vec{B}/B^2$ [16]. Since the magnetic field is axial and the electric field is radial the resulting motion is parallel to the walls of the drift tube and transverse to the z-axis. Charges at a distance $r = 5 \times 10^{-4}$ meters in a magnetic field of 4×10^{-3} webers/meter^2 (40 gauss) would have a drift velocity of about 1.7×10^{-4} meters/sec. This motion in turn leads to an additional magnetic moment $qvr/2 = 7 \times 10^{-27}$ amp meters^2 (7×10^{-24} ergs/gauss) which is comparable to the anomalous magnetic moment of the electron, but in the opposite direction. It is interesting to note that at one value of r the total magnetic moment is actually zero, so there are no interactions with small magnetic field gradients. Beyond that distance, the interaction caused by the drift velocity increases rapidly (as r^2), providing a limitation on the usable size of the cathode emitting surface. Since the low energy charged particles follow the magnetic flux lines, electrons or ions having $r = 10^{-3}$ meters in the 40 gauss region of the drift tube must come from a cathode surface of radius 10^{-4} meters if the cathode is in a 4000 gauss field.

3. Vacuum

The particle concentration of background gases in the drift tube had to be made low enough to make unlikely any collisions which would change the direction of electrons having energies of more than 10^{-11} eV. One of the main reasons for doing the experiment at 4.2°K was to reduce out-gassing from the walls, thus greatly reducing the background gas pressure.

In addition the cold walls served as a pump by condensing all gases except helium and hydrogen. The only gas likely to be present was helium. Hydrogen, whose equilibrium vapor pressure is about 10^{-6} torr at this temperature [17], is pumped very efficiently by the ion pump used in the experiment and was probably present in much smaller quantities than helium gas.

The interaction of greatest importance in determining the vacuum requirement is the attraction of the electron to the induced dipole moment of the helium atom. The dielectric strength K of helium gas is about 1.000065 [18]. The polarizability α is $(K-1)\epsilon_0/n_0$, where n_0 is Loschmidt's number, 2.69×10^{25}, so for a helium atom, α is about 0.21×10^{-40} farad m^2. The electric field strength due to the electron is $E = q/4\pi\epsilon_0 r^2$ where r is the distance from the electron. Thus the induced dipole moment $p = \alpha E = \alpha q/4\pi\epsilon_0 r^2$. The potential of the dipole is $p \cos \theta/4\pi\epsilon_0 R^2$, where R is the distance from the atom and θ is the angle between the observation point and a line connecting the atom and the electron. For the electron, of course, $\theta = 0$ and $R = r$. The potential energy of an electron near a helium atom is thus $-\alpha q^2/(4\pi\epsilon_0)^2 r^4$. This quantity exceeds 10^{-11} eV when $r < .72 \times 10^{-5}$ cm. The cross section σ for undesirable collisions is therefore 1.66×10^{-10} cm^2. We want the mean free path $1/n\sigma$ to be greater than $h = 25$ cm, the drift tube length. This determines the background pressure. Evidently we must have $n < 1/\sigma h = 2.4 \times 10^{8}$ cm^3 which corresponds to a pressure of 1.04×10^{-10} torr at 4.2°K.

During most of the experiments the pressure was monitored by a gauge in the warm part of the system. If no condensible gases were involved we would read a pressure in the gauge p_g related to that in the drift

tube p_d by $p_g = (T_g/T_d)^{1/2} \; p_d = (300/4.2)^{1/2} p_d$ [19]. Then the mean free path is long enough if $p_g < 8.8 \times 10^{-10}$ torr. This requirement is probably too severe since much of the pressure in the warm part of the system is due to such gases as N_2 and O_2 which condense before reaching the drift tube.

The potential energy of an ion near a helium atom is the same as that of an electron at the distances of interest here. In work with ions we require $\alpha q^2/(4\pi\epsilon_o)^2 r^4 < 10^{-8}$ eV. This means that we must have $r > 1.3 \times 10^{-6}$ cm. Thus the particle concentration must be less than $8.0 \times 10^9/cm^3$ corresponding to a pressure of 3.5×10^{-9} torr. at 4.2°K and a room temperature gauge pressure of 3.0×10^{-8} torr.

4. Thermal Effects

A homogeneous metal with no applied voltage may still have a potential difference from one part to another if these parts are at different temperatures. The potential difference V_T varies with the temperature T according to the equation $V_T = \sigma_T T$, where σ_T is the Thompson coefficient. For metals it is usually a few microvolts per degree. Measurements have been made of σ_T for copper at 4.2°K, but the coefficient changes drastically with the purity and history of the sample [20]. In view of the uncertainty in the Thompson coefficient for any given sample it is clearly desirable to do one of the following:

(1) Insure that the liquid helium bath temperature is constant to 10^{-5} $^\circ$K or better over the length of the drift tube.

(2) Isolate the drift tube from the bath in such a way that thermal contact is made in one place.

(3) Use a superconducting drift tube. The Thompson coefficient of

a superconductor is zero [21].

The third method would solve the problem most conclusively, but introduces several difficulties. First the magnetic field in the drift tube would be more troublesome to vary, since the tube itself would have to be driven normal in order to change the field. Second the surface texture of the available materials (niobium or lead) could not be as carefully controlled as copper or graphite. Finally the walls of the drift tube would have zero D.C. resistance, so it would be impossible to set up a weak axial electric field by running current through the drift tube. Such a field performs a mass analysis as described in Chapter 4.

In the second method the drift tube would be connected to a heat sink at just one end and insulated by vacuum along its entire length. The OFHC copper tube used in the experiment was about 2 cm in diameter with 0.2 cm wall and 20 cm long. Suppose a 10^{-1}°K temperature difference existed across the length of the tube. Because of the low heat capacity of copper at 4°K, the temperature over the length of the tube would be uniform to 10^{-5}°K in about 0.1 second. A temperature gradient could exist if there were a heat leak into the walls of the tube or into the insulated end. We wish to know what sort of heat leak dQ/dt would cause a temperature difference of 10^{-5}°K over a length of 25 cm. The rate of energy flow is related to the temperature gradient by $dQ/dt = KA \, dT/dx$, [22] where K is the thermal conductivity which is about 10 watts/cm°K for annealed OFHC copper near 4.2°K [23] and A is the cross sectional area, about 1.3 cm². Thus $dQ/dt = 10$ watts/cm deg x 1.3 cm² x 10^{-5}deg/25 cm = $.5$ x 10^{-5}watts = 50 ergs/sec. It should not be hard to reduce the heat leaks to this size or smaller in a vacuum (10^{-11} torr) insulated tube whose

container is within 10^{-2}°K of the drift tube temperature.

If the drift tube is in intimate contact with the helium bath over its full length any variations in liquid helium temperature with depth could cause temperature gradients in the drift tube. Factors tending to cause thermal gradients in the liquid are the hydrostatic pressure and heat leaks from the dewar walls and from the top of the system. As the pressure rises the boiling point rises, so helium boils at a higher temperature at the bottom of the drift tube than at the top. This effect should result in a temperature gradient of 0.34×10^{-3} degrees/cm, which is in the neighborhood of experimentally observed values in a system with no good conductors present [24]. In practice the drift tube and the thick aluminum frame for the guide magnet (figure 5) help to equalize the bath temperature. However, if the liquid is maintained below its boiling point, most of the heat radiated into the system from the nitrogen shield or otherwise brought into the bottom of the liquid helium must be conducted through the walls of the apparatus. The radiation heat input to the bottom of the dewar used in this experiment was at least 10^{-3} watts which would lead to a temperature gradient of about 10^{-4} deg./cm.

If the helium bath is maintained below the λ-point (2.17°K) it becomes an extremely good conductor and presumably would allow the drift tube temperature to stay uniform to less than 10^{-5}°K. While this method was not used in experiments discussed in this report, it may be the most practical for a drift tube several meters high.

5. Cathode

The principal requirement on the cathode was that it emit one ground state electron with axially directed kinetic energy below 10^{-9} eV from

1 sq. mm. area during each millisecond pulse, but no electrons at all at any other time.
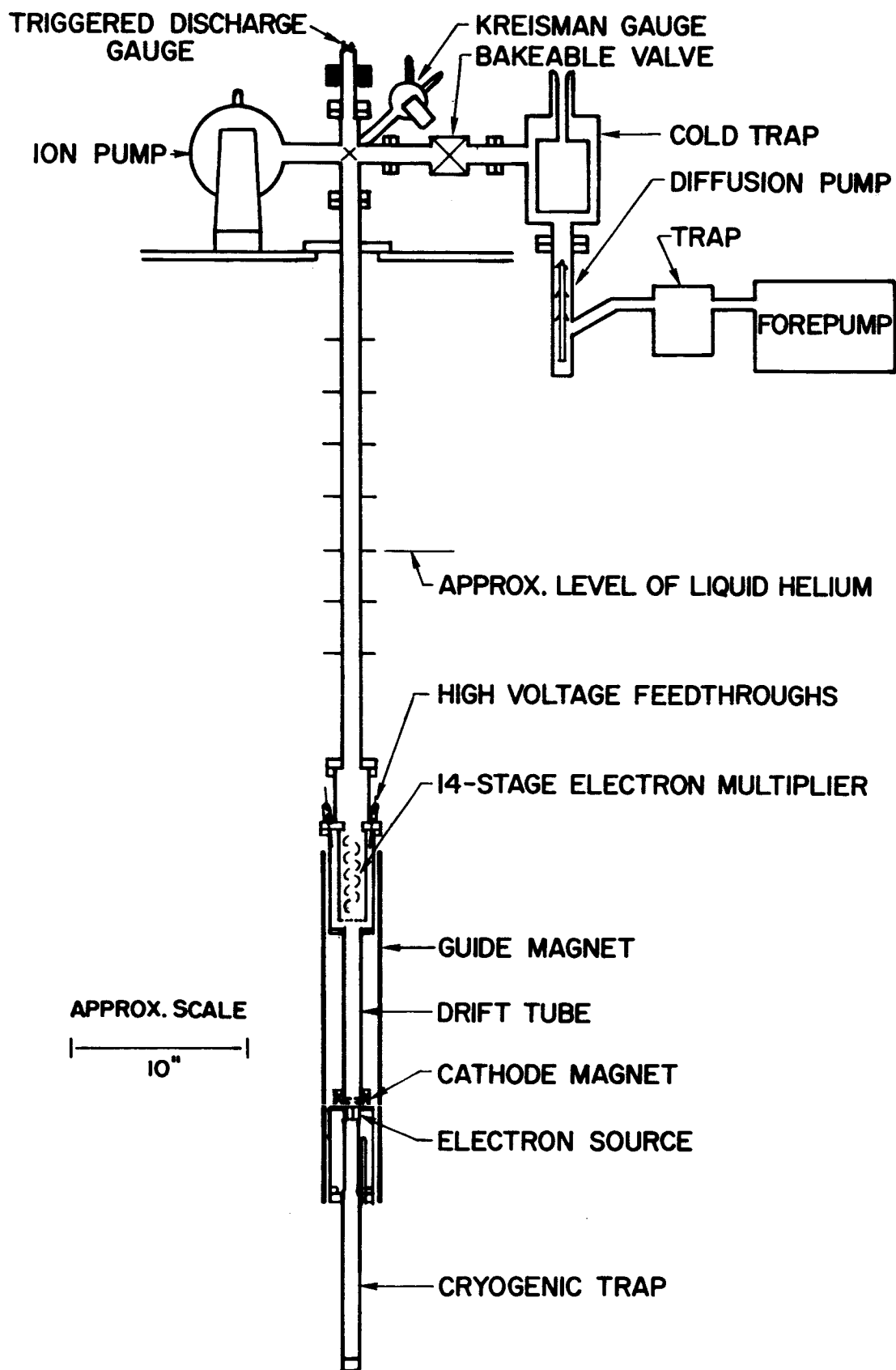
The number of electrons having z-directed velocities between v_z and $v_z + dv_z$ in a Maxwellian distribution is [25],

$$dN(v_z) = \frac{N}{\sqrt{\pi}} \left(\frac{m}{2kT}\right)^{\frac{1}{2}} \exp\left(\frac{-mv_z^2}{2kT}\right) dv_z \tag{10}$$

where T is a temperature which is characteristic of the type of cathode being used, and k is Boltzmann's constant. (It is not necessary to use Fermi-Dirac statistics for emitted electrons, because the energy levels outside the metal are very sparsely populated.) In continuous emission the distribution of energies in a beam of emitted electrons is calculated by integrating over $v_z dN(v_z)$, but in pulsed emission only the distribution function should be used. The number of electrons ΔN in the small energy range 0 to ΔE is $\int_0^{\Delta v_z} dN(v_z)$, where $\Delta v_z = \sqrt{\frac{2\Delta E}{m}}$. Since $\Delta E = 10^{-9} eV$ $\ll kT$ for the cathodes to be examined, the exponential term remains essentially equal to unity in the integration. Thus $\Delta N = \frac{N}{\sqrt{\pi}} \left(\frac{m}{2kT}\right)^{\frac{1}{2}} \sqrt{\frac{2\Delta E}{m}} = N\sqrt{\frac{\Delta E}{\pi kT}}$. The total number of emitted electrons is $dN(v_z) = N/2$, since half the electrons are going in negative z direction and are thus not emitted. The fraction of emitted electrons in the energy range 0 to $10^{-9} eV$ is therefore $\frac{2\Delta N}{N} = 2\sqrt{\frac{\Delta E}{\pi kT}} \simeq 2 \times 10^{-5}$, using $kT \approx 3eV$ which is characteristic of many thermionic cathodes.

In practice the ratio of low energy electrons calculated above is unattainable. The electrons emitted from the cathode must pass over a potential hill in the drift tube which is slightly higher than the potential at the cathode. (If it were lower none of the electrons would traverse the drift tube slowly.) The potential level of the cathode can be adjusted to come

FIGURE 5. Semi-schematic drawing of time of flight apparatus. The dewars, transfer tube, feedthroughs, connecting wires, and electronics are not shown.

TRIGGERED DISCHARGE GAUGE

KREISMAN GAUGE

BAKEABLE VALVE

ION PUMP

COLD TRAP

DIFFUSION PUMP

TRAP

FOREPUMP

APPROX. LEVEL OF LIQUID HELIUM

HIGH VOLTAGE FEEDTHROUGHS

14-STAGE ELECTRON MULTIPLIER

APPROX. SCALE

10"

GUIDE MAGNET

DRIFT TUBE

CATHODE MAGNET

ELECTRON SOURCE

CRYOGENIC TRAP

very close to that of the potential hill, but because of changing cathode conditions it would be very difficult to hold this potential difference Φ to less than 0.001 eV. The electrons which will end up with 0 to 10^{-9} eV of kinetic energy must have between Φ and $\Phi + 10^{-9}$ eV in the distribution of emitted electrons. In this case v_z is such that $\Delta E = \frac{m}{2}(v_z + \Delta v_z)^2 - \frac{m}{2} v_z^2$, where $\frac{m}{2} v_z^2 = \Phi$. Since $v_z \gg \Delta v_z$, $\Delta E = m v_z \Delta v_z$, so $\Delta v_z = \frac{\Delta E}{(2m\Phi)^{\frac{1}{2}}}$. The number in the energy range Φ to $\Phi + \Delta E$ is

$$\Delta N = \int_{v_2}^{v_2 + \Delta v_2} dN(v_z) = \frac{N}{\sqrt{\pi}} \left(\frac{m}{2kT}\right)^{\frac{1}{2}} \Delta v_z = \frac{N}{2} \frac{\Delta E}{(\pi kT \Phi)^{\frac{1}{2}}} \tag{11}$$

where again the exponential term was considered to be unity in the integration. Finally

$$\frac{2\Delta N}{N} = \frac{10^{-9}}{10^{-1}} = 10^{-8} . \tag{12}$$

If the orbital angular momenta are assumed to be in thermal equilibrium outside the cathode (where Maxwell-Boltzmann statistics is a good approximation even for electrons), then the fraction f_g of electrons in the ground state is

$$\exp\left[-\frac{\mu_\beta B}{kT}\left(1 - \frac{g_s}{2}\right)\right] \div Z_{rot} , \tag{13}$$

where Z_{rot} is the rotational part of the partition function.

$$Z_{rot} = \sum_{n=0}^{\infty} \sum_{s=-\frac{1}{2}}^{+\frac{1}{2}} \exp\left[-\frac{2\mu_\beta B}{kT}\left(n + \frac{1}{2} + \frac{s g_s}{2}\right]\right.$$

$$= \frac{\exp[-\mu_\beta B(1 + g_s/2)/kT] + \exp[-\mu_\beta B(1 - g_s/2)/kT]}{1 - \exp(-2\mu_\beta B/kT)} , \tag{14}$$

using the sum rules for geometric progressions. Since $B = 3000$ gauss at the cathode and $\mu_\beta \cong 10^{-20}$ ergs/gauss, $\frac{\mu_\beta B}{kT} = 10^{-5} \ll 1$, where we

-30-

have again set $kT = 3eV \cong 5 \times 10^{-16}$ ergs. Using the approximation $e^{-x} = 1-x$, the partition function simplifies to $Z_{rot} \cong \frac{kT}{\mu_\beta B}$, and $f_g \cong \frac{1}{Z_{rot}} \cong \frac{\mu_\beta B}{kT} \cong 10^{-5}$.

Thus such a cathode must provide 10^{13} electrons per pulse. Since the pulse is one millisecond wide, the required current is about 2×10^{-5} amps. This is a very reasonable amount for a hot filament cathode.

Hot cathodes have several serious disadvantages. The cathode remains hot enough to emit photons in the ultraviolet for several milliseconds after the electron forming pulse. These photons would look like slow electrons to the electron multiplier detector. This difficulty could be alleviated by making the detector solid angle no larger than necessary for the slow electrons to enter, or by magnetically bending the electrons around a corner. Another problem is the outgassing from the hot filament. This can be reduced if the filament is given prolonged baking much above its normal operating temperature, but even cathodes operated considerably below their melting points continue to emit small amounts of volatile impurities indefinitely. These could condense out on the drift tube wall in sufficient quantities to change the contact potential near the cathode which would cause unpredictable electrostatic forces on the electrons. Finally the hot filament would constitute a serious heat leak.
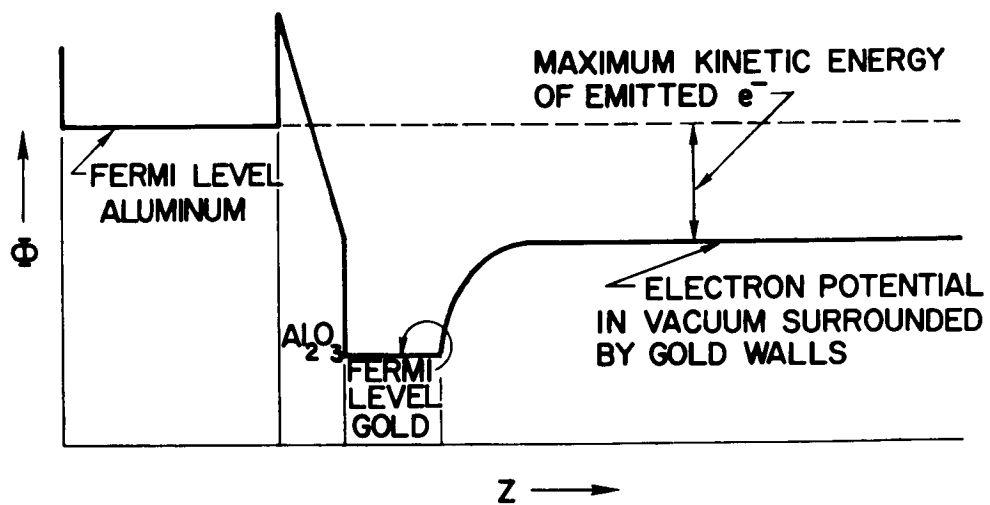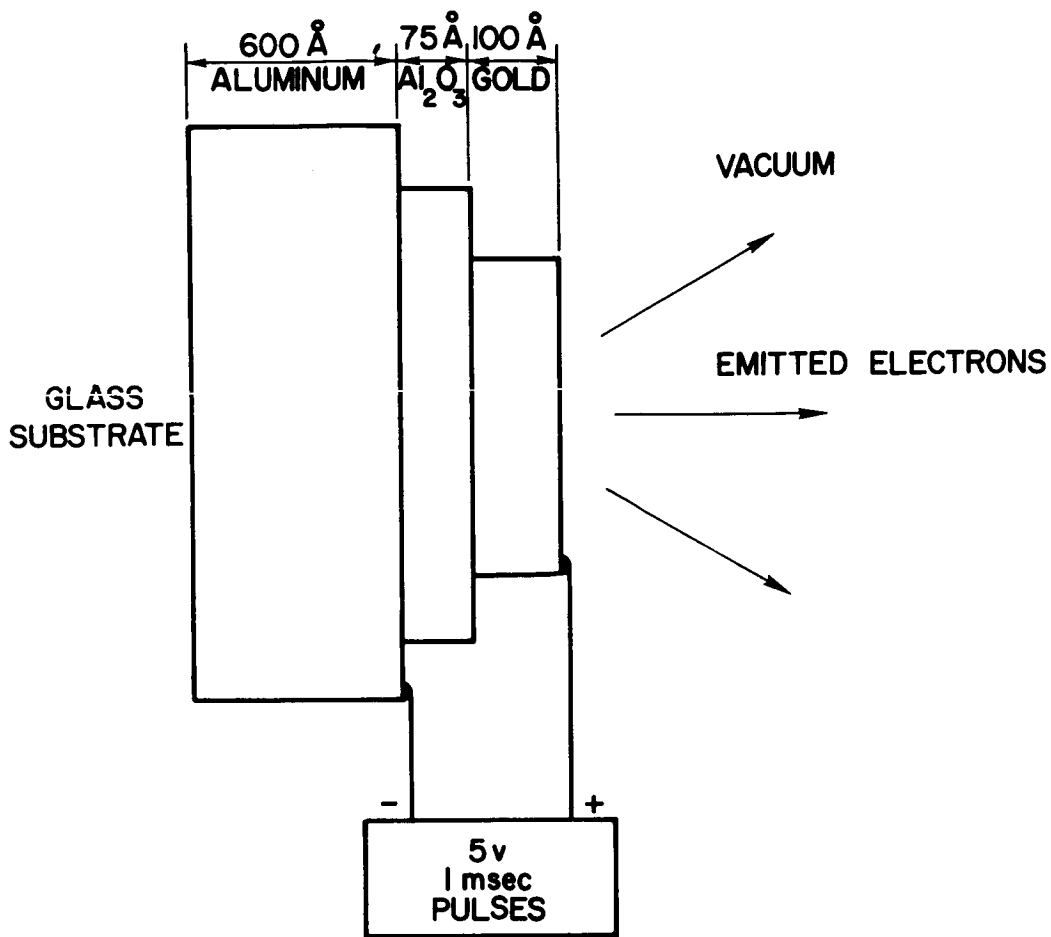
A photoelectric source has the advantage of operating when cold. Unfortunately, the cathode materials that have high photoemission rates for visible or near ultraviolet light are volatile enough even at room temperature to contaminate the system. The problems of building a high

intensity quartz ultraviolet source in liquid helium or of bringing the light in from outside via quartz optics are considerable, but could probably be solved.

Instead of the conventional cathodes, however, it was decided to try first the newly developed tunnel diode emitters [26,27]. A detailed report on the type used in our experiments was written by J.W. Hall, II [28] of General Electric Co. who generously provided us with a large number of these devices. A schematic diagram of a tunnel diode emitter (or tunnel cathode) is shown in figure 6. If a sufficient positive voltage is applied to the top metal film, electrons from the aluminum base metal may tunnel through the thin ($75^{\circ}A$) insulating film into the top film. If now the top film is also very thin, some of the electrons will continue on into the vacuum above the top metal film. Since the emission ceases when the voltage across the insulator is removed, the device provides very well defined pulses. The operation is essentially "cold", although some heat is generated by the current passing through the various films. The current available from the tunnel cathodes was limited to about 10^{-5} amps under the conditions of our experiment. However, we found that the spread in z-directed kinetic energy at $4.2^{\circ}K$ was less than 1 eV and sometimes as low as 0.1eV.

Similar energy spreads with tunnel cathodes at room temperature were observed by Collins and Davies [29] who concluded from the energy distribution of emitted electrons that they reached a thermal equilibrium in the Al_2O_3 film near 3000° K. Using this temperature and $\Phi = 10^{-3}$ eV in the expression for the fraction of electrons with z-directed energy between Φ and $\Phi + 10^{-9}$eV, we have $\frac{2\Delta N}{N} = \frac{10^{-9}}{\sqrt{10^{-3}}} = 3 \times 10^{-8}$. At $3000^{\circ}K$,

FIGURE 6. Tunnel cathode schematic diagram. Upper diagram is a greatly enlarged cross sectional view of a tunnel cathode. When a positive voltage is applied to the gold film, electrons in the aluminum may tunnel through the oxide layer. The lower diagram shows the potential energy at positions corresponding to the upper diagram, when the voltage is on.

600 Å
ALUMINUM

75 Å
Al$_2$O$_3$

100 Å
GOLD

VACUUM

EMITTED ELECTRONS

GLASS
SUBSTRATE

−

+

5 v
I msec
PULSES

MAXIMUM KINETIC ENERGY
OF EMITTED e$^-$

Φ

FERMI LEVEL
ALUMINUM

ELECTRON POTENTIAL
IN VACUUM SURROUNDED
BY GOLD WALLS

Al$_2$O$_3$

FERMI
LEVEL
GOLD

Z

$f_g = 10^{-4}$, so now we need only 3×10^{11} electrons per pulse, which requires a current of 5×10^{-5} amps during each one millisecond pulse. It will be shown in Chapter 5 that the temperature of the Al_2O_3 and gold films during emission is about $100^\circ K$. Since there are no accelerating fields in directions transverse to emission, the temperature appropriate to transverse degrees of freedom may be considerably lower than $3000^\circ K$. Thus tunnel cathodes should provide sufficient slow electrons for the experiment.

Further thermalization of the electrons after leaving the cathode and possible ion formation mechanisms are discussed in Chapter 5.

6. Detector

The detector had to be capable of detecting single electrons. The use of electron multiplier dynode structures for this purpose is well known and is discussed by Z. Bay in [30]. From the discussion of mutual repulsion of electrons and the limitations of the cathode it is apparent that no more than one very slow electron per pulse could be obtained. The maximum time of flight of an electron acted on by a force mg through a distance $h_{eff} = 15$ cm is about 170 milliseconds. An electron in the last 100 milliseconds could be expected about once every 10 pulses (see Chapter 5 for typical distributions), so the background noise level should be kept below 1 count per second if the signal is to be above the noise level.

CHAPTER III

THE APPARATUS

The preceding chapter described the conditions required to make time of flight measurements on charged particles with energies below 10^{-9} eV. In this chapter are given the details of the actual apparatus used to provide such conditions and make the measurements. (See figure 7 for overall view of the apparatus.)

The cryogenic part of the system consisted of a liquid nitrogen jacketed liquid helium dewar having 3.3 inches inside diameter and 70 inches inside length. After cooling to liquid nitrogen temperature for several hours, the dewar could be filled with liquid helium through a vacuum jacketed transfer tube whose outlet was at the bottom of the dewar. Liquid helium cooling served primarily to permit operation of the superconducting magnets, but also greatly improved the vacuum, reduced the detector noise, and improved the possibility of reducing thermal gradients in the drift tube.

The vacuum system, superconducting magnets, detector, and cathode are shown schematically in figure 5. A more detailed view of the cathode region, drift tube, and detector is in figure 8. The cathode consists of a General Electric tunnel diode discussed in the previous chapter. Above it is an aperture 0.046 inch diameter made of OFHC copper and usually maintained at a small positive voltage to reduce space charge near the emitting film. To shield the drift tube region from the voltages on the extraction aperture and the cathode, a grounded OFHC copper shield surrounds them both. The hole in the shield is also 0.046 inches diameter

FIGURE 7. Overall view of the apparatus with dewars lowered beneath the floor.
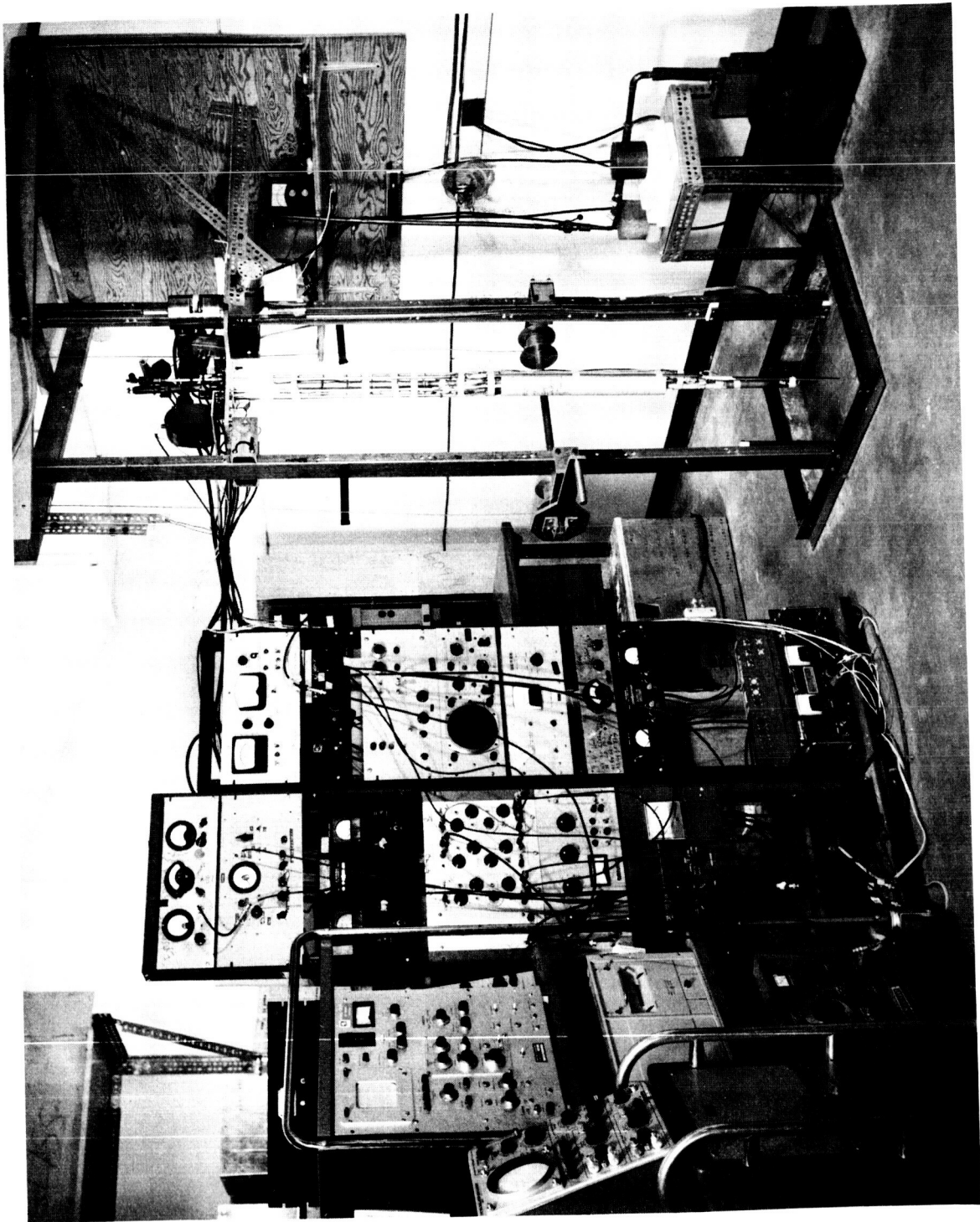
FIGURE 8. Cross section of drift tube region.

TO PUMPS AND FEEDTHROUGHS

14-STAGE ELECTRON MULTIPLIER

GUIDE MAGNET (40 gauss)

DRIFT TUBE

CATHODE MAGNET (3000 gauss)

EXTRACTION APERTURE

COLD CATHODE

QUARTZ BULB

INDIUM SEAL

ELECTRICAL FEEDTHROUGHS

CATHODE SUPPORT PLATE

CRYOGENIC TRAP HOUSING

0   1
INCH

-40-
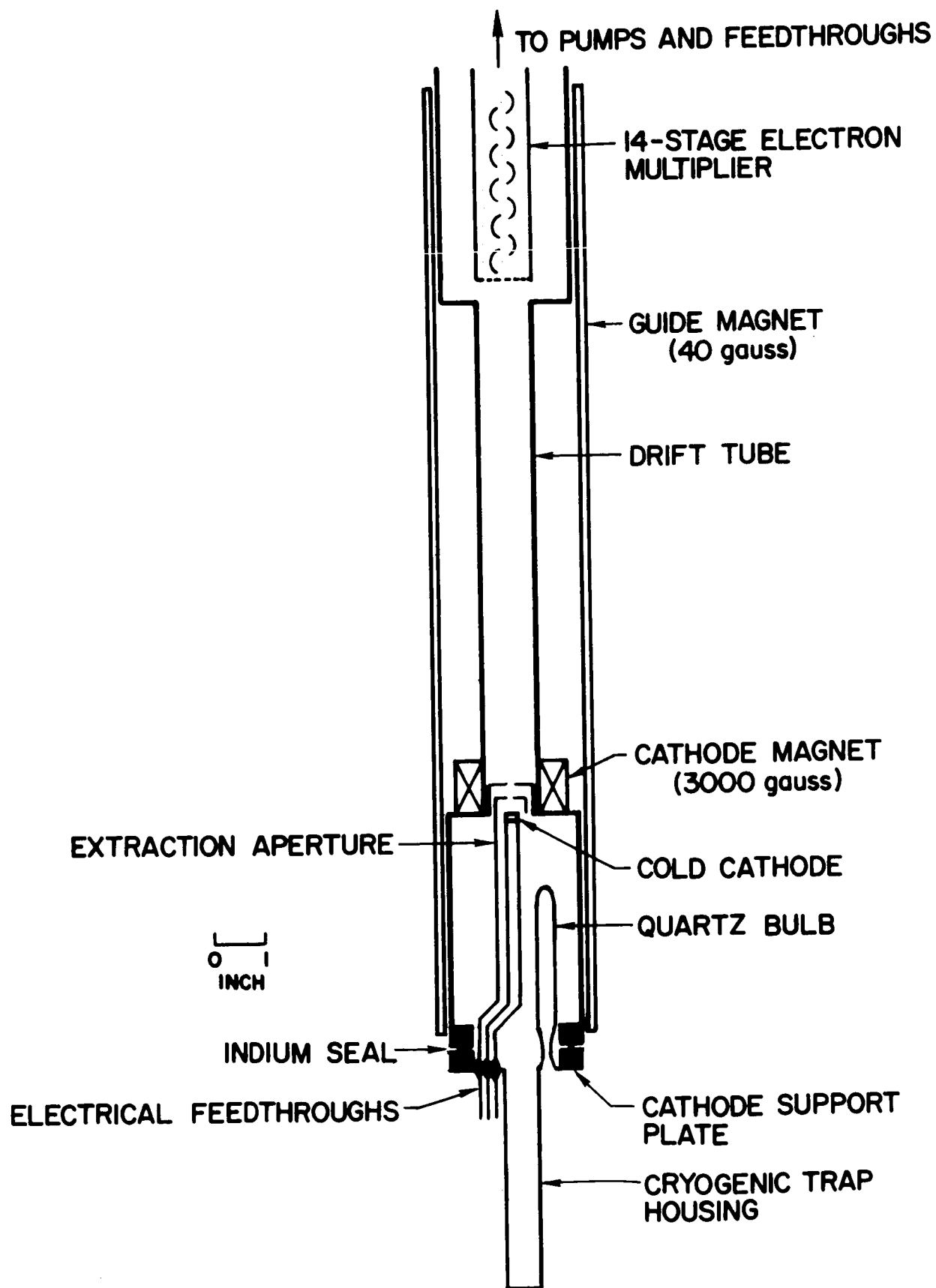
and is visually aligned with the gold emitting film and the other aperture. Spacers (not shown) align the shield axis with the center of the drift tube. This entire section is removable and demountable, since the limited life-time of the tunnel cathodes (30 hours or so of pulsed operation) dictates occasional replacement. The quartz bulb was built into the system to accommodate an ultraviolet source in case a photoelectric cathode was chosen. The long extension below the cathode feedthroughs was to house a cryogenic pump, but usually was empty.

The cathode housing, drift tube and detector housing were made of OFHC copper. The end flanges were made of type 304 stainless steel to prevent denting by metal "O" rings and to match the expansion coefficient of the mating stainless steel flanges. The assembly was brazed together in a hydrogen atmosphere oven with alloys containing only gold, silver, and copper. Electropolishing of the drift tube to a uniform texture was done before the brazing. No deterioration of the surface was noted as a result of the brazing. Insert drift tubes may be hung from the detector chamber or supported from the cathode assembly. Insert tubes were used to test the effects of different surface preparations. They can be thermally isolated at either end and along their length more conveniently than the outer tube. They are also more isolated from mechanical deformations, so that dimensions are more likely to be maintained.

The detector is an RCA CE 70131 electron multiplier containing 14 oxidized beryllium copper dynodes. Its gain, rated at 10^6 at 3.5 KV, was entirely adequate for detecting single electrons. The voltage divider consists of 14 glass encapsulated 5-megohm resistors (Pyrofilm PT-1000) spot welded onto the dynode supports. The structure is suspended from a

flange which contains four high voltage feedthroughs to provide electrical access to the detector entrance grid, the first dynode, the 14th dynode and the anode.

The requirement that pressure be below 10^{-10} torr ruled out the use of organic or other volatile materials in the vacuum system. Only stainless steel (300 series to minimize distortion of magnetic fields), OFHC copper, indium, quartz, glass, and ceramic were used in that part of the system ordinarily exposed to the drift tube. This was continuously pumped by a 5 liter per second ion pump. An all metal bakeable valve separated the ultra high vacuum part of the system from the liquid nitrogen trapped 5 liter per second oil diffusion pump and its molecular sieve trapped mechanical forepump. The diffusion pump used low vapor pressure Dow Corning 705 fluid and was only opened to the ultra high vacuum side of the system during initial pump down and bakeout.

Bakeout of the ion pump, the flanged cross, the gauges and the all metal valve was performed at $400^{O}C$ for 4 hours after every exposure to air, using an oven that completely enclosed the top part of the system. The metal valve was pinned open during bakeout. That part of the system which was to be in liquid helium was only baked with a heat gun. The cathode section could not be baked because the tunnel diodes would short out if heated above about $100^{O}C$.

The ultra high vacuum gauges mounted at the top of the system are a GE triggered discharge gauge and a Vactek Kreisman gauge both of which are supposed to be able to measure pressures below 10^{-12} torr. Even when the gauges function properly they measure a pressure which might be more closely related to the room temperature wall outgassing rate than to

pressures in the drift tube. In principle, a direct measurement of particle concentration in the desired location may be made with the same components used to study the electron free fall. If the cathode is biased at about -100 volts, the electrons guided through the drift tube by the magnetic field will ionize some of the background gas. If the detector grid and first dynode are biased at -150 and -200 volts respectively, only positive ions formed in the drift tube can reach the detector (about half of the ions will go to the cathode.) Thus if the electron current, ionization cross sections, and ion detection efficiency are known, the pressure may be calculated from the ion current to the detector. This is just the configuration of the Lafferty gauge [26], but in this case there is no x-ray limit since a cold cathode is used.

A magnetic field of about 3000 gauss may be set up in the cathode region by running 10 amps through the 1650 turn coil (cathode magnet) wound around the base of the drift tube. The superconducting wire is copper clad 0.010 inch niobium zirconium insulated with a thin epoxy coating. The 22 layers are additionally insulated by 0.001 inch mylar tape. A superconducting shunt with a wire wound heater permits the magnet to be run in either the persistent or the normal mode.

The 20 inch long guide solenoid is wound on an aluminum frame which may be removed from the vacuum system to provide access to the cathode magnet and the outside of the drift tube. The frame is supported by metal tabs projecting out from the cathode support flange. It is aligned with the drift tube to better than $\pm$ 0.010 inch by slipping wires of equal diameter at equal intervals between the frame and detector housing at the top, and between the frame and the cathode housing at the bottom. The

guide solenoid is made with the same kind of wire as the cathode magnet. It too can be run in either the normal or the persistent mode. It has 300 turns per inch. Although it can produce fields above 1500 gauss, it was usually run at only 40 gauss, since low fields produced smaller absolute gradients.

Electrical leads from the magnets and the cathode section were placed outside the guide magnet. Those carrying pulsed currents were shielded. All wires passed through vacuum feedthroughs in the support plate above the dewars. The high voltage leads were brought in through demountable teflon insulated connectors. Glass and teflon were used to insulate the leads to the anode and 14th dynode (both about 3000 V.) In the part of they system not covered by liquid it was necessary to make tight seals between various sections of insulation so that the effective surface leakage path was at least several inches. The insulating layer was surrounded by a grounded stainless steel tube which acted as an electrical shield. Flexible stranded copper shielding was used where bends were required. Failure to properly shield the anode lead resulted in greatly increased background noise.

A considerable amount of electronic equipment is required to provide time varying voltage biases to various parts of the system and to monitor the signals from the detector. The functions must be performed in the proper sequence and repeated at close intervals, usually every 0.4 second. A block diagram of the time sequencing units, the voltage supplies, and the detector monitoring apparatus is shown in figure 9. The timing of the entire operation is controlled by the time base generator. It delivers one microsecond wide pulses at some prescribed interval as small as 20 microseconds but usually 1.00 millisecond to the channel selector of a

400 channel scalar. Suppose a pulse of electrons is being emitted from the cathode. During the time of electron emission, the scalar counts all the signals that come to its signal input from the detector and stores them in its first channel. Then a channel advance pulse arrives from the time base generator, whereupon the scalar begins storing signals in its second channel. This continues at equal time intervals until the counting of signals has taken place successively in each of the 400 channels. At this time the 400 channel scalar restarts the cycle by sending out a pulse to trigger the cathode supply and simultaneously begins adding signals to those already stored in its first channel. During this time interval the cathode supply provides a 5 or 6 volt negative pulse to the aluminum film while the gold emitting film is held at some fixed bias (usually ground.) This injects electrons into the drift tube. Most of the electrons are very fast and hit the detector during the first or second time interval.

After the first time interval the cathode stops emitting electrons. If we assume that the time intervals are one millisecond wide, then those signals counted in the second channel represent electrons taking from 0 to 2 milliseconds to reach the detector, since they may have left the cathode at any time during the first millisecond and arrived at any time during the second millisecond. The signals counted in the tenth channel represent electrons which took between 8 and 10 milliseconds to traverse the drift tube.

When an electron nears the detector, it is accelerated by the electrostatic field from the first dynode which is at + 200 volts so that it hits the first dynode with enough energy to eject several secondary electrons

FIGURE 9. Block diagram of electronics for time of flight distribution
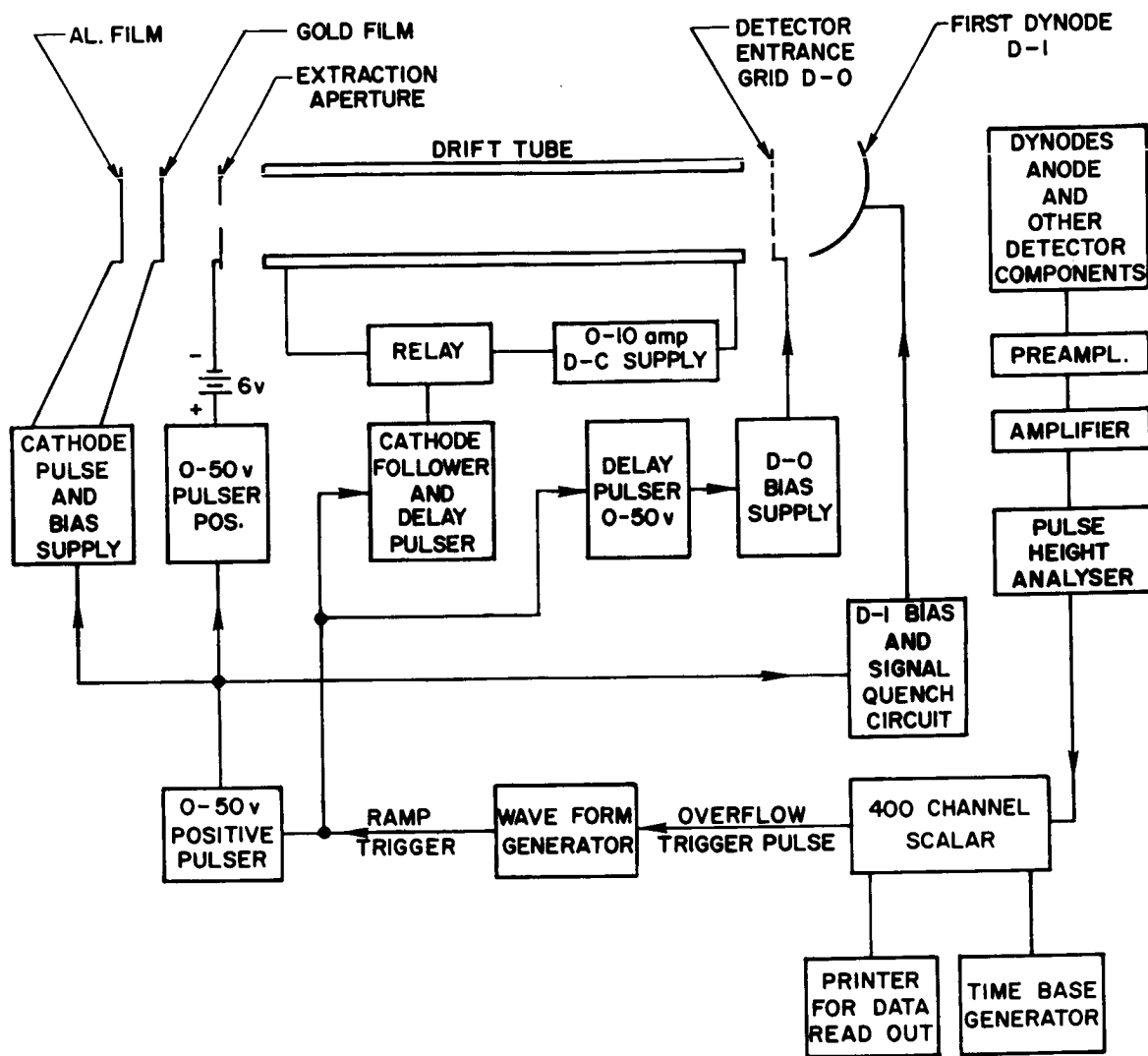
measurements.
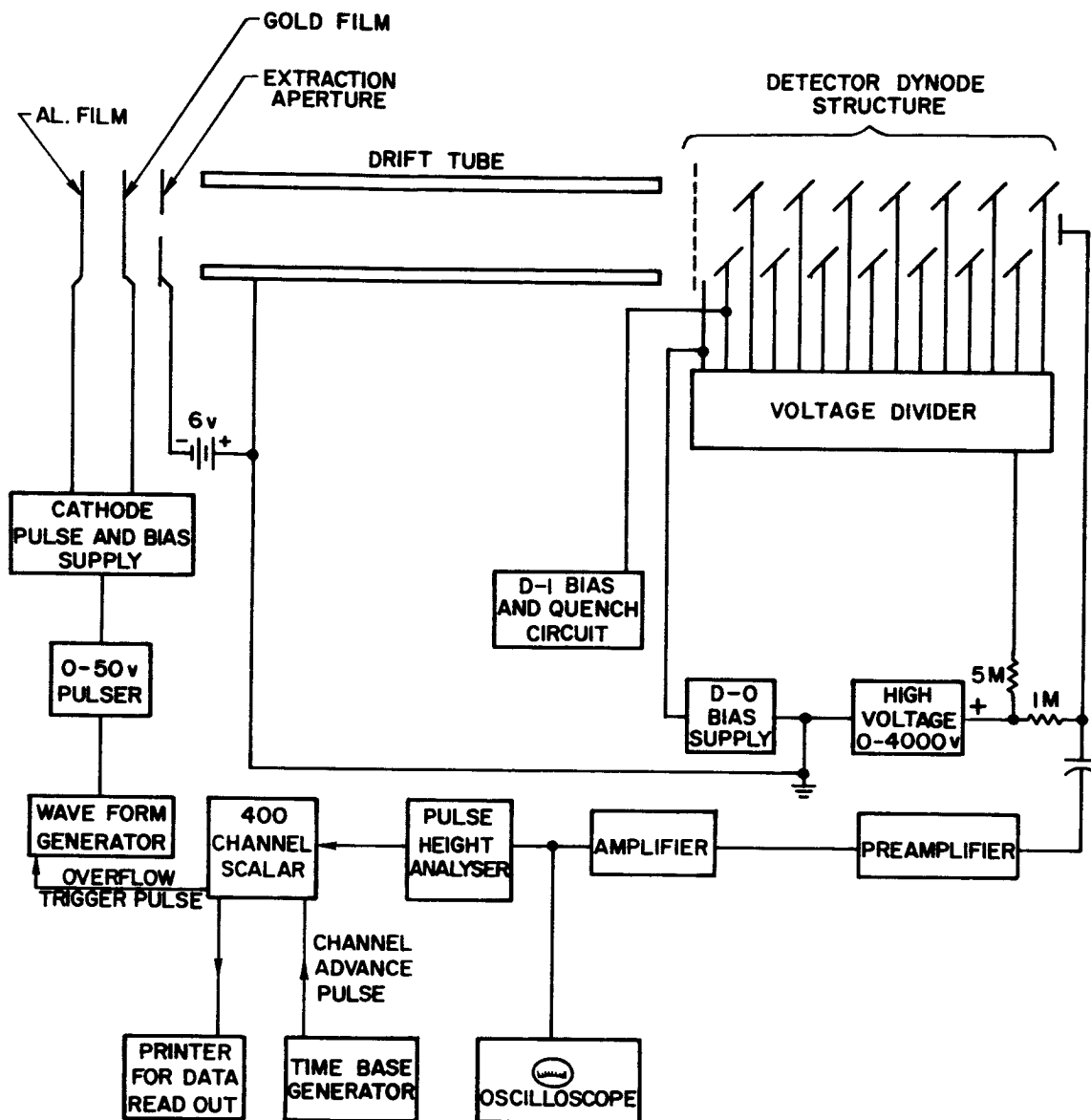
which are accelerated to the second dynode and so on, until about 10^6 electrons reach the anode. The signals from the anode pass successively through a preamplifier, an amplifier and a pulse height analyzer, before reaching the signal input of the 400 channel scalar. The preamplifier, a Franklin 359, differentiates the anode signal and provides impedance matching into the amplifier. The gain of the amplifier, Franklin 358 may be set as high as 7000, but was usually kept at 1000. The pulse height analyzer was only used as a discriminator. It sends equal sized pulses into the 400 channel scalar for each signal above a minimum amplitude that it receives from the amplifier.

So many electrons reach the detector during the first millisecond that the detector becomes overloaded, thus losing its ability to detect further pulses for a few milliseconds. Since we are not interested in the number of fast electrons, the gain of the detector was greatly reduced during the first time interval by electronically grounding the first dynode during this time, or in some cases by turning back the electrons during the first millisecond with a negative voltage at the entrance grid.

By supplying voltage pulses to the detector entrance grid and to the extraction aperture at the appropriate times, it is possible to bounce electrons in a desired energy range back and forth before allowing them to be detected. A block diagram of the electronics required for this mode of operation is shown in figure 10. Also included are the units which can set up a weak axial electric field at any desired time by sending a current through the drift tube.

FIGURE 10. Block diagram of electronics for producing electric fields near the detector and in the drift tube during appropriate time intervals. All the apparatus shown in figure 9 is also used in this mode of operation, but some is omitted or abbreviated in this diagram.

AL. FILM

GOLD FILM

EXTRACTION APERTURE

DETECTOR ENTRANCE GRID D-O

FIRST DYNODE D-I

DRIFT TUBE

DYNODES ANODE AND OTHER DETECTOR COMPONENTS

RELAY

0-10 amp D-C SUPPLY

PREAMPL.

— 6v +

CATHODE PULSE AND BIAS SUPPLY

0-50 v PULSER POS.

CATHODE FOLLOWER AND DELAY PULSER

DELAY PULSER 0-50 v

D-O BIAS SUPPLY

AMPLIFIER

PULSE HEIGHT ANALYSER

D-I BIAS AND SIGNAL QUENCH CIRCUIT

0-50 v POSITIVE PULSER

RAMP TRIGGER

WAVE FORM GENERATOR

OVERFLOW TRIGGER PULSE

400 CHANNEL SCALAR

PRINTER FOR DATA READ OUT

TIME BASE GENERATOR

CHAPTER IV

EXPERIMENTAL PROCEDURE

The actual procedure followed in any given experiment was not always the same. The initial phases depended on the condition of the apparatus after the previous run. Later phases depended on the ease with which slow electrons or ions could be obtained and on the particular test to be applied to them. In this chapter is given first a description of the procedure used in obtaining time of flight distribution data, starting with the apparatus at room temperature and atmospheric pressure. Then a procedure is described for distinguishing delayed emission of relatively fast particles from those which travelled slowly through the drift tube. This is followed by the method used to determine the approximate masses of the particles in a distribution. The details of analyzing the data to deduce the forces acting on the particles is deferred to the next chapter.

The reduction in sensitivity caused by exposure of the detector dynodes to air dictated that the detector be kept under vacuum as much as possible. Similarly the drift tube surface had to be kept under vacuum to minimize the formation of non-uniform oxide layers. The tunnel cathodes were also subject to deterioration in air and were thus stored in a vacuum desiccator. Consequently when the apparatus was not in use, the bakeable metal valve was kept closed and the ion pump left on. Repairs or revisions to the inside of the apparatus were made as quickly as possible and followed by rapid reassembly and pump down.

The rough pumping was done by a mechanical pump through an adsorption trap. Rough pumping reduced the pressure to about 10^{-2} torr. Then the diffusion pump was turned on and its liquid nitrogen trap filled. When

the pressure was reduced to less than 10^{-6} torr, the top section of the apparatus was baked for 4 hours at 400°C with the all metal valve open. The top section includes the ion pump, the vacuum gauges, the all metal valve and the flanged cross which connects them together. The lower section was baked briefly with a heat gun near the end of the bake-out period of the top section. When prolonged baking of the drift tube or the detector was necessary, the apparatus was immersed in water up to the top of the cathode magnet. This protected both the magnet winding and the tunnel cathode inside, as well as the indium seal between the cathode support plate and the cathode housing (fig. 8). Had the cathode section been bakeable, the indium seal would have been replaced with annealed gold or copper. The flanges above the detector were sealed with indium most of the time, but when baking above 100°C was necessary (to restore detector gain or to degas a graphite coated drift tube), annealed O.F.H.C. copper gaskets were used.

After the bakeout was finished, the ion pump was turned on. When the ion pump reduced the pressure to that previously achieved by the diffusion pump, the all metal valve was closed. This procedure usually led to pressures of 10^{-8} torr or lower within a few hours after the ion pump was started. During this pumping time the wires were attached and the guide magnet put in place and aligned. The dewars were then raised into position and the volume to be occupied by liquid helium was pumped out and replaced with dry helium. The liquid nitrogen jacket was filled at least five hours before filling with liquid helium.

After enough liquid helium had been transferred to immerse the drift tube and detector, a persistent current of 10 amps was set up in the

cathode magnet. This maintained a field of over 3000 gauss, which was sufficient to separate ground state electrons from those in other states. The guide solenoid was kept normal until the cathode field was established and the cathode itself had been turned on. The latter was accomplished by increasing the voltage of the pulses applied across the tunnel cathode until the current through the insulating film was about 10^{-3} amp. The voltage of the aperture just above the emitting film was set at about 10 volts or more. When the high voltage for the detector was turned on, many voltage spikes coincident with the pulse could be observed on an oscilloscope which monitored the detector output. These were "fast" electrons. Putting a small current through the guide solenoid increased the number of fast electrons. As the guide field strength was further increased the number and amplitude of the spikes went through a maximum and decreased to zero. This decrease results from the decrease in gain of the detector when placed in a magnetic field. In the early experiments the detector was shielded by a third superconducting magnet, but this was later removed to improve the field uniformity. The guide solenoid was made persistent when the maximum number of fast electrons was observed. In the successful experiments slow electrons were also detected at this time or sooner. Their presence was indicated by voltage spikes appearing after the initial burst of fast electrons (see figure 11). To verify that the signals were due to negative particles the voltage of the detector entrance grid could be made negative. -10 volts was sufficient to stop all signals. This did not mean that the particles detected with the grid at -8 volts had this much energy, because the +200 volts on the first dynode caused a considerable penetration of field through the entrance grid.

The number of slow electrons could be altered by varying the voltage

level of the emitting film and also the voltage of the extraction aperture just above it. Once these were at their optimum values, the collection of data in the 400 channel scalar was begun. The total number of counts stored in each channel was displayed on an oscilloscope so that the distribution of flight times could be observed as the data was collected. After sufficient data had been stored to show a cutoff in the distribution or some other interesting feature, the total of counts in each channel was recorded. The data storage time was usually between 10 minutes and one hour.

Pulses of electrons were emitted from the cathode every 400 milliseconds. Since the slowest particles were expected to arrive in less than 200 milliseconds, the data stored in the last 200 milliseconds gave a measure of the background noise.

To test the possibility that the signals arising after the initial burst were not due to slow particles but rather to particles emitted at relatively high speeds from potential traps near the cathode or the drift tube, a modified procedure was used. The extraction aperture was made positive only during electron emission and afterwards to time t_1. At time t_1 the extraction aperture became several volts negative and a short negative voltage pulse of length τ was applied to the detector entrance grid. Negative particles reaching the detector between t_1 and $t_1 + \tau$ were turned around by the potential there and returned to the extraction aperture. But since the latter was also negative, the particles had to return to the detector which in the mean time had been returned to its normal voltage level. If the particles that turned around between times t_1 and $t_1 + \tau$ had actually taken that long to travel from the bottom of the drift tube without being trapped on the way, they would take an

FIGURE 11. Oscilloscope trace of amplified detector output. This is

actually a superposition of 10 successive pulses. The horizontal scale

is 1 millisecond per centimeter. The nearly solid band on the left is

the initial burst of fast electrons. Spikes to the right of it represent

the arrival of slow electrons. The spikes are both positive and negative,

because the preamplifier differentiates the pulses. The black band across

the center is from a piece of tape used to shield the camera from the un-

deflected oscilloscope trace.
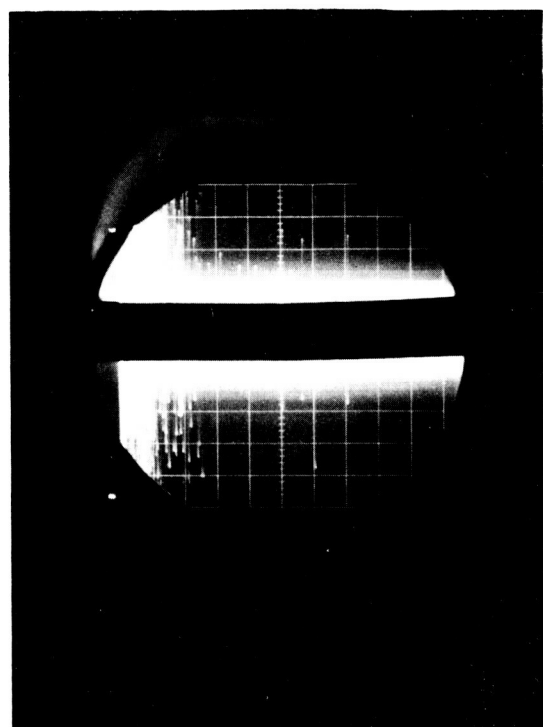
additional time $2t_1$ to $2(t_1 + \tau)$ to return to the detector. These would form a peak in the distribution between $3t_1$ and $3t_1 + 3\tau$. (This peak is further broadened by the finite width of the initial electron emission pulse.) On the other hand if the particles arriving after t_1 had been relatively fast particles escaping from potential traps, they would enter the detector very soon after $t_1 + \tau$. Particles whose velocities had been changed by collisions during transit through the drift tube would not be present in the peak even though they were turned around near the detector between times t_1 and $t_1 + \tau$. This method is a very powerful one for checking the validity of the experiment. Its only drawback is that the fields in the drift tube are changed somewhat by the changes in extractor and detector voltages, making the second and third trips through the tube slightly different in time from the first. Since the resulting potentials are attenuated below 10^{-11} volts throughout the middle section of the drift tube where the particles spend the most time, the peak should appear very nearly where predicted by the above simple analysis.

If a known field could be set up in the drift tube it would be possible to vary the position of the cut-off in time of flight distributions. For example by setting up a field that just cancelled gravity, the cut-off time would be extended to some point determined by the field irregularities in the drift tube. By setting up a field much larger than gravity, the cut-off time should be greatly reduced. Such a field was produced by running a d.c. current, I, through the drift tube and parallel to its axis. The drift tube resistance R was measured at liquid helium temperature and found to be $2.8 \times 10^{-7}\Omega$. A one amp current through such

a tube should cause an abrupt cut-off in electron flight times and considerably reduce the cut-off time for ions. Neglecting end effects, the cut-off time is $t_{max} = \sqrt{\frac{2hm}{qE}}$, where E is the electric field strength: $E = \frac{IR}{h}$. Unlike the gravitational cut-off time, this one is dependent on the particle's mass and thus provides a method of distinguishing electrons from ions. The proper interpretation of the shifts in cut-off times requires a careful analysis of the fields produced by superposition of uniform electric fields and the exponential fields arising from voltages at either end of the drift tube. These fields do not in general result in an actual cut-off in the distribution of flight times, but rather to a marked change in the distribution that is almost as clear as a cut-off experimentally. The distribution of flight times obtained experimentally, the effects of applied fields, and their interpretations are discussed in the following chapter.

CHAPTER V

RESULTS AND ANALYSIS

1. Electron Time of Flight Distributions

The results of our first time of flight experiment are summarized in figure 12. The 400 channel scalar had not been obtained in time for that test, so the delayed pulses were counted by photographing traces of an oscilloscope monitoring the detector output. Not very much data could be obtained this way, but the distribution of flight times illustrates remarkably well the form which one would expect to find if the density of emitted electrons were low enough that they did not interact. The number of electrons $N(t)$, arriving after time t is very nearly given by $N(t) = Ct^{-2}$ as shown by the solid curve in figure 12.
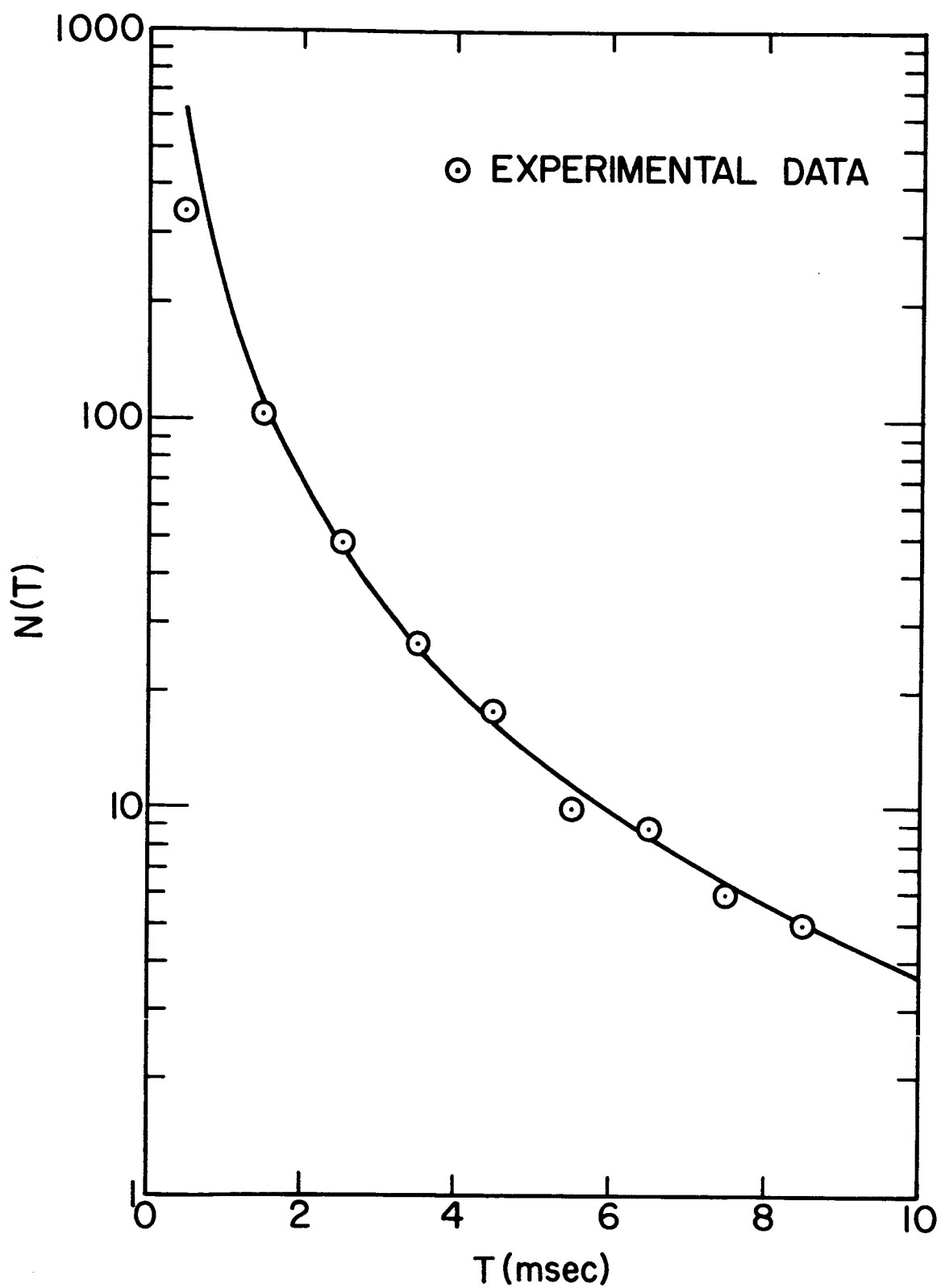
The t^{-2} dependence may be derived from the expected energy distribution of electrons emitted from the tunnel cathode or indeed any common cathode. Electrons taking longer than one millisecond to traverse the drift tube do so with average kinetic energies between 0 and $1.6 \times 10^{-7} \text{eV}$. As shown in section 2.5, the number of electrons $N(\epsilon)$ emitted in the small energy range ϵ above the maximum drift tube potential Φ is given by

$$N(\epsilon) = C_1 \epsilon \, , \tag{15}$$

where C_1 is a constant. In a tube of length h in which no forces act $\epsilon(t) = \frac{1}{2} mv^2 = \frac{m}{2} \frac{h^2}{t^2}$, so

$$N(t) = \frac{C_1}{2} mh^2 t^{-2} = C_2 t^{-2} \, . \tag{16}$$

FIGURE 12. Data from our first time of flight experiment. $N(t)$ is the sum of all signals coming later than time t. (semilog plot) The solid curve is $\dfrac{C}{t(t-1\ \text{millisec.})}$. C was chosen to fit the data.

The figure shows a semi-log plot of $N(T)$ versus T (msec), with experimental data points and a fitted curve.

⊙ EXPERIMENTAL DATA

If one takes into account the fact that the electrons were not all emitted at time $t = 0$, but assumes a uniform frequency of emission between $t = 0$ and $t = \tau_o$, then

$$N(t) = \frac{mh^2}{2\tau_o} \int_0^{\tau_o} \frac{d\tau}{(t-\tau)^2} = \frac{mh^2}{2} \left(\frac{1}{t-\tau_o} - \frac{1}{t}\right) = \frac{C_2}{t(t-\tau_o)} \qquad (17)$$

τ_o was always one millisecond or less. The flight times of interest were usually so much longer than this that τ_o is taken to be zero in all further analysis.

The data taken after the first experiment followed approximately the Ct^{-2} distribution within limits of deviation expected from statistical considerations, but under the original operating conditions very little data could be obtained beyond 10 milliseconds even with the aid of a 400 channel scalar. It was apparent from the distribution function that if 10 minutes of data collection were required to get 10 electrons with flight times greater than 10 milliseconds, 10^3 minutes would be required to observe this number beyond 100 milliseconds, where the effect of gravity on the distribution might be observable. Thus the intensity of electron emission had to be greatly increased over that used in the first few experiments.

The factor limiting the amount of current that could be used was the overloading of the detector by the initial burst of fast electrons. This was accompanied by an overloading of the amplifier and usually followed by a long series of spurious signals. To prevent this overloading it was first decided to maintain the detector entrance grid at a negative voltage while the cathode was emitting. This certainly stopped the overloading of the detector, but introduced a complication in calculating the electron energy distribution because of the collisions between fast electrons turned

around at the detector and those still rising from the cathode.

The results of an experiment in which the initial pulse of electrons was returned to the cathode are shown in figure 13. The distribution still followed the Ct^{-2} dependence for the first 10 channels (milliseconds). The advantage of the increased electron current allowed by this method is apparent from the large numbers of late detector signals observed compared to the background noise of 5 counts per channel per minute. Background noise could be determined by averaging the counts per channel in the last 50 channels of the 400 channels of data. If no particular trend appeared in the last 200 channels, as was often the case, the noise was determined from an average of the last 200 channels. The data in figure 13 appears with the noise subtracted. Apparently there is a cut-off between 30 and 40 milliseconds.

If the 23 cm drift tube were completely free of vertical electric and magnetic forces then gravity alone would cause a cut-off given by $t_{max} = \sqrt{\frac{2h}{g}}$ = 220 milliseconds. From figure 4 it is apparent that electrostatic forces from the end potentials and the force due to the magnetic field gradient require that the electron move through much of the drift tube at high speeds. The effective drift tube length in which the electrostatic and magnetic potentials change more slowly than gravitational potential appears to be only about 2 cm. This makes gravity hard to observe unless the field free region is lengthened.

Before analyzing the 30 to 40 millisecond cut-off more carefully, it should be mentioned that electrons falling through a metal tube with no applied electric or magnetic fields would probably not have a gravitational cut-off if their gravitational and inertial masses were identical. The

-63-

FIGURE 13. Comparison of experimental data with some calculated electron distributions. (semilog plot) The $N(T) \propto T^{-2}$ curve describes the distribution expected from particles emitted from the cathode with a constant distribution in energy and no interaction with the fringe field. The $N(T) \propto E(T)$ curve should describe electrons in the ground state emitted with a constant distribution in energy. The $N(T) \propto E^{0.6}(T)$ curve describes ground state electrons whose space charge interaction near the cathode has partially thermalized the energy distribution.
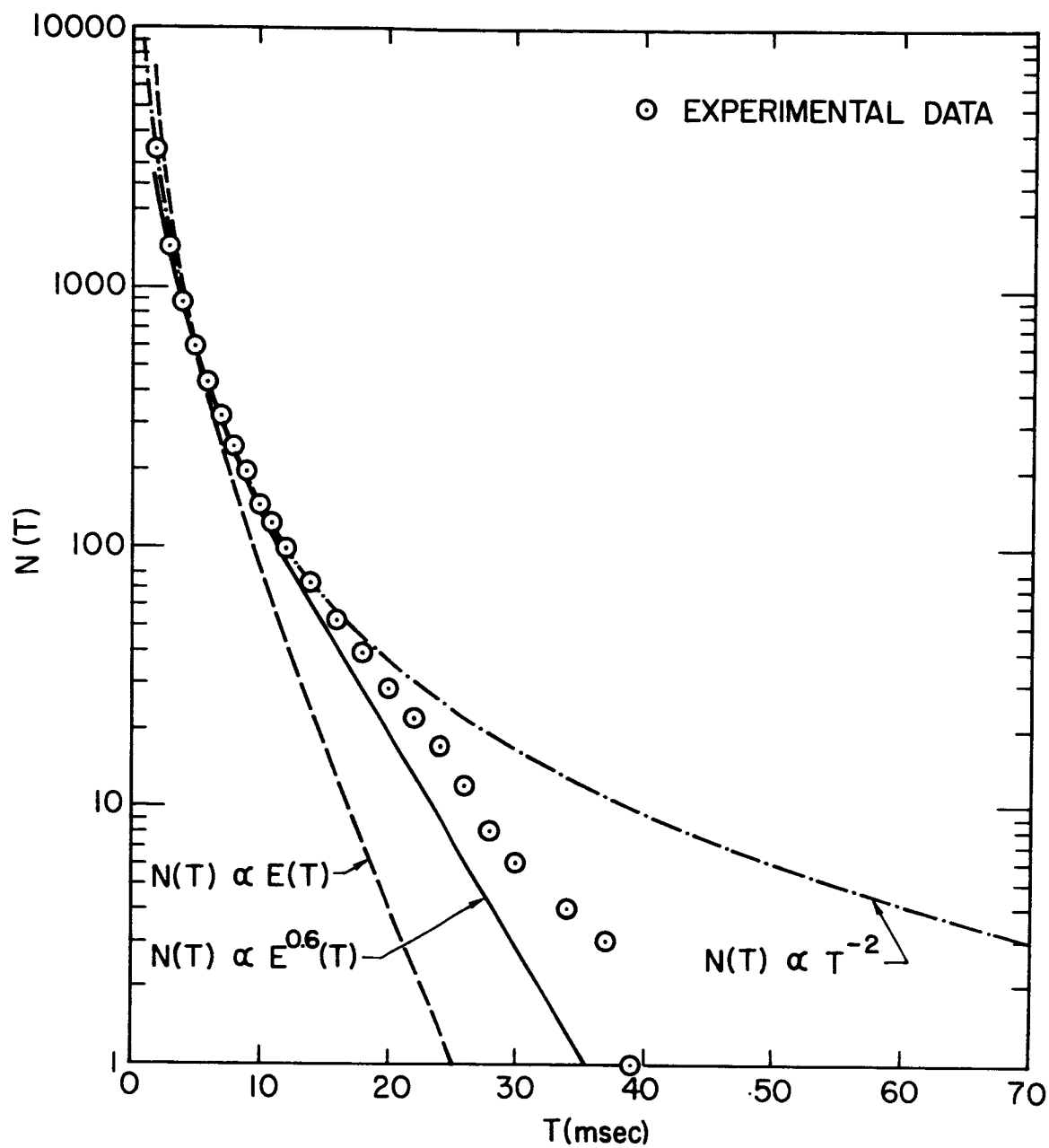
electrons in the metal walls of the drift tube are free to respond to the earth's gravitational field. Since on the free electron model they adjust their distribution to form a force free region inside the metal, an electric field $E = \frac{mg}{q}$ must be set up which just cancels the gravitational force for electrons. Since the tangential component of E is continuous across a metal boundary, the electron in the center of the drift tube is also in this electric field. The behavior of the ionic lattice is not taken into account in this argument, however, one would expect the weight of the ions to be compensated by a slight rearrangement of the electron density. This question is still open, and until it is cleared up, it will be difficult to interpret electron time of flight data properly. In any event, it is interesting to note that a gravitationally induced electric field would act in the opposite direction on positrons. Thus if positrons have the same gravitational constant as bulk matter and the above argument is correct they will experience a downward acceleration of 2g in a metal drift tube. By making measurements on both electrons and positrons, we can determine the sum of the force of gravity on the electron and the positron. The electrostatic cancellation of the gravitational force on electrons will have a negligible (less than 0.1%) effect on ions, so normal gravitational cut-offs should appear when slow ions are studied.

We now study in detail the effect of the fringe fields on the distributions. The time of flight of an electron in an arbitrary potential field $V(z)$ is found from the energy integral:

$$t = \sqrt{\frac{m}{2}} \int_0^h \frac{dz}{\sqrt{E - qV(z)}} \tag{18}$$

where $E \geq qV_{max}(z)$ has the same meaning as before. If the only forces acting on the electron are due to the electrostatic fringing fields shown in figure 2, then since $qV(z) = 0.027(1-e^{-2.405z/cm})eV$ for $1 \text{ cm} < z \leq 10.5 \text{ cm}$, and a nearly symmetrical relation holds for the other end of the drift tube,

$$t = \sqrt{2m} \int_0^{10.5cm} \frac{dz}{\sqrt{\epsilon + 0.027e^{-2.405z/cm} - 0.027e^{-2.405 \times 10.5}}} \quad (19)$$

where $\epsilon = E - qV_{max}(z)$.

Plots of ϵ versus t for several potential are shown in figure 14. From Eq. (15) we see that $C_1 \epsilon(t) \propto N(t)$ so the energy distribution function in appropriate units is also the time of flight distribution. This distribution goes out to about 40 msec., so the voltages near the ends of the drift tube almost completely account for the 30 to 40 millisecond cut-off. Now the effect of the magnetic field gradient must be examined.

A plot of the magnetic fields due to the cathode magnet and guide solenoid is shown in figure 3. The resulting magnetic potential energy for ground state electrons plus the electrostatic potential are plotted in figure 4. Numerical integrations of Eq. (18) for this potential distribution were made for several values of E. The results are included in figure 14 and compared with the data in figure 13 assuming $N(t) \propto E(t)$. The constant C_1 in Eq. (15) was chosen to make N(10 msec) equal to the experimental values. The calculated distribution falls off even more steeply than the experimental data. It is immediately apparent that the observed distribution could not result from electrons in excited magnetic

-67-

FIGURE 14. Minimum kinetic energy versus flight time for ground state electrons. (log-log plot) The flight time for a given electron energy was obtained by numerical integration of the energy integral (Eq. (18)) for cases: (1) No forces; (2) Electrostatic force only as in figure 2, (3) Electrostatic and magnetic potential of figure 4. The minimum kinetic energy is reached about halfway up the drift tube and is fairly constant over a distance of only about 2 cm.
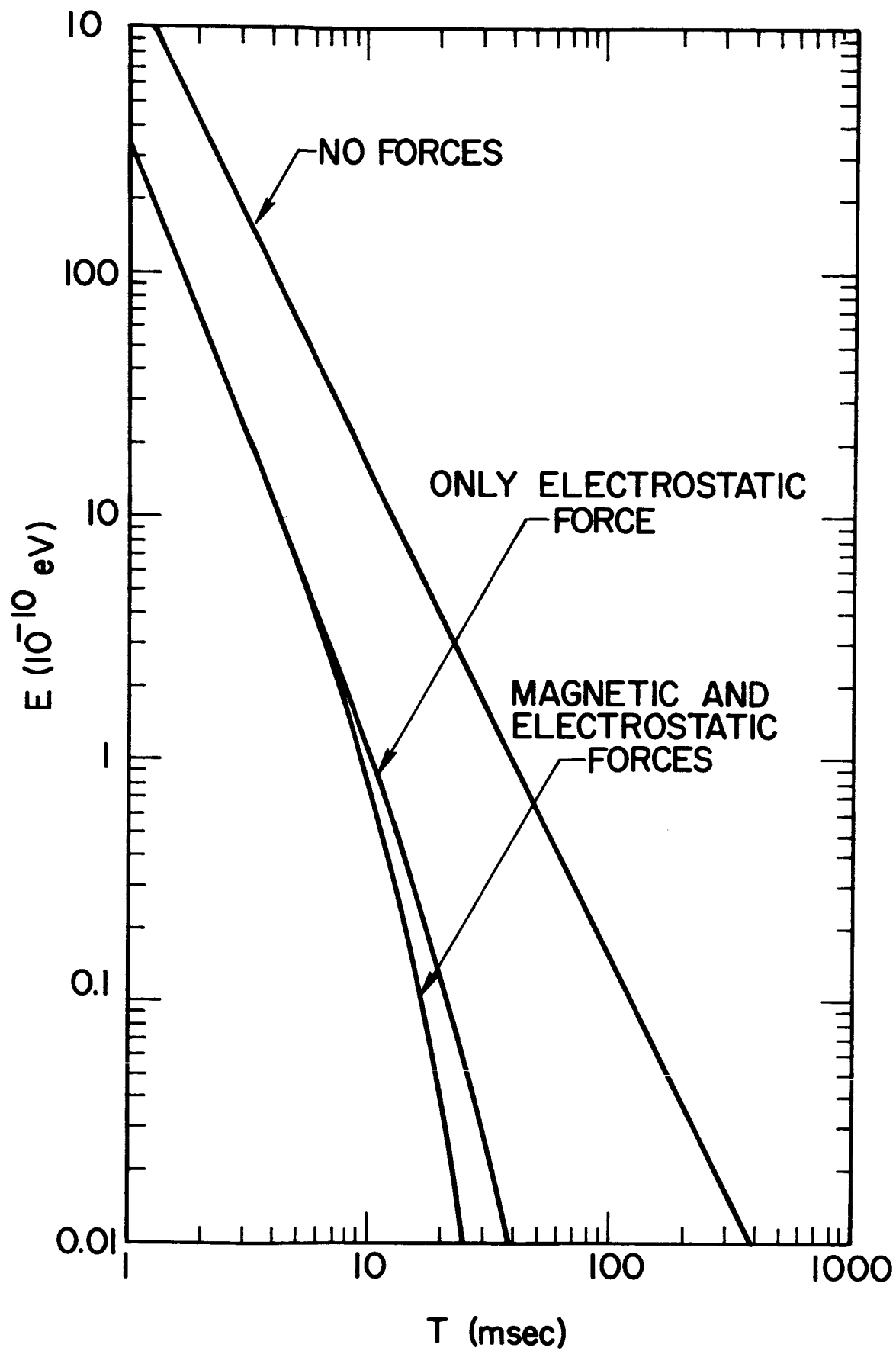
states, because their magnetic potential gradient would be at least

1000 times steeper, causing a much shorter cut-off time. Thus the

data indicates that the distribution of figure 13 was formed from

electrons in the ground state provided an explanation can be provided

for the small but disturbing difference between the calculated curve

and the data. The mechanism for the extension of the cut-off time be-

came apparent from the results of a later experiment.

In a subsequent run the electron density was further increased to

speed data collection. In this case the cut-off (figure 15) was at

about 80 milliseconds, far beyond what reasonably could be expected

for electrons in the potential of figure 4. So far the interactions

of the electrons with each other have been ignored in interpreting the

data. Changes in both $N(E)$ and in the potential distribution that

could result from such interactions are discussed next. It will be

seen that these changes are sufficient to account for the unusually

long flight times.

The data of figure 15 was accumulated from 9000 pulses each one

millisecond wide. According to the data, about 60,000 particles re-

quired 2 milliseconds or more to reach the detector. The corresponding

energy range is seen from figure 14 to be 7×10^{-9} eV. The density of

particles in z-directed energy space is therefore $\dfrac{60,000}{9,000} \div 7 \times 10^{-9}$ eV $=$

1×10^{9}/eV. For each electron that passes through the drift tube in the

energy range 0 to 10^{-9} eV, there is one in a similar energy width that

is turned around below the center of the drift tube. An electron in

this energy range will spend at least 10 milliseconds in the drift tube,

mostly in the region of highest potential energy (see figure 4) where

its velocity is lowest. As shown in Chapter 2, the electrostatic potential due to this charge exceeds 10^{-10}eV for 2.5 tube radii (2.5 cm in our apparatus) above and below the electron. Indeed for charge separations greater than 1 cm, the mutual repulsion potential falls with precisely the same form as the potential energy from end voltages rises. Thus the region of flat potential may be extended by space charge effects by 2 cm or even more for times on the order of 10 milliseconds. This effect would be most noticeable on the slowest particles whose flight times are most sensitive to changes in the potential. Since the chance of getting two electrons in the same energy interval ΔE is proportional to ΔE^2 or t^{-4}, the distribution must still drop off quite sharply. This behavior is in qualitative agreement with the data of figures 13 and 15. The former had about one tenth the electron density of the latter and should have been much less affected, as was evidently the case. So far we have only discussed the effects of mutual repulsion on the potential energy in the drift tube. These involved electron interactions or collisions which could also affect the kinetic energy distribution, as shown below.

If the electrons reached a thermal equilibrium with each other in a region of the drift tube in which the applied electric fields were relatively weak they would have a velocity distribution discussed in Chapter 2 and given by $dN(v_z) \propto e^{-mv_z^2/2kT} dv_z$ [25], so $dN(E_z) \propto e^{-E_z/kT} \dfrac{dE_z}{E_z^{\frac{1}{2}}}$.
Then

$$N(t) \propto \int_0^{E(t)} \frac{dE_z}{E_z^{\frac{1}{2}}} \propto E^{\frac{1}{2}}(t) \propto t^{-1} \qquad (19)$$

where we have made use of the fact that $E(t) \ll kT$ for flight times of interest. The flow of electrons through the drift tube clearly is not a

-71-

FIGURE 15. Experimental data from a run with a high electron density.

(semilog plot)

-73-
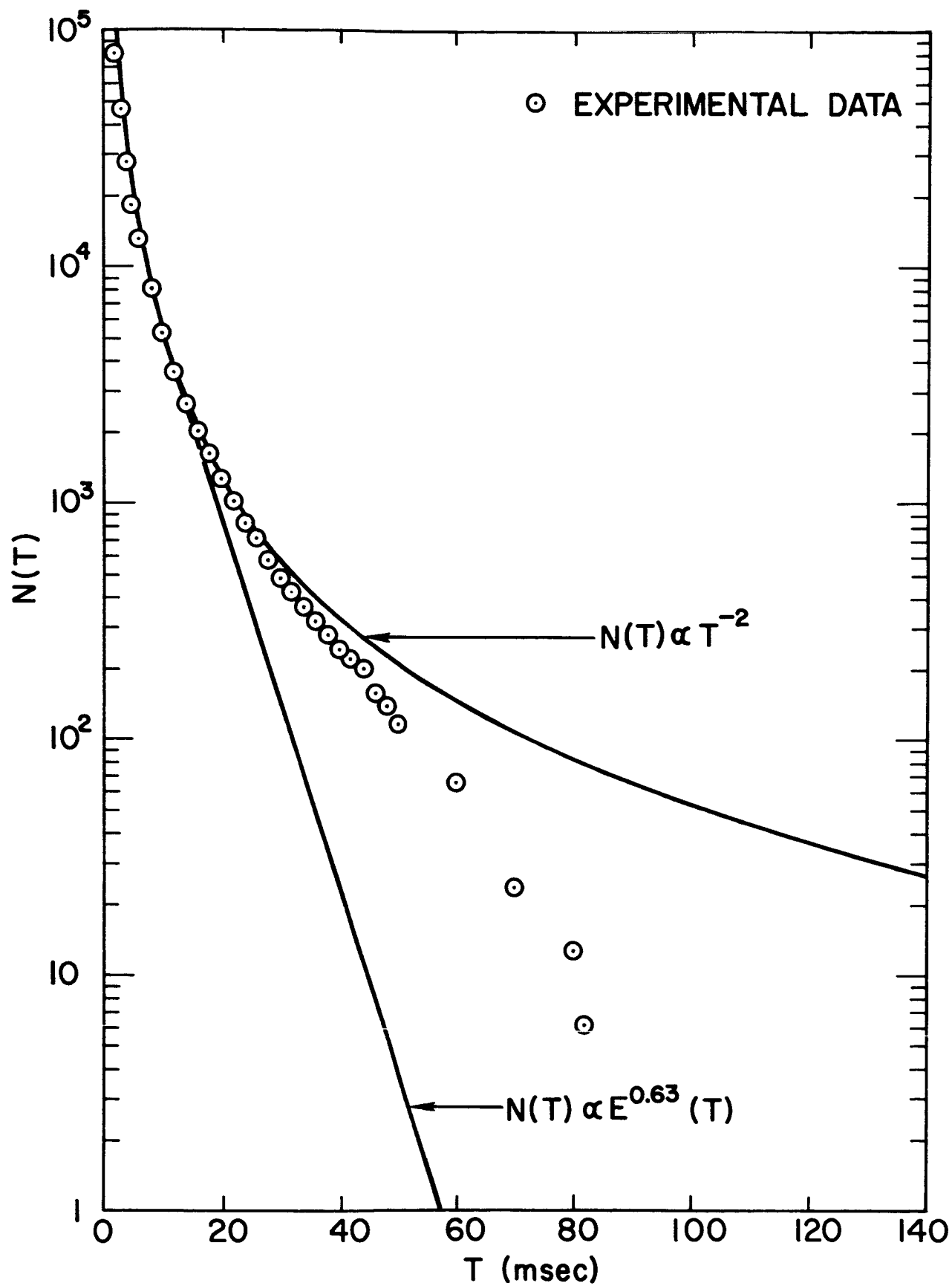
case of thermal equilibrium, which is only a limiting case. From equations (15) and (19), one would expect the relation $N(t) = C_1 E^\gamma(t)$, where $0.5 \leq \gamma \leq 1.0$, to hold for a range of space charge conditions.

Another effect of partial thermalization is to leave some electrons trapped in the potential well near the extraction aperture. Electrons not in the ground state could also be trapped between the cathode magnet and the center of the drift tube. Electrons may be ejected from such traps by 3-electron collisions, by binary collisions with background gas, or in the case of magnetic trapping, by binary electron collisions. Let $n(t)$ be the number of density of the electrons left in a trap at time t. If the principal means of escape is by 3-electron collisions then $\frac{dn}{dt} = -s_3 n^3$, so $\frac{dn}{n^3} = -s_3 t$, where s_3 is a constant. Thus $\frac{1}{n^2(t)} - \frac{1}{n^2(0)} = 2s_3 t$. Now clearly $n^2(0) \gg n^2(t)$ for large t, so

$$n(t) = \frac{1}{\sqrt{2s_3 t}} \qquad (20)$$

Furthermore $n(t)$ is proportional to the number of electrons likely to arrive at the detector after time t. Therefore experimental values of $N(t)$ may include a $t^{-\frac{1}{2}}$ component. Similarly if binary collisions provide the principal escape mechanism from traps then $\frac{dn}{dt} = -s_2 n^2$ which may be integrated to give

$$n(t) = \frac{1}{s_2 t} \qquad (21)$$

This could apply only to ions or electrons in excited states trapped by magnetic gradients, since the relative velocity between particles is unchanged in a binary collision unless the internal energy changes. If collisions with the background gas were predominant then $\frac{dn}{dt} = -s_1 n$ which

leads to

$$n(t) = n(0)e^{-s_1 t} \qquad (22)$$

where s_1 is a constant proportional to the background pressure. An example of a distribution described by Eq. 22 is shown in figure 16 which shows time of flight data taken when the pressure was at least ten times as high as ordinarily used. The data in figure 17 was obtained with the detector entrance made 9 volts negative so that the whole drift tube served as a very shallow trap. It shows a $t^{-\frac{1}{4}}$ dependence for several milli-seconds which drops off to the $t^{-\frac{1}{2}}$ dependence of Eq. (20) and then falls off sharply. This suggests multi-body collisions, as might be expected for this situation. (It should be emphasized that the particles did not need $9eV$ of kinetic energy to enter the detector, because of the penetration of field from the first dynode.) Still other sources of modifications to the expected distributions exist.

The presence of irregular surface potentials in the drift tube, for example can shorten the observed flight times through the drift tube by blocking all but the fast electrons. Such potentials could also form traps. A large amount of data had to be accumulated under a variety of experimental conditions before the time of flight distributions could be understood.

It might be argued that the long cut-off times observed in the data of figures 13 and 15 were caused by a few negative ions formed near the cathode. In fact it will be shown that this was the case in a few of the later experiments. A series of short runs taken on the same day as the data in figure 13 provides very convincing evidence that the data in at least the first 10 milliseconds was due to electrons. In these runs time of flight data was accumulated for 2 minutes at each of 17 values of the

FIGURE 16. Data taken with high background gas pressure. (semilog plot)
The solid line is an exponential distribution normalized to the data at
10 milliseconds. Note that the data decreases exponentially from 3 milli-
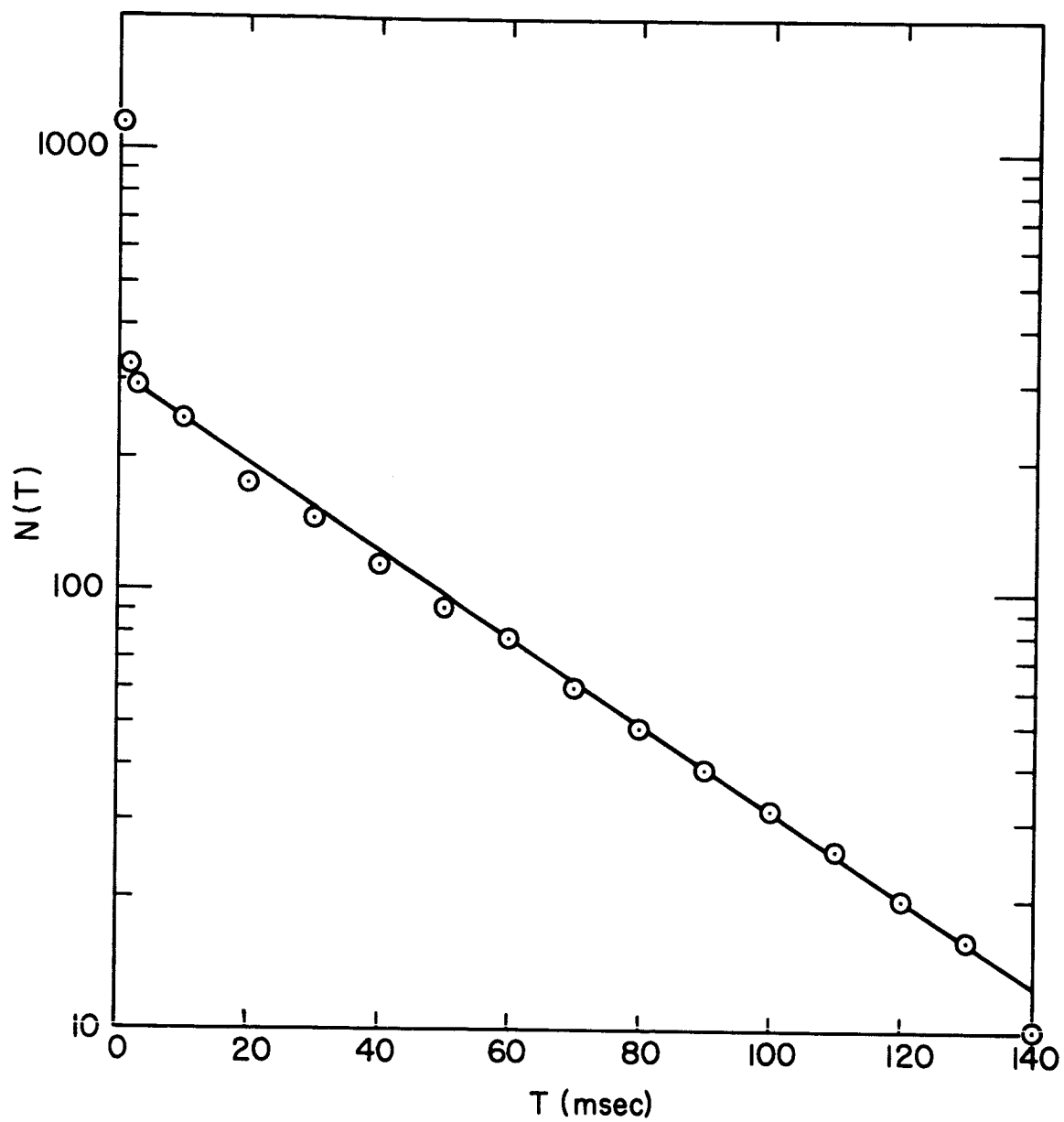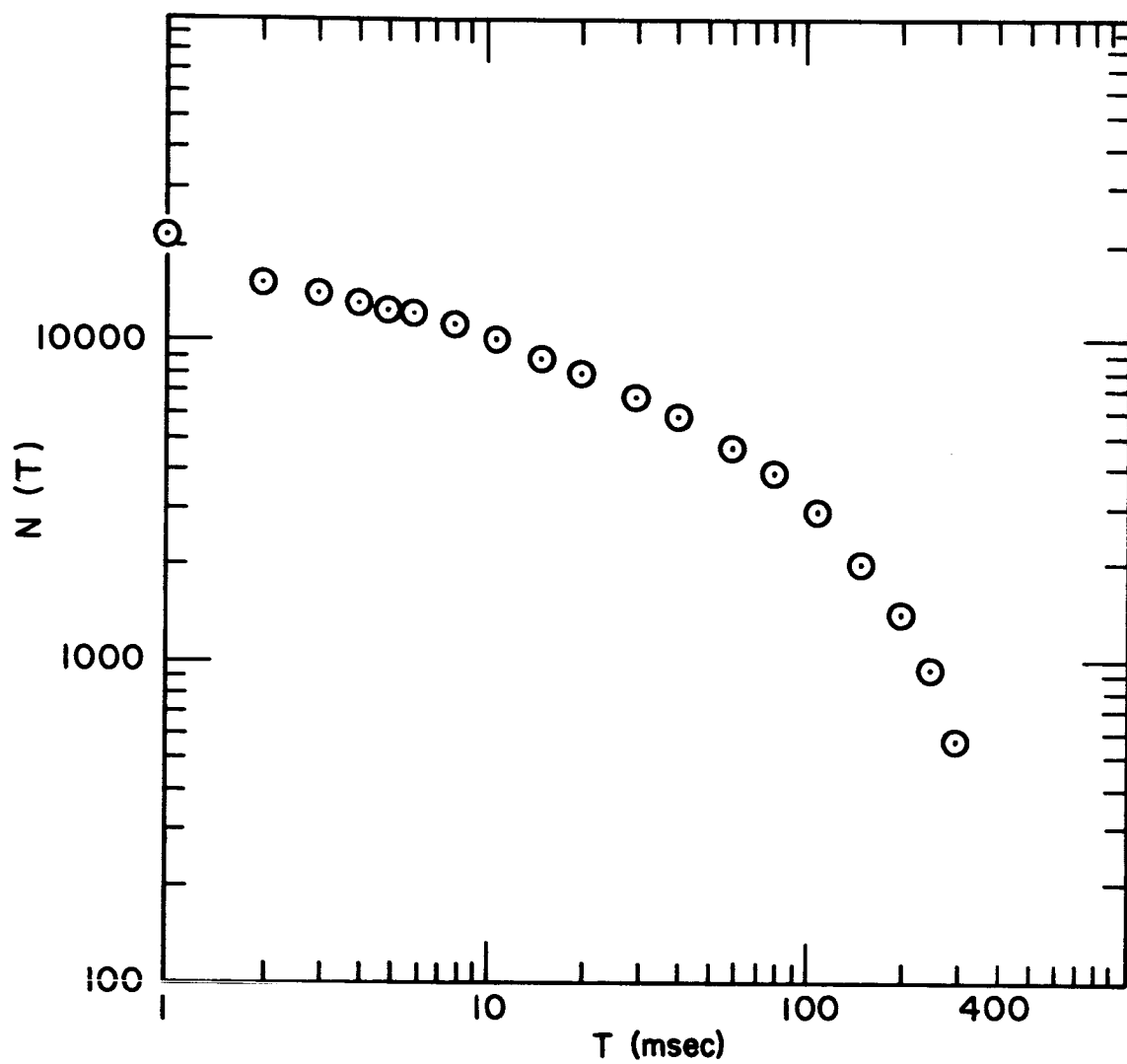seconds on.

FIGURE 17. Data taken with the entire drift tube serving as an electro-
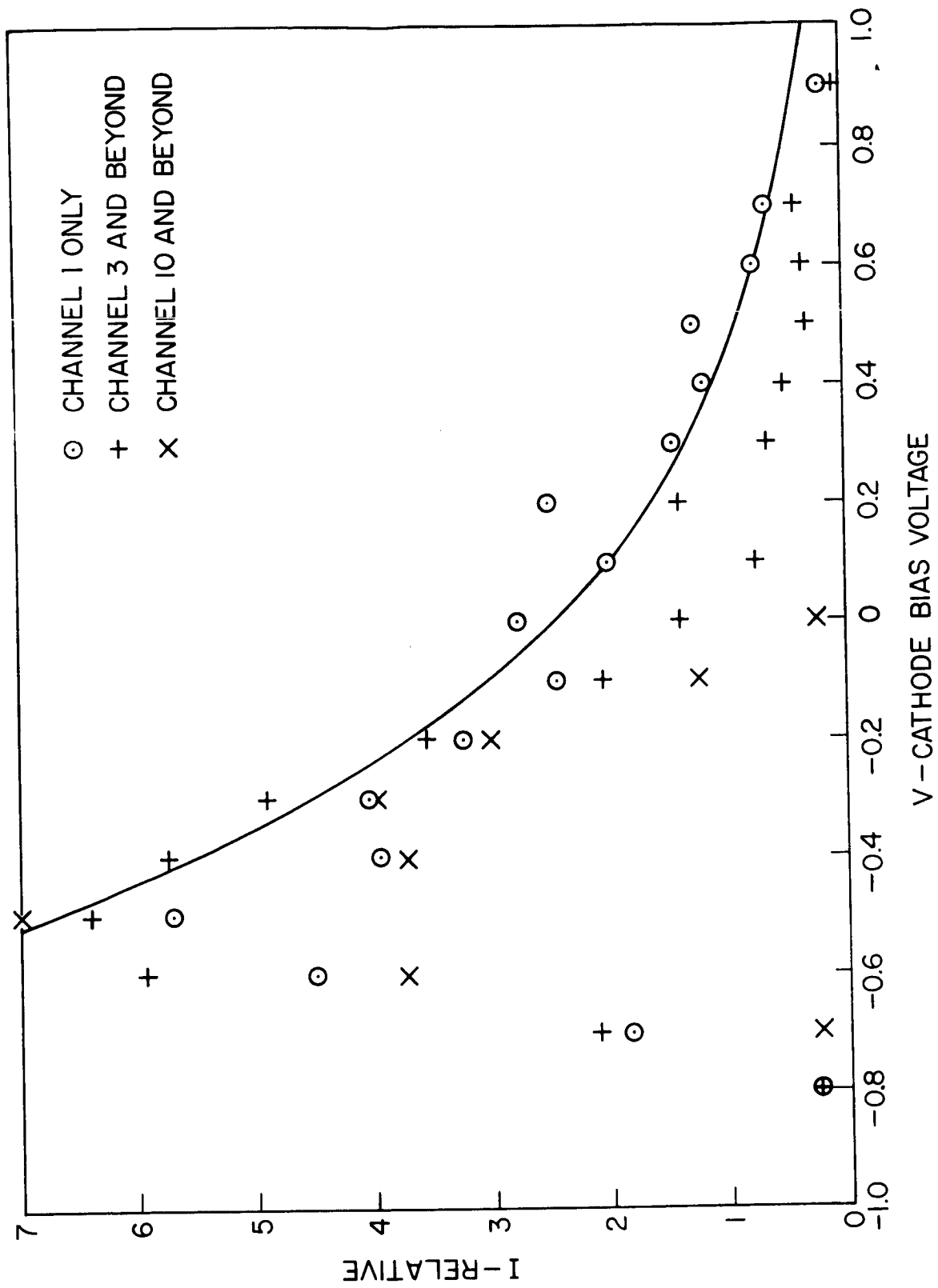static potential trap. (log-log plot)

cathode voltage (relative to the drift tube). This amounts to a retarding potential measurement of the energy distribution of emitted electrons. It is an unusual retarding potential measurement in that only slow electrons are used to determine the energy distribution. Thus if the cathode to drift tube potential difference was set at + 0.1V, only detector signals from electrons with energies between 0.1000000 eV and about 0.1000001 eV were stored in channels 1 through 399 of the scalar. All electrons with higher energy arrived in the first channel, channel 0. All with lower energies failed to get through the drift tube.

Electrons arriving in channel 10 or beyond must have passed through the drift tube with minimum kinetic energies below 10^{-10} eV. The data plotted in figure 18 shows that the particles arriving in channel 10 and beyond had the same energy distribution as those arriving in the first millisecond. Furthermore, these distributions had the same form as retarding potential measurements made at another time on the fast electrons by a different method. They are of the same form as the distributions reported by Collins and Davies [29] in their retarding potential measurements of energy distributions of electrons emitted from tunnel cathodes.

Ions formed in the drift tube would have had a narrower energy distribution than that of figure 18 since they must be formed from gas near 4.2°K. Ions formed on the surface of the cathode would also have a narrower energy spread, since they are formed from gas at $T \sim 100^{\circ}$K. The energy spread could be broadened if the ions were formed over a range of potentials (e.g. on different patches of the cathode), but then the distribution would not be likely to have such a long exponential tail as that in figure 18. The fact that the flight time distributions had a t^{-2} form for each

FIGURE 18. Energy distribution of emitted electrons. The solid curve is a plot of $e^{-|q|V/kT}$ with $kT = 0.5$ eV. The zero of the voltage scale is arbitrary. The vertical scale is relative and is different for each channel number. This was done to facilitate comparison between the shapes of the I versus V curves for each time of flight interval.

Legend:
- ⊙ CHANNEL 1 ONLY
- + CHANNEL 3 AND BEYOND
- × CHANNEL 10 AND BEYOND

Y-axis: I-RELATIVE

X-axis: V-CATHODE BIAS VOLTAGE

of the runs at each cathode voltage setting is good evidence that the particles observed were not emitted from traps. It must be concluded that the particles forming these distributions were electrons with energies as low as 10^{-10} eV.

2. Separation of Slow Electrons From Trapped Electrons

As mentioned in the chapter on procedure, it is possible to distinguish between delayed detector signals coming from slow particles and those from other sources. Particles turned back from the detector at time t_1 should take an additional $2t_1$ to travel to the extraction aperture (at negative potential after $t = t_1$) and back to the detector if they were actually particles with average velocity h/t_1 throughout their flight in the drift tube. The expected distributions from such an experiment are shown in figure 19, both for the case in which genuine slow particles are present and that in which the distribution consists of particles emitted at relatively high speeds from traps. Data from a run in which this method was tried appears in figure 20. The peak at 22 milliseconds is very pronounced. The initial cathode pulse width was one msec. and the detector was negative from 8 msec to 11 msec. Thus the peak should lie between 21 msec and 33 msec. The peak should lie nearer the lower time limit because the distribution favors the faster particles. The data satisfies these criteria quite well. The extraction voltage was kept at 16 volts, so helium ions could not form. It is fairly certain that the particles observed were electrons. Under some conditions of operation in which delayed signals were observed, there was no peak near $3t_1$. In future work with electrons these conditions are to be avoided. They include working with large detector overloads and negative

FIGURE 19. Distribution expected if negative delayed pulse is applied to detector entrance grid.

Top: Delayed signals result from particles traveling with average z-directed speed h/t.

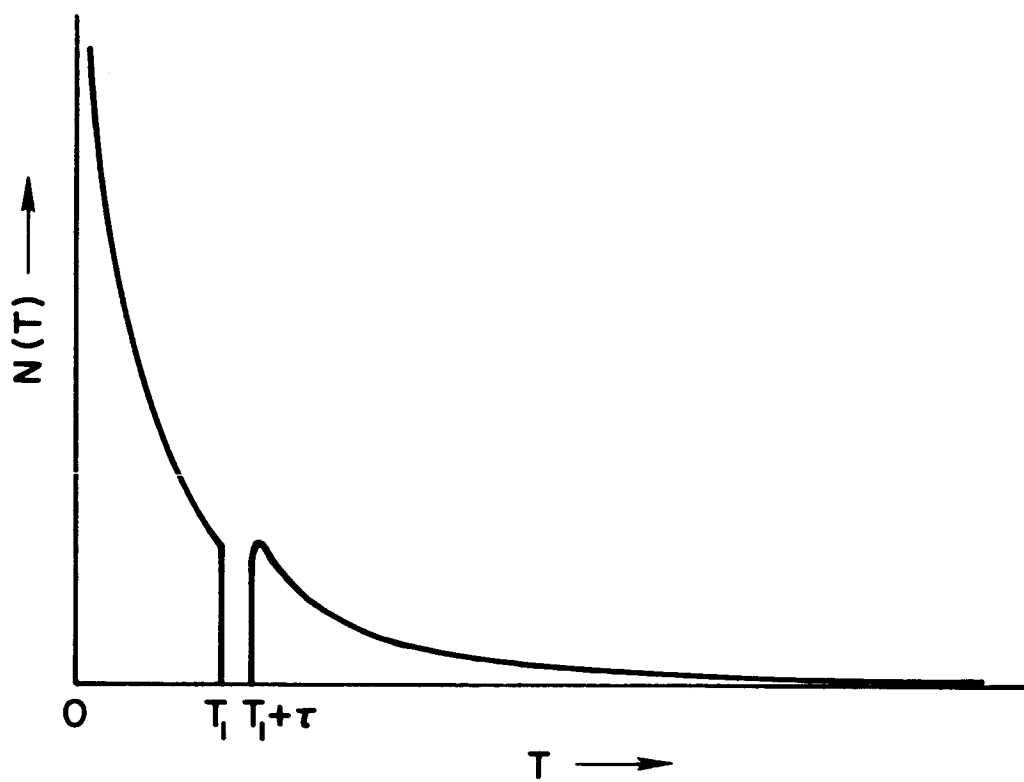Bottom: Delayed signals result from particles emitted from traps at relatively high speeds.
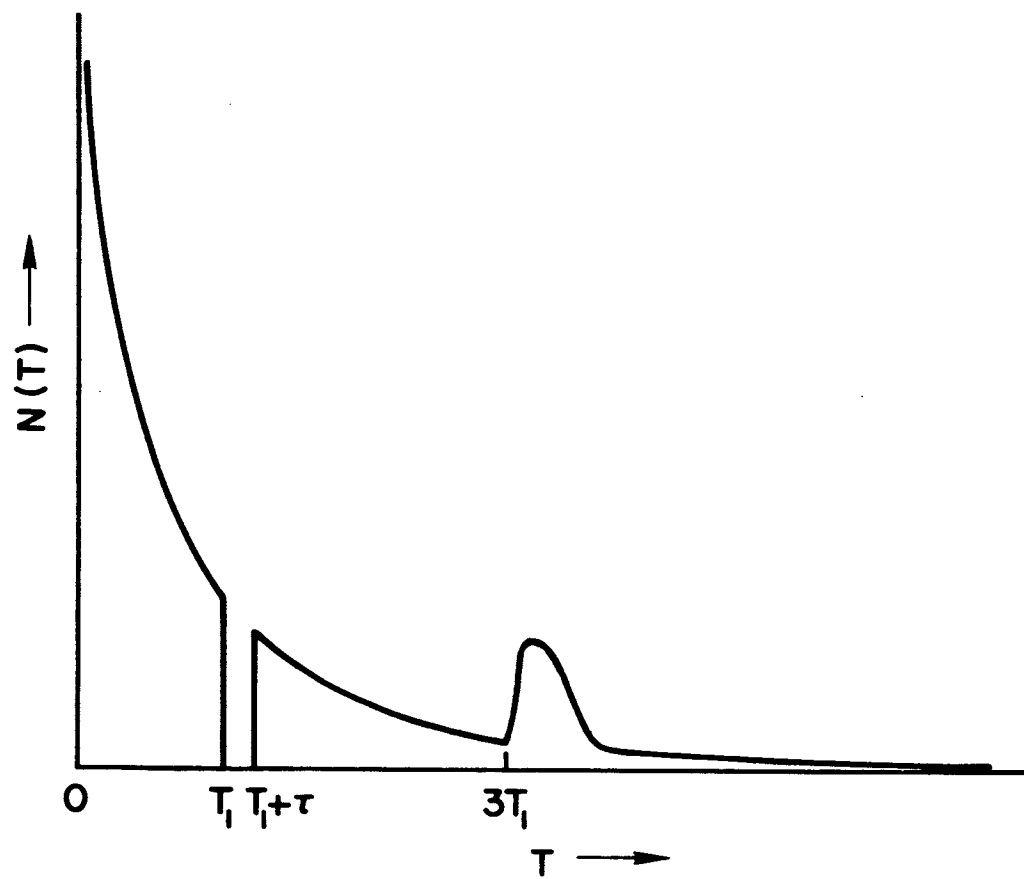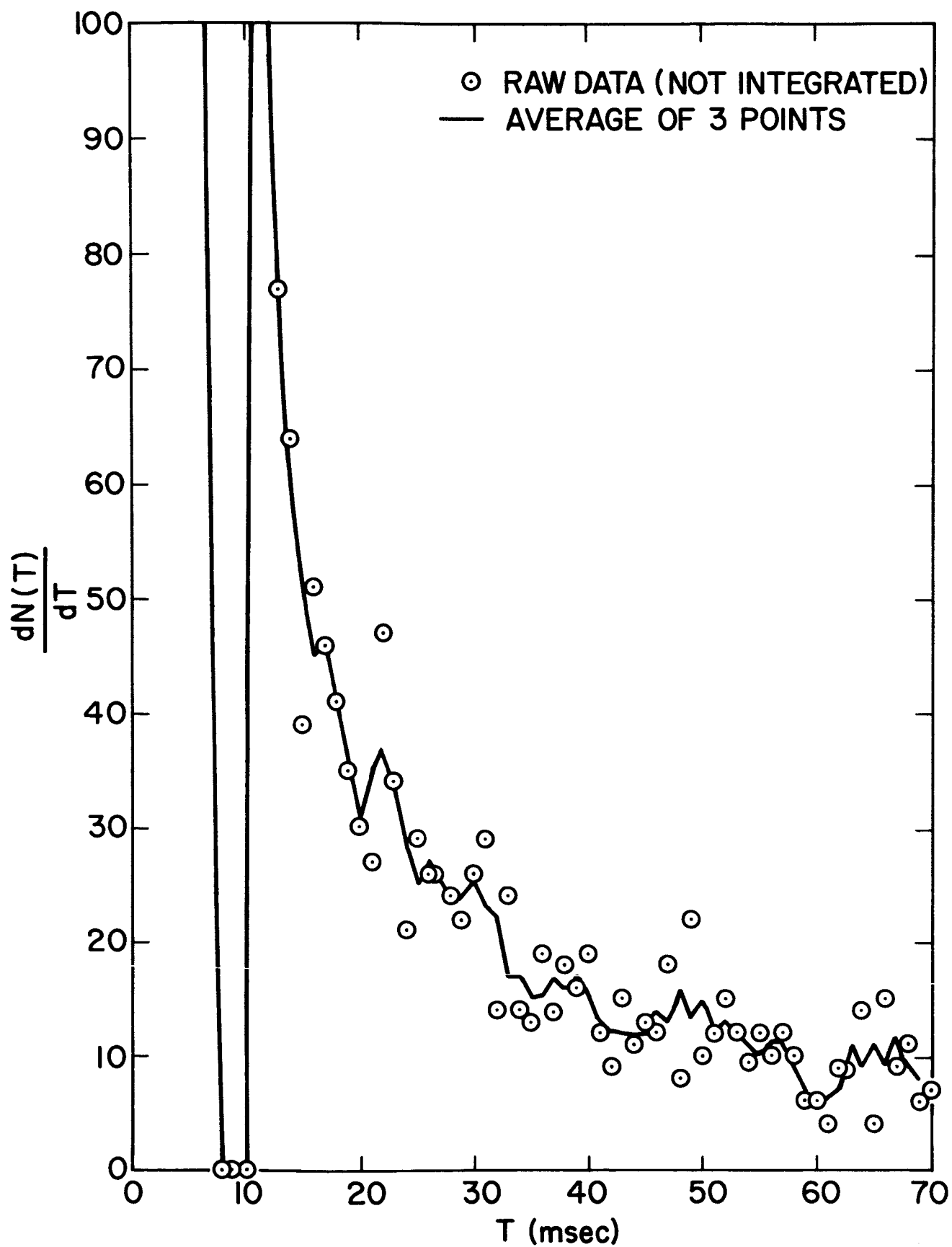
FIGURE 20. Experimental data using delayed pulse to detector entrance grid. The negative delayed pulse was applied 7 milliseconds after the end of the emitting pulse and lasted 3 milliseconds. Note the peak at 22 milliseconds.

biasing of the detector entrance grid. The overloading of the detector

probably causes gas desorption either from the dynodes or the resistors

in the voltage divider. This could be a source of noise that would decrease

with time after the initial pulse. The negative biasing is an obvious source

of trapping.

3. Ions

When the apparatus for the free fall experiments was first built,

the possibility of measuring the gravitational force on ions without ex-

tensive modifications was not even considered. It was thought that a

special source would be needed. The unusually long cut-off time for the

data in figure 15 suggested that possibly a few ions were being formed

even though other evidence showed that electrons predominated at least

out to 10 milliseconds. If as many as one or two slow ions were formed

in each pulse, they would control the distribution of flight times by

sweeping out electrons ahead of them and turning back electrons trying

to pass them. Distributions resulting from ions should be distinguishable

by their insensitivity to small changes in magnetic and electric fields.

The first ion time of flight distributions were obtained accidentally

during an attempt to test the effect of reducing the magnetic field gradi-

ents in the drift tube. This was done by constructing a superconducting

shield from 200 individual coils of niobium zirconium superconducting

wire. A long resistance wire wrapped around the inside and outside of

the loops and in good contact with every loop served as a heater for

driving the shield normal when required. Data typical of several runs

made with the shield installed is shown in figure 21. The distribution

shows a definite cut-off at about 170 msec. During one of the runs a

10 milliamp d.c. current was run vertically through the walls of the drift tube. This should have set up an electric field of 2×10^{-10} volts/cm along the axis of the drift tube. The resulting time of flight distribution should be similar to that for electrons in figure 22 obtained by numerical integration of Eq. (18), using a superposition of the potential field of figure 4 and the applied potential. Instead of a drastic change in the distribution, with a cut-off near 12 msec., similar data with the same cut-off was observed, indicating that most of the particles arriving after 12 msec. were not electrons. The distribution was also relatively independent of whether the shield was being used. The shield could be allowed to persist before or after the strong cathode magnet was turned on. Time of flight data accumulated in either mode of operation yielded about the same cut-off time. Unfortunately, during the series of runs in which this data was obtained (all in one day) the failure to affect the distribution with a 10 milliamp current through the drift tube was incorrectly assumed to result from a short circuit causing the current to bypass the drift tube. Thus no large electric fields were applied at that time. After the data had been examined and the consistent cut-offs noticed, the possibility of ions was considered.

Several features of the data in figure 21 suggest that it is affected by ions. The distribution follows a $t^{-\frac{3}{2}}$ curve which indicates it is partially thermalized. This would be expected for ions since they would be formed from atoms in thermal equilibrium with the walls of the system. The electrostatic potential distribution and a gravitational potential plot appropriate for ions of mass number four is shown in figure 23. Numerical integrations of the flight time through this potential and one appropriate

FIGURE 21. Time of flight data compared with expected distributions for a charged particle without a gravitational interaction, He⁻ with an ordinary gravitational attraction, and H⁻ with ordinary gravitational attraction. (semilog plot) Magnetic forces are assumed negligible. The electrostatic fringe field is shown in figure 23.
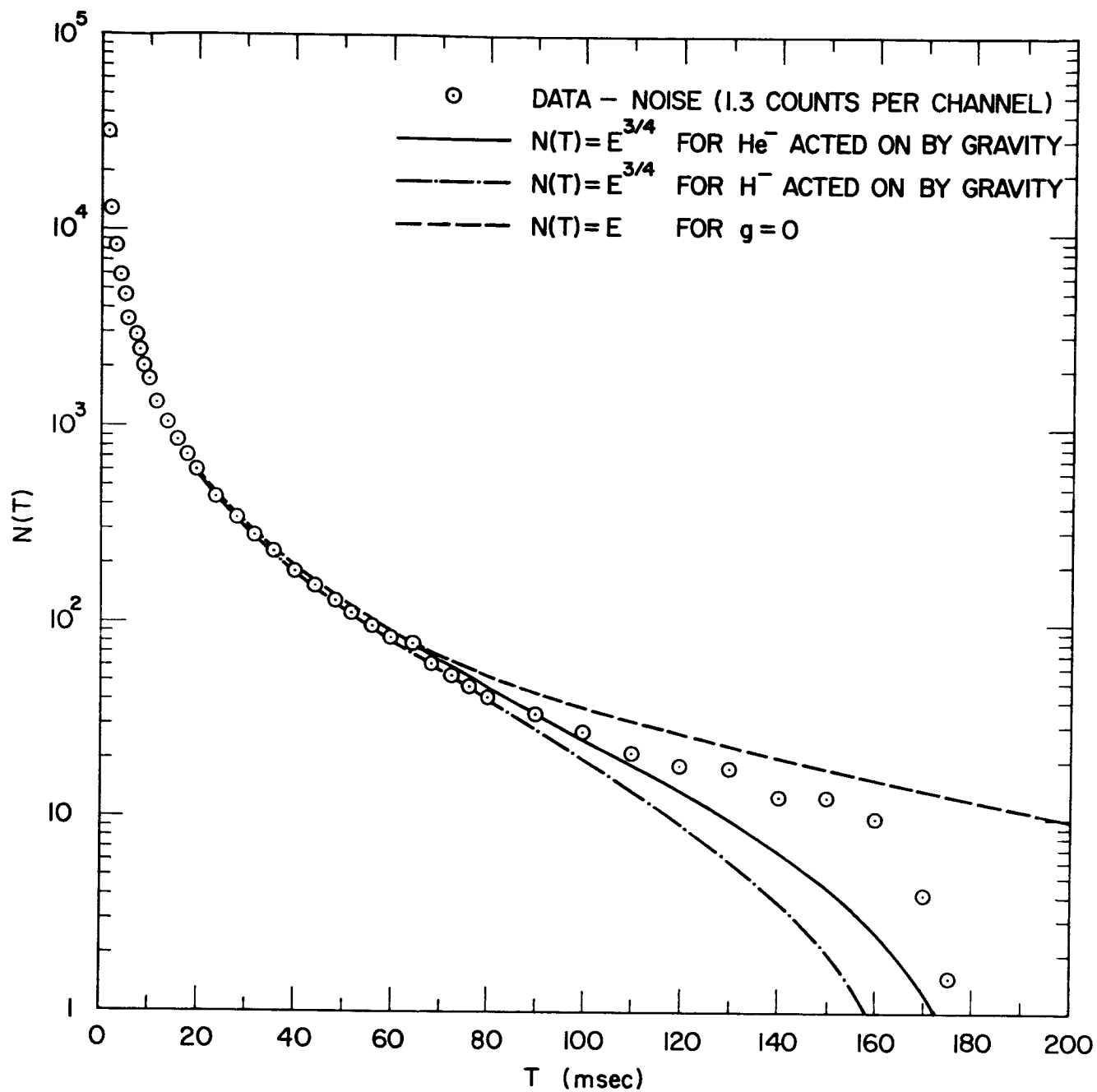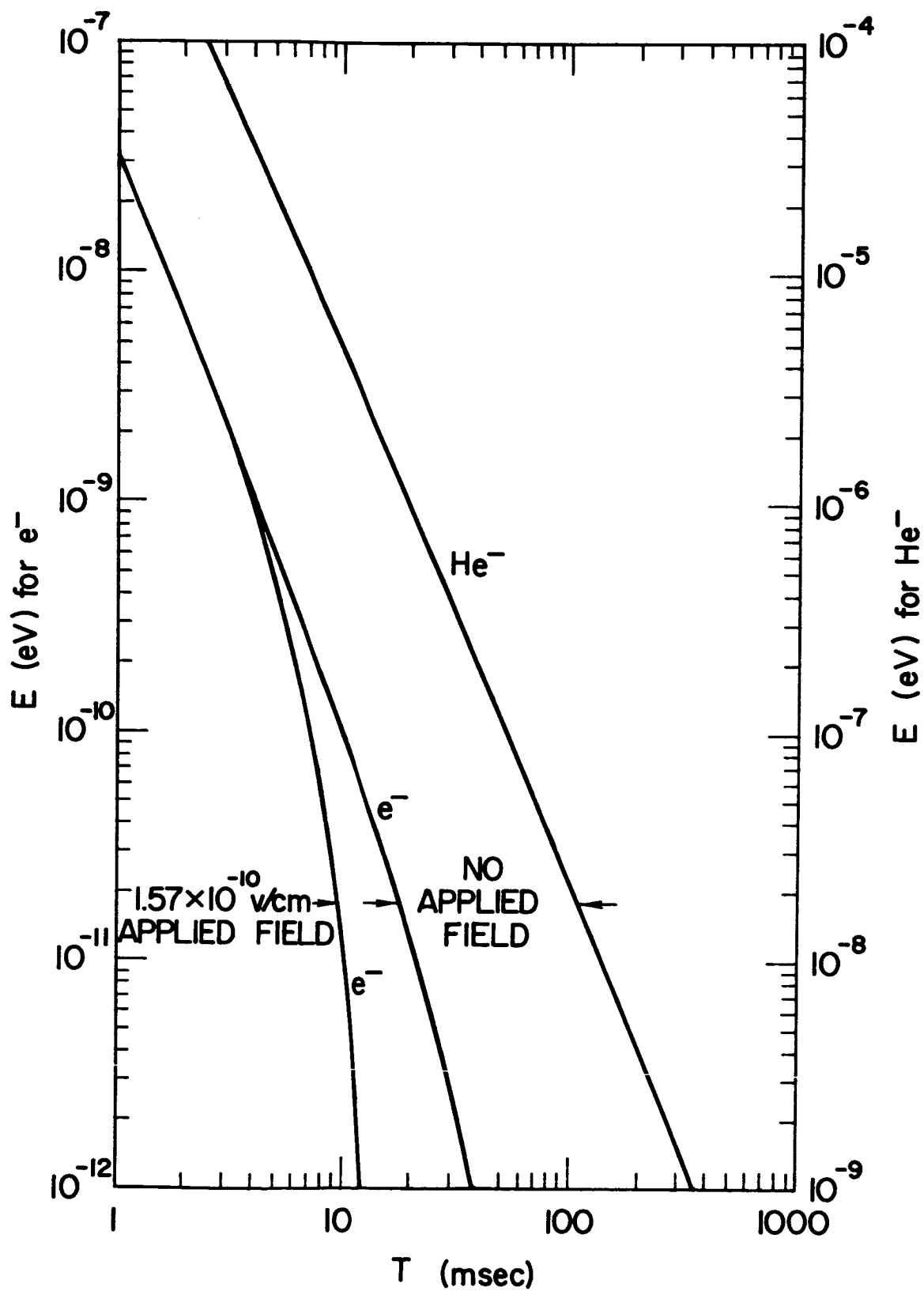
FIGURE 22. Zero gravity curves for electrons and ions in the electro-
static field of the drift tube. (log-log plot)

for negative hydrogen ions were made at various energies. The resulting

E versus t curves are shown in figure 24. To match the $t^{-\frac{3}{2}}$ behavior

of the data, $N(t)$ was chosen equal to $CE^{\frac{3}{4}}$, where C was chosen to

make the data and both calculated curves agree at t = 20 milliseconds.

These curves are plotted in figure 21 for comparison with the data. The

difference in the calculated cut-off times for H^- and He^- results from

the electrostatic end effects which are more important for lighter ions.

The long cut-off time cannot be attributed primarily to space charge

effects, because the densities used for the figure 21 data were only one

third as large as those used in obtaining the figure 15 data. Four other

runs made the same day using electron densities differing by factors of

two above and below the figure 21 data yielded similar cut-offs and dis-

tribution shapes. Space charge effects might be reasponsible for a slight

lengthening in flight times and for the rather abrupt cut-off shape. It

is apparent from figure 23 that the potential in the tube appears flat

to ions for a much longer distance than electrons, so that the fractional

lengthening of flight times by space charge broadening of the potential

plateau cannot be nearly as large.

4. Measurement of g

　　We must now examine to what extent the data of figure 21 and the

two other sets of data taken under similar conditions constitute a mea-

surement of the gravitational constant for ions. If the electrostatic

potential in figure 23 is approximated by a flat potential of length h

bracketed by infinitely steep walls, the gravitational cut-off time is

an absolute one given by $t_c = \sqrt{\frac{2h}{g}}$, so $g = \frac{2h}{t_c^2}$. This simple form

is used here only to estimate the error in the measurement. The fractional

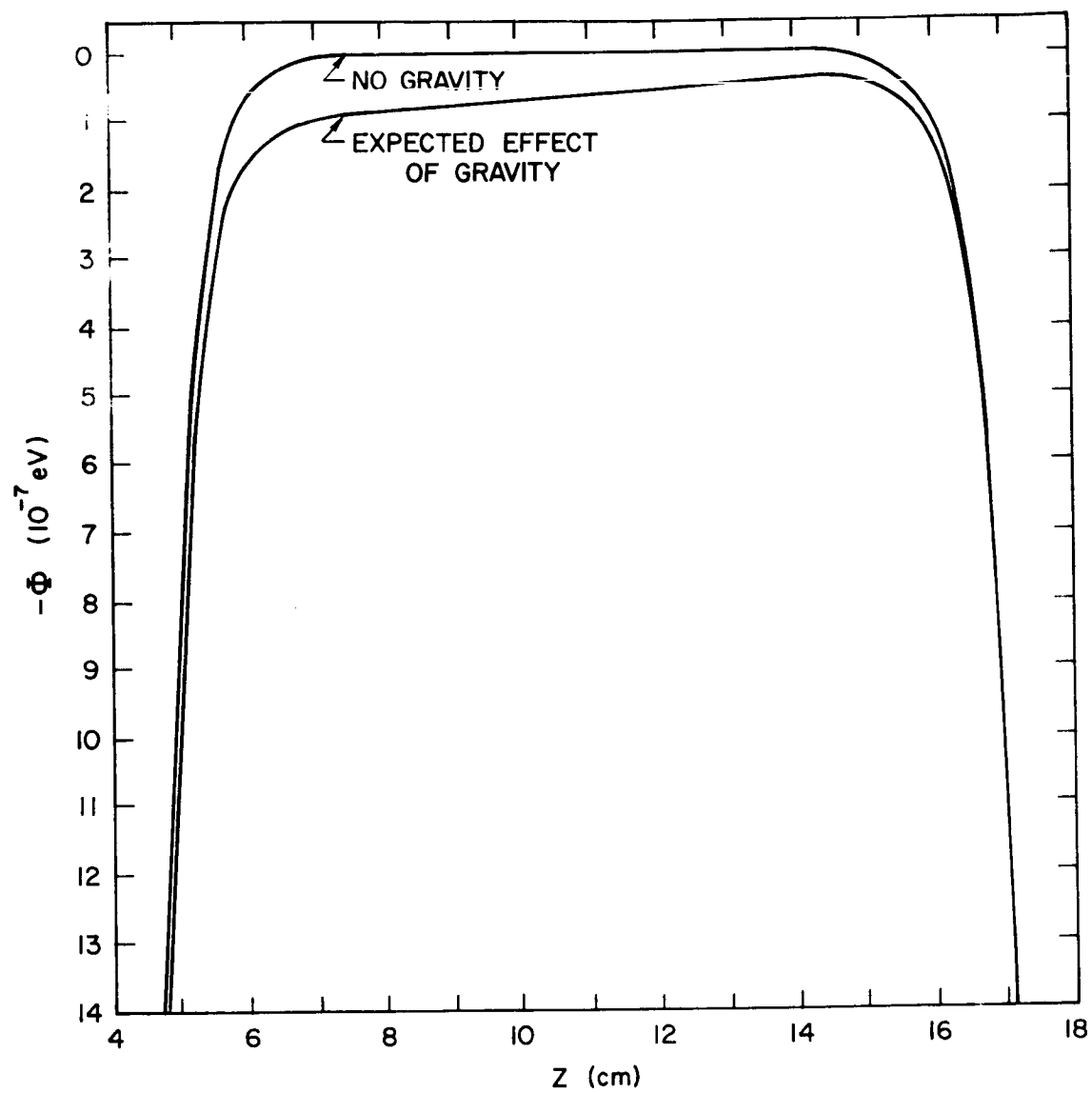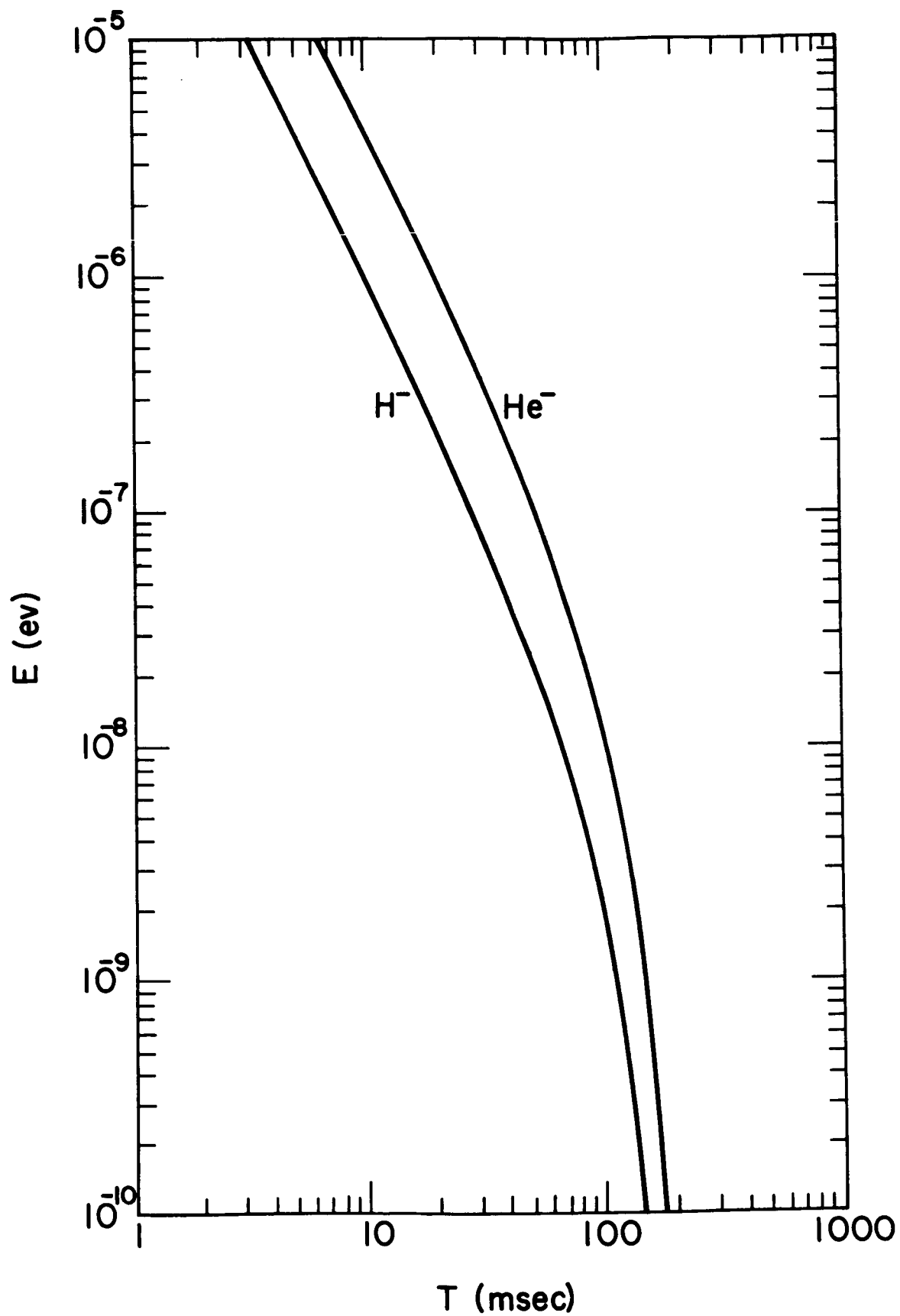FIGURE 23. Potential energy for negative helium ion in the drift tube.

FIGURE 24. Time of flight versus energy for H^- and He^- acted on by gravity and electrostatic fields of the drift tube. (log-log plot)

error in g is thus given approximately by

$$\frac{\Delta g}{g} = \frac{\Delta h}{h} + \frac{2\Delta t_c}{t_c} \quad .$$

(23)

The major contributions to Δh come from the lack of knowledge of the exact potential distribution in the drift tube and lack of information about the mass of the ions, which is required to calculate the effect of fringe fields on flight times, and, therefore the effective h. Later experiments fixed the mass between 2 and 5 times that of the proton, with strong indications that the mass was that of helium. The effect of the mass uncertainty is a contribution to $\frac{\Delta h}{h}$ of $\pm$ 0.12. This can be seen from the difference in cut-off points for the calculated flight times for H^- and He^- shown in figure 21. Lengthening of the potential plateau by space charge effects by more than 1 cm is very unlikely because the potential changes so rapidly away from the flat region. Irregularities in the electrostatic potential due to patch fields would shorten the effective length of the plateau. They would tend to decrease the number of long flight times. The effect of the irregularities would be very large for the slowest particles and progressively smaller for the faster ones. The observed distributions did not have such a progressive reduction below the calculated value for the potential of figure 23. Calculations of flight time distributions resulting from some likely potential configurations strongly indicate that a shortening of the plateau of more than 1 cm as a result of small potential bumps could not have produced data with such a sharp "knee" at 160 milliseconds as that in figure 21 and the two other runs taken under similar conditions. Therefore we may estimate that the uncertainty in the drift tube potential contributes $\pm$ .08 to $\Delta h/h$. The total fractional uncertainty in h is thus $\pm$ .12 $\pm$ .08 = $\pm$ .20.

The cut-off times of the eight runs made in the series of runs with the data of figure 21 were 172, 170, 172, 110, 140, 198, 100, 162 milliseconds. To facilitate comparison between runs, the "cut-off" was chosen as the time t_c at which $N(20 \text{ msec})/N(t_c) = 200$. The average of these is 153 milliseconds with a standard deviation of 31.6. Only the first three of these were made with the superconducting shield working properly. In the subsequent runs some of the 200 or so independent superconducting loops could not be driven normal when desired. This resulted in unknown magnetic field gradients that could have affected the ion flight times. The average of the first three is 171 msecs. with an approximate standard deviation of $\pm$ 1 msec. An additional $\pm$ 1 msec uncertainty arises from the time width of the data storage channels. Inserting the last two values of Δt and the values of $\frac{\Delta h}{h}$ into Eq. (23) gives

$$\frac{\Delta g}{g} = (\pm .12 \pm .08) \pm (.01 \pm .01) = \pm .22 \quad . \tag{24}$$

The error may be put in the form of a standard deviation by adding the squares of the independent contributions to the error. Then

$$\frac{\Delta g}{g} = \sqrt{.12^2 + .08^2 + .01^2 + .01^2} = .15 \tag{25}$$

is the standard deviation. There is a 68% chance that the error falls within these limits.

Considering the wide limits of error just calculated, no further determination of g is necessary than to note that the distribution and cut-off for He$^-$ shown in figure 21 and that calculated using the value $g = 980 \text{cm}/\text{sec}^2$ agree almost precisely with the experimental data.

5. Determination of Ion Mass

In a later experiment successive runs were taken with an electric field of 1.57×10^{-6} volts per meter opposing the upward motion of negative particles, then aiding this motion, and finally with the electric field turned off. The results appear in figure 25. The curves were calculated using the potential of figure 23 with a 1.57×10^{-6} volt/meter electric field superimposed, but without the gravitational potential of the ion included. The effect of gravity would be to split the curves, since gravity adds to the electric field in one direction and subtracts from it in the other. The calculated curves are for H^-, H_2^-, and He^- normalized to the same value at 20 msec. The calculated distribution is assumed to have the t^{-1} form of Eq. (19), although the experimental data follows a $t^{-\frac{2}{3}}$ curve more closely. The He^- curve fits the data best. This is in conflict with the theoretical results of Pietenpol [32] who has calculated the He^- halflife to be about 1.7×10^{-3} seconds, which would not have permitted the observed distribution.

The only gases that could be present in the liquid helium cooled regions are hydrogen and helium. They would not usually be present in sufficient number to form enough ions to yield a time of flight distribution. However, there would be a surface layer of either one or both of these gases. During emission of electrons, the cathode dissipates 5×10^{-3} watts in its insulating and emitting films. Since the tunnel cathode has a glass backing and very small connecting wires, a considerable fraction of this heat, say 3×10^{-3} watts must go to heating the gold film. It is $100^{\circ}A$ thick and one millimeter square, so since the density of gold is 19.3 gms/cm^3, the film weighs about 2×10^{-7} grams. The film is

FIGURE 25. Mass analysis data compared to ion distributions. (semilog plot)
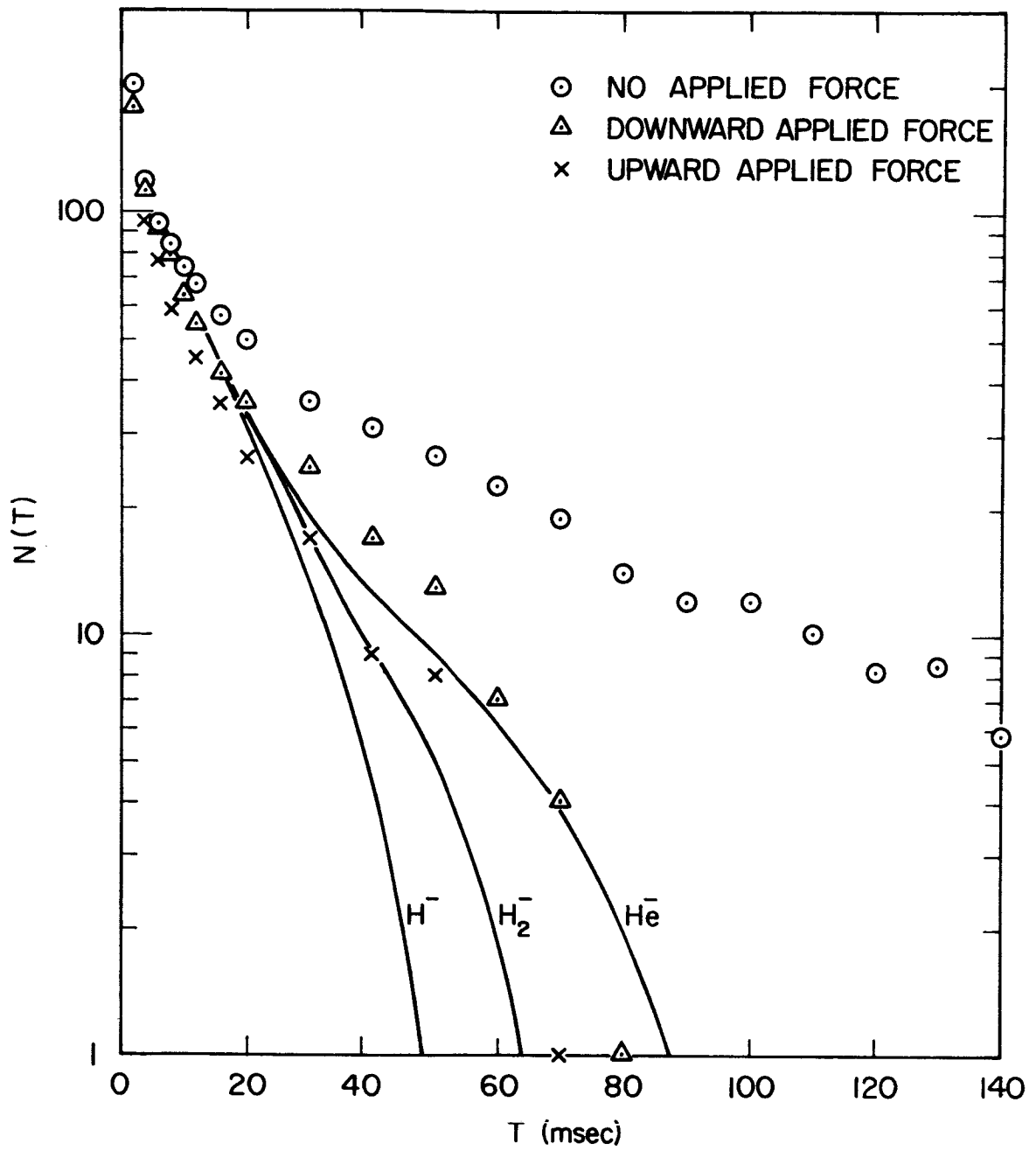
carrying current for one millisecond, so about 3×10^{-6} joules $\cong 7 \times 10^{-7}$ calories are available to heat 2×10^{-7} grams. Since the specific heat of gold is less than 0.03 cal/gram almost up to room temperature and decreases at lower temperatures, the temperature of the gold could rise above $100°K$ during each pulse. This would be warm enough to desorb any gas that had condensed on it during liquid nitrogen or liquid helium cooling. At first the gases given off would include all atmospheric gases, but as the condensible gases condensed on surrounding cold surfaces only the hydrogen and helium would remain as background gases and thus be available for readsorption to the cooling surface. Thermal He atoms strike the surface with an average speed of 10^4 cm/sec, and H_2 molecules with twice that speed. If the background gas concentration is $3 \times 10^8/cm^3$ ($\sim 10^{-10}$ torr) and the pulses are emitted every 0.40 seconds, then 1.2×10^{10} He atoms or twice that many hydrogen molecules would strike the gold film between emission pulses. Assuming that the sticking coefficient is nearly unity, the cathode can emit and readsorb on the order of 10^{10} atoms or molecules in each cycle.

It does not seem likely that the fraction of hydrogen in the background gas would be appreciable. The ion pump, which operates continuously for days before and during the data taking, is 20 times as efficient in pumping H_2 as in pumping He. Furthermore, the cross sections for formation of negative hydrogen ions by various processes are not especially large. The most likely mechanism appears to be by the reaction $e^- + H_2 \rightarrow H^- + H$ which has a cross section $\sigma(H^-)$ of about 10^{-20} cm^2 [33]. Negative ions formed near the extractor would be trapped in its positive potential and would not reach the detector, so we are considering only the negative

ions formed at the surface of the cathode, or in the force free part of the drift tube. In the latter region the concentration n of atoms or molecules at 10^{-10} torr is 2.4×10^8/cm^3. Since the emission current was about 10^{-7} amps in most of the experiments and the pulses lasted 10^{-3} seconds, the number $N(e)$ of electrons given off was 10^9 per pulse. Even if .1 of the background gas were H_2 the number of H^- ions formed would be only $N(H^-) = N(e)n(H_2)\sigma(H^-)z = 10^9 \times 2 \times 10^7 \text{cm}^{-3} \times 10^{-20} \text{cm}^2 \, 10^1 \text{ cm} = 2 \times 10^{-3}$, where z is the approximate length of force free drift tube. The same 10^9 electrons also pass through the 10^{10} atoms at or very near the cathode surface, but this number is only 50 times larger than the number in the drift tube yielding $N(H^-) = 10^{-1}$, so dissociative ionization of H_2 does not appear to be the main source of negative ions. Formation of H_2^- by direct attachment has an even smaller cross section.

Höløien and Midtdal [34] who first proved that He^- should exist in a metastable state, suggest a two step process for its formation in low energy interactions. The first step is the production of the short lived $(1s,2s)^3S$ state of He. This could form in the process of recombination of He^+ with an electron. This must be followed by the capture of a second electron into the $2p$ orbital of the atom to form the $(1s,2s,2p)^4P_{5/2}$ state. The cross section $\sigma(He^+)$ for ionization of helium in the vicinity of the extraction aperture (at + 200 volts) is 10^{-16}cm^2 [33], so $N(He^+) = N(e)\sigma(He^+)n(He)1\text{cm}$ where 1cm is the length having $V > 100v$. Most of the ions formed near the aperture would be driven into the cathode with energies near 200 eV. Measurements by Hagstrum [35] show that about 1% of the 200 eV helium ions would leave the surface as metastable atoms. In our experiment the surface which the He^+ would hit is already emitting

electrons. Since the affinity of the metastable He atom for an electron

is at least .075 eV, it seems quite possible that He$^-$ would be emitted

instead of the metastable atom. This would yield one He$^-$ ion per pulse.

If these were assumed to be near thermal equilibrium at 100^OK (the cathode

temperature during emission), their energy spread would be on the order

of 9×10^{-3} eV. The flight time through the drift tube of an He$^-$ ion

with average energy would be about 0.3×10^{-3} seconds. The resulting dis-

tribution could be described by $N(t) = \dfrac{0.3}{t(msec)}$ per pulse. Thus it would

take 3000 pulses to get 10 counts past 100 msec. In practice the ion dis-

tributions are at least that intense.

Another possible ion formation mechanism is through a 3 or more body

process involving the electrons being emitted from the cathode and the ad-

sorbed surface gases that are not thermally desorbed. Probabilities for

3-body attachment are considerably higher than in the case of binary

collisions if there is sufficient concentration. If this were in fact

the mechanism for ionization it would suggest that the He$^-$ formed was

not the metastable $(1s,2s,2p)^4P_{5/2}$ state, but the ground state He$^-$ ion

so far thought not to be a bound state. The disappearance of the slow

particle signals when the extraction voltage was lowered below about 25

volts is fairly strong evidence against this possibility, however.

An interesting feature of figure 25 is that the shortest cut-

off comes when the gravitational field was opposing the applied electric

field for negative particles. This would appear to indicate that the ions

in question were actually positive. While positive ions could have formed

either near the extraction aperture where electrons were accelerated to

100 eV, or near the first dynode of the detector which was +200 volts,

it is hard to understand how any ion formed at such a high potential could travel through the drift tube with an energy less than 10^{-8} eV as suggested by the distribution curve. Low energy positive ions would simply remain trapped in the drift tube until neutralized by electrons.

A more likely explanation for the behavior of the cut-offs is that the heat dissipated by the one amp current required to produce the electric field caused a temperature gradient in the tube which, because of the Thompson effect, was sufficient to generate a voltage on the order of the IR drop. Since the thermal gradient would be in the same direction regardless of the direction of current flow, the Thompson voltage would add to the IR drop in one case and subtract from it in the other. Ordinarily one would expect the liquid helium bath to dissipate part of this heat, but in the experiments in which the applied field was used, the drift tube was wrapped in tape to thermally insulate it from the surrounding superconducting shield. The temperature difference that would arise from Joule heating in the drift tube is only about 10^{-7} degrees, so if one assumes McDonald's value [20] of 3×10^{-6} volts/degree for the Thompson coefficient of a very pure copper sample, the voltage drop is at least 10^{3} times too small to explain the effect. However, the Joule heating in the contacts to the drift tube could account for more than 10^{-2} watt heat input into the drift tube. The liquid level had gone below the top contact, so the bath could not dissipate the heat there. This could easily cause a thermal gradient as high as 10^{-2} °K. The resulting 3×10^{-8} volt potential drop has the proper sign and magnitude to account for the peculiar behavior of the cut-offs.

The presence of small Thompson emf E_T does not spoil the mass measurement. In the case of the downward applied field $(-E_A)$ the force

F_1 on a particle of mass m and charge q is $F_1 = -mg + qE_A - qE_T$. For the upward applied field $+E_A$, the Thompson emf is the same as before so

$$F_2 = -mg - qE_A - qE_T \; . \tag{26}$$

The cut-off time is approximately

$$t_{max}(F_1) = \sqrt{\frac{2h\,m}{F}} = \sqrt{\frac{2h\,m}{|+mg - qE_A + qE_T|}} \quad \text{for} \quad F = F_1 \; , \tag{27}$$

$$t_{max}(F_2) = \sqrt{\frac{2h\,m}{|-mg - qE_A - qE_T|}} \quad \text{for} \quad F = F_2 \; , \tag{28}$$

where h is the length of the region not strongly affected by fringe fields, and q is negative. The calculated curve is made assuming $F = |-qE_A|$ which is just the average of $|F_1|$ and $|F_2|$. The corresponding cut-off time $t_{max}(F)$ must lie between $t_{max}(F_1)$ and $t_{max}(F_2)$. If $|qE_A|$ is considerably larger than $|qE_T|$ and $|mg|$, then $t_{max}(F) = \dfrac{t_{max}(F_1) + t_{max}(F_2)}{2}$ is a good enough approximation for mass analysis. In practice the whole distribution curves are used for comparison rather than just the cut-off times.

The experiment with applied axial electric fields was repeated at a later time with a different drift tube. One run was made in which the liquid helium level was above the contacts. The data is shown in figure 26 together with calculated curves for He^- and H^-. In this case the data taken with the applied field aiding gravity falls off more steeply than taken with the applied field in the other direction, as expected. The separation between the two curves could be used to obtain a lower limit on the gravitational force except that the data is too meager to give an accurate value. The possibility of heat dissipation at the electric

FIGURE 26. Mass analysis data compared to calculated distributions for ions. (semilog plot)
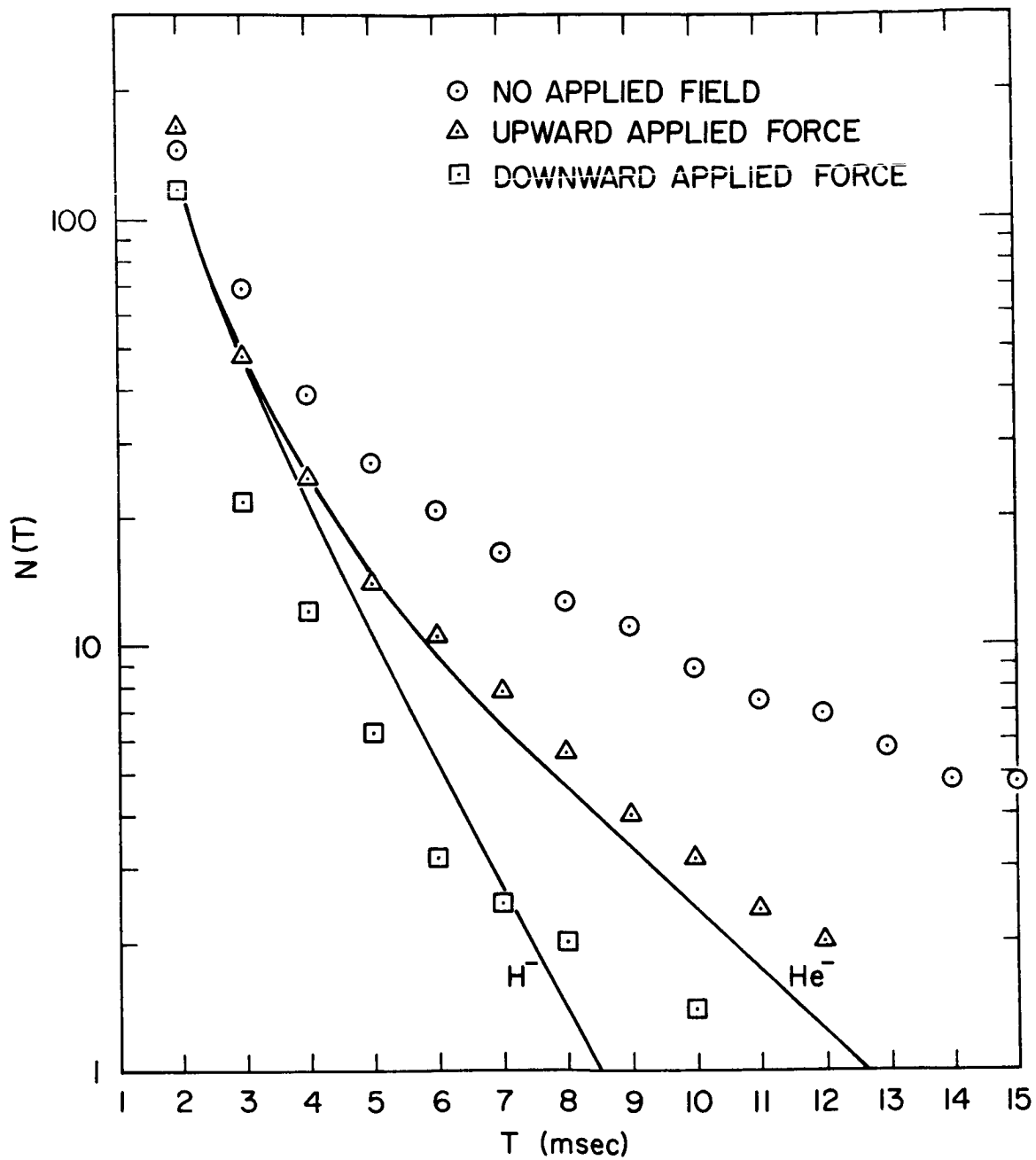
contacts had not been considered at that time yet, so several more runs were made with the liquid level below the upper contact. They showed a reverse separation of the data taken with applied fields, just as in the data of figure 25.

6. The Patch Effect

By comparing the experimental distribution curves of figure 21 with the time of flight versus energy curves in figure 22, it is clear that regardless of which of the possible light ions actually constitute the distributions, they had energies as low as 5×10^{-10} eV through part of the drift tube. The early runs (figures 13,15) suggest energies down to 10^{-11} eV if the particles in the tails of those distributions were really electrons. Passage of charged particles having such low energies through 2 cm diameter drift tubes should provide information on the nature of the patch effect.

Contact differences of potential on a copper surface are on the order of 0.1 volt [12]. The crystal size of annealed OFHC copper (used for the drift tube in most of our experiments) is about 0.045 mm on a side [36]. We will assume that only two patch potentials exist: +0.1 V and -0.1 V. We first assume that the two kinds of patches are present in about equal numbers but with local statistical fluctuations. Out of N patches randomly chosen from the two possible types, the probable excess of one type over the other is $\sqrt{N}$. Consider a group of N_1 patches at equal distance r_1 from a test charge. The potential from each patch is either $+\Phi(r_1)$ or $-\Phi(r_1)$. The probable difference of potential from the average (i.e. zero) is just $\pm N_1^{\frac{1}{2}}\Phi(r_1)$. Let N_i be the number of patches at distance r_i from the test point. Then the probable fluctuation in the total

-111-

potential of the test point as it is moved along is

$$\Delta\Phi = \sqrt{\sum_i N_i {\Phi_i}^2} \cong \sqrt{\int \Phi^2(r)dN(r)} \qquad (29)$$
$$\text{over surface}$$

Let A be the area of each patch, τ be the surface dipole moment, a be the radius of the drift tube, and z be the distance from the test charge chosen to be on the drift tube axis. Patches at equal distances have the same z value, since $r = (a^2 + z^2)^{\frac{1}{2}}$. If Φ is due to dipole double layers,

$$\Phi = \frac{Aa\tau}{4\pi\epsilon_o (a^2 + z^2)^{3/2}} \qquad (30)$$

The number of patches between 0 and z is $N(z) = \frac{2\pi az}{A}$, so $dN(z) = \frac{2\pi a}{A} dz$. Thus

$$(\Delta\Phi)^2 = \int_{-\infty}^{\infty} \frac{A^2 a^2 \tau^2}{(4\pi\epsilon_o)^2 (a^2 + z^2)^3} \frac{2\pi a}{A} dz = \frac{3A\tau^2}{8\epsilon_o^2 a^2} , \quad \text{so} \quad \Delta\Phi = 2.7 \times 10^{-3} V, (31)$$

where the $\tau/\epsilon_o = 0.1$ V is the potential change across the dipole double layer. Even on a surface that is atomically smooth, $A^{\frac{1}{2}}$ would be on the order of the lattice spacing of copper, about 3.6×10^{-10} meters, which would make $\Phi = 2.2 \times 10^{-9}$ V, still too large!

If one makes the assumption that the gas molecules adsorb to the surfaces in such a way as to reduce contact potential differences to values on the order of kT, then $\frac{\epsilon}{\tau} = 3.62 \times 10^{-4}$ eV making $\Delta\Phi = 10^{-5}$ eV if $A^{\frac{1}{2}} = 4.5 \times 10^{-5}$m.

If the patch fields were periodic in spacing, the potential at a distance z above a surface in the x,y plane with patches of dimension X,Y would be (with an appropriate choice of origin): [12]

$$\Phi = \Phi_{ave} + \sum_{m=1}^{\infty} \sum_{m=1}^{\infty} (a_{n,m} \sin \frac{2\pi nx}{x} \sin \frac{2\pi mx}{y}) \exp[-2\pi z(\frac{n^2}{x^2} + \frac{m^2}{y^2})^{\frac{1}{2}}] \qquad (31)$$

If the patches vary by $\pm$ 0.1 volt then $a_{n,m} = \frac{0.1}{2\pi nm}$. For $z > X = Y$ we have approximately for the maximum potential change

$$\Phi_{max} - \Phi_{ave} = \frac{0.1}{2\pi} \exp[\frac{-2\pi z \sqrt{z}}{X}] \qquad (32)$$

For $z = 1$ cm and $X = 0.1$ cm (a very large patch), $\Phi_{max} - \Phi_{ave} =$ $0.016e^{-89} = 6.3 \times 10^{-38}$ V. It is unlikely that the patch field could be completely periodic, but this result shows the strong effect of removing the assumption of randomness in the patch distribution.

The small effect of contact potential differences on the particles passing through the drift tube may be explained either by a considerable reduction of contact potential differences by the adsorbed gases, or by a partial removal of randomness in the patch distribution. Such a removal of randomness would also have to arise from the adsorbed gases. This might be accomplished by preferential adsorption to the stronger patch fields and by polarization of gas particles adsorbed near patch boundaries. Whatever the mechanism, it is an extremely fortunate one for the study of very low energy charged particles.

CHAPTER 6

CONCLUSIONS

It has been experimentally demonstrated that electrostatic and magnetic fields can be reduced sufficiently to allow charged particles with energies of 1×10^{-10} eV and possibly lower to pass through a 2 cm diameter copper tube. The effect of gravity on light negative ions was measured in such a tube using time of flight techniques. The gravitational constant was found to have the same magnitude as bulk matter to an accuracy of $\pm 15\%$ with a certainty of 68%.

The close agreement of the mass analysis data to calculated distributions for He^- suggests either that this ion has a much longer lifetime (at least 170 msec) than the predicted value of 1.7 msec. or that a negative ion of mass 2, 3, 4, or 5 other than He^- is readily formed in the drift tube at low temperatures. The latter possibility seems unlikely since helium was the only gas likely to be present in the drift tube.

The successful passage of 1×10^{-10} eV electrons through the present drift tube lowers the energy in which charged particles can be studied by seven orders of magnitude below that expected by other investigators. It shows that forces as small as that of gravity acting on a free electron or positron should be observable in a drift tube 5 cm in diameter and 250 cm high. An apparatus of this type has been designed and is now under construction.

The boundary conditions (at the ends of the drift tube) used to calculate the electrostatic potentials shown in figure 2 are derived in this appendix.

A cross section of the actual electrode configuration used in most of the experiments is shown on the left hand side of figure 27. On the right are cross sections of the simple configurations used to approximate the experimental ones in the neighborhood of each end of the drift tube. At the bottom, the extraction aperture at voltage V and the shield hole at ground are replaced respectively by an infinite conducting plane at voltage V and a grounded infinite conducting plane with a hole in it. The hole size is the same as that in the shield and the separation between planes is set equal to the distance between the shield and the extraction aperture. Clearly the potential for this model can hold only at distances smaller than the drift tube radius, since the effect of the grounded drift tube wall is not considered in the model.

The potential on the axis of the configurations on the right of figure 27 is found from a more general expression by Spangenberg [37], to be
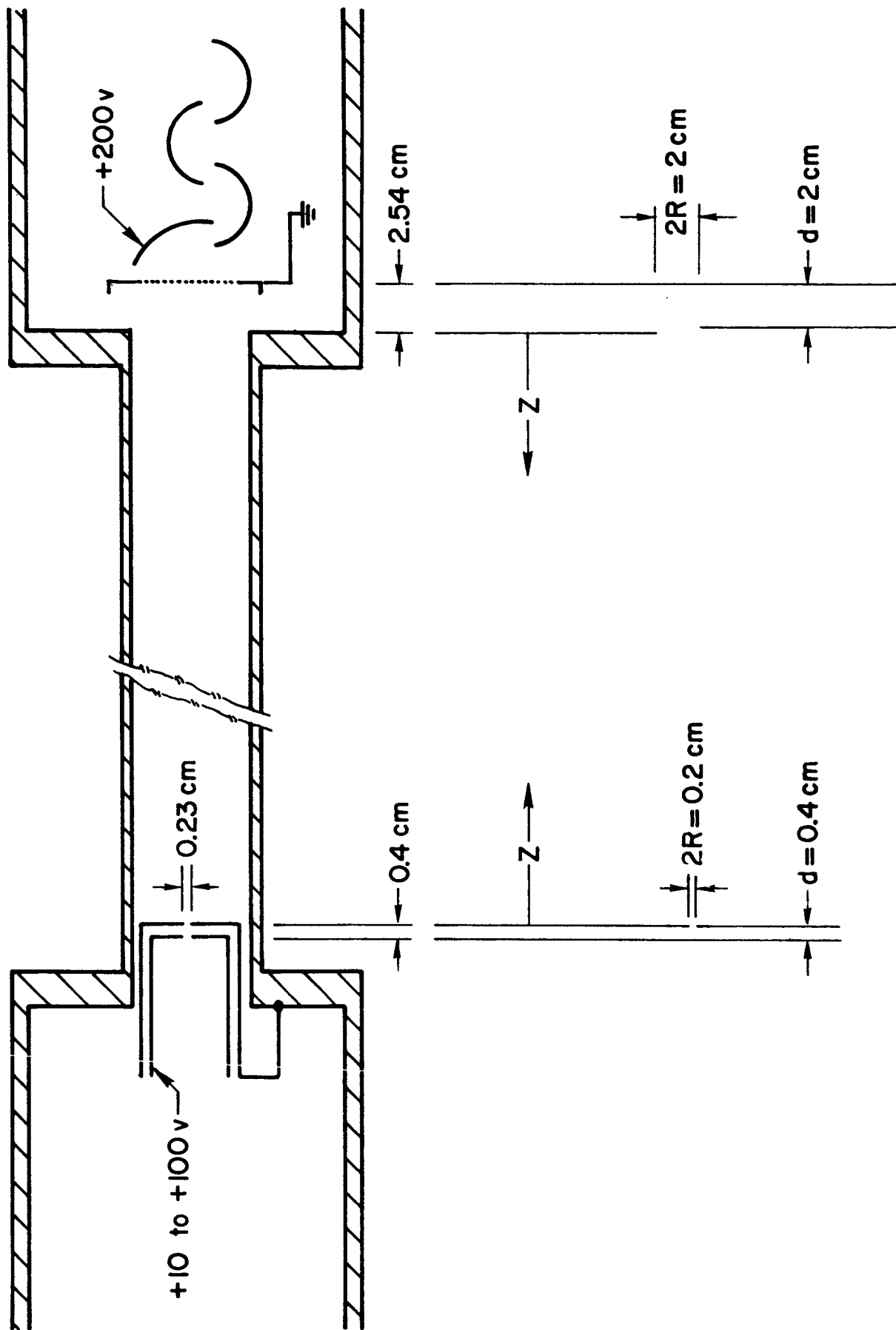
$$V_o(z) = \frac{V_1}{2d} \left\{ |z| - \frac{2R}{\pi} \left[\frac{z}{R} \tan^{-1}\left(\frac{R}{z}\right) - 1 \right] \right\} - \frac{V_1 z}{2d} \tag{33}$$

For $z \geq 0$ this simplifies to

$$V_o(z) = \frac{V_1 R}{\pi d} \left[1 - \frac{z}{R} \tan^{-1}\left(\frac{R}{z}\right) \right] \tag{34}$$

We already know from our previous consideration of a charged disc at one end of the drift tube, that the effect of the tube is to make the potential

FIGURE 27. Electrode configuration near ends of drift tube.

fall off as

$$V_e(z) = C \exp (-2.4z/a)$$ (35)

By comparing this potential with the expression for $V_o(z)$ valid near the shield hole we may determine the values of C appropriate at the bottom of the drift tube. The change from exponential dependence occurs near $z = a$, so C was evaluated by setting $V_e(a) = V_o(a)$ yielding

$$Ce^{-2.4} = \frac{V_1 R}{\pi d} [1 - \frac{a}{R} \tan^{-1} (\frac{R}{a})]$$ (36)

In the case of the shield hole, $R \ll a$, so using a series expansion for $\tan^{-1}(\frac{R}{a})$ the relation is $Ce^{-2.4} = V_1 R^3/3\pi dz^2$, good only for $R \ll a$. If $V_1 = 100$ volts, $R = 1.0 \times 10^{-3}$ meters, $d = 4.0 \times 10^{-3}$ meters, then $Ce^{-2.4} = 0.027$ volts. $C = .30$ volts. If $V_1 = 10$ volts, $C = .030$ volts. Both cases are shown in figure 2. Values calculated from Eq. (35) will have a 0.64 cm displacement from those in figure 2 in which z was measured from the center of the magnet.

The same method was applied to the detector region. The configuration and values used are apparent from figure 27. In this case $R = a$ so from Eq. (36) we have:

$$Ce^{-2.4} = \frac{V_1 R}{\pi d} [1 - \tan^{-1} 1] = \frac{V_1 R}{\pi d}(1 - \frac{\pi}{4}) .$$ (37)

$Ce^{-2.40} = 0.270$ volts, so $C = 2.97$. (In using Eq. (35) to find the contribution of the detector to the potential in figure 2, substitute $h-z$ for z with $h = 23.5$ cm.) The value of 10 volts for V_1 was chosen from an experimental measurement of the penetration of the dynode field through the grounded entrance grid of the detector.

Since changing V_1 at either end by a factor of 10, changes the effectively field free length by only 1 cm, the approximations in this section were considered adequate for the analysis of the data.

The image solution for the potential of a charge and a conducting sphere will be used to find the potential energy change in displacing a charge a small distance from the center of a sphere. The result was used in Chapter 2 to estimate the effect of moving a charge off the axis of a cylinder. The same potential expression is then used to find the difference in potential of a charge in a sphere of radius a and one of slightly larger radius, $a + da$. This is compared with the analogous problem of a charge midway between two infinite conducting planes separate by distance $2a$. The close agreement between the result for the planes and that for the sphere justifies the application of the result to the problem of a charge in a cylinder for which there is no image solution.

The potential V due to a point charge q_o at a distance b from the center of a grounded sphere of radius "a" may be found by the method of images. The grounded sphere is replaced by a charge q at distance a^2/b from the center of the sphere on the line between the center and q (see figure 28). The resulting potential satisfies the boundary conditions that $V = 0$ on the surface of the sphere provided $q = -\frac{a}{b} q_o$ [38]. The force between two charges q_1 and q_2 separated by x is just

$$F = \frac{q_1 q_2}{4\pi\epsilon_o x^2} = \frac{-q^2}{4\pi\epsilon_o ab(1 - \frac{a^2}{b^2})^2} \tag{38}$$

using $q_1 = q_o$, $q_2 = -q\frac{b}{a}$ and separation $x = b - \frac{a^2}{b}$. Let $r = \frac{a^2}{b}$.
Then

$$F(r) = \frac{-q^2 r a}{4\pi\epsilon_o (a^2 - r^2)^2} \tag{39}$$

The work required to displace a charge q to a distance r from the center of a sphere is therefore

$$W = \int_0^r F(r')dr' = \frac{-q^2 r^2}{8\pi\epsilon_0 a^3 (1 - \frac{r^2}{a^2})} \tag{40}$$

For $r \ll a$,

$$W = \frac{q^2 r^2}{8\pi\epsilon_0 a^3} \tag{41}$$

In Chapter 2 this result is used to estimate the potential energy change of a charge displaced from the axis of a cylinder. The potential of the charge q due to its image q_0 is

$$- \frac{q_0}{4\pi\epsilon_0 (b - \frac{a^2}{b})} = \frac{q}{4\pi\epsilon_0 a (1 - \frac{a^2}{b^2})} = \frac{q}{4\pi\epsilon_0 a (1 - \frac{r^2}{a^2})} = V(r) \tag{42}$$

The potential energy of the charge is $\Phi(r) = \frac{1}{2} qV(r)$.

The expression for $\Phi(0)$ may be used to estimate the change in potential energy if the radius is changed by a small amount $da \ll a$. By taking the differential of $\Phi(0)$ we have:

$$d\Phi(0) = - \frac{q^2 da}{8\pi\epsilon_0 a^2} \;. \tag{43}$$

This expression for a sphere may be compared with the corresponding potential energy of a charge midway between two grounded infinite conducting planes separated by a distance $2a$.

Consider a charge q at point c (figure 28) between the two planes. The image solution for this situation requires an infinite number of image charges q placed successively farther out on a line through c and perpendicular to the planes. The resulting potential is [39]:

FIGURE 28. Image Constructions.

Top: Point charge and grounded conducting sphere.

Bottom: Point charge between two parallel infinite grounded conducting planes.
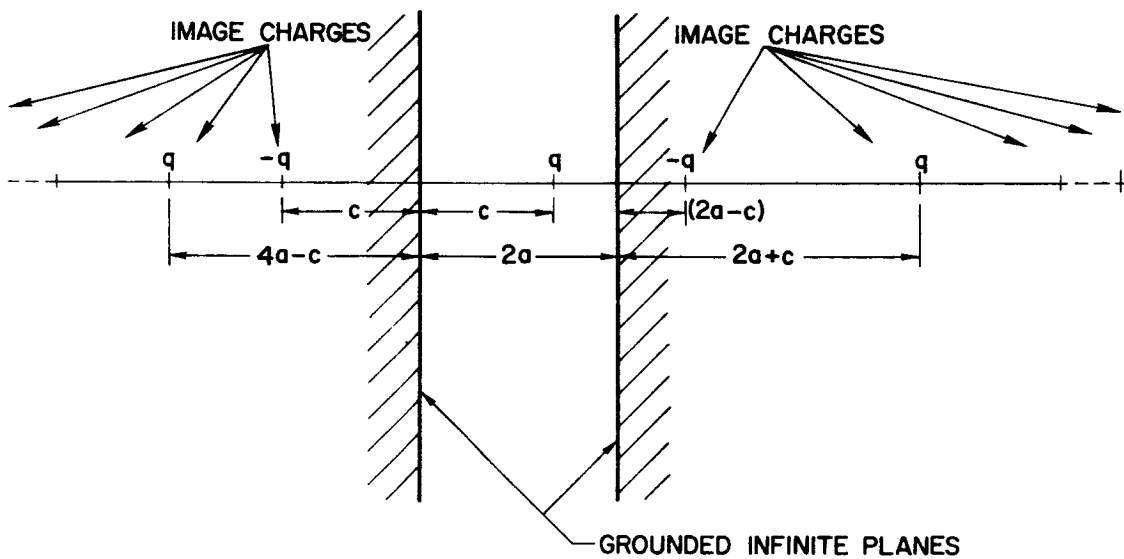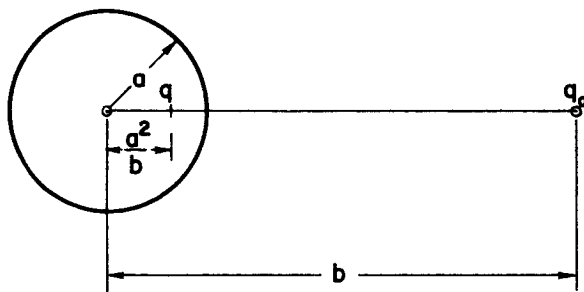
$$4\pi\epsilon_o V(x,y,z) = \sum_{n=-\infty}^{\infty} \left\{ \frac{q}{\sqrt{(x-4na-c)^2+y^2+z^2}} - \frac{q}{\sqrt{(x-4na+c)^2+y^2+z^2}} \right\} \tag{44}$$

At the position of the charge, $x = c$, we have

$$4\pi\epsilon_o V(c,0,0) = 2q \sum_{n=1}^{\infty} \left[\frac{1}{-4na} - \frac{1}{2c-4na} \right] . \tag{45}$$

We are interested in the case where $c = a$:

$$4\pi\epsilon_o V(a,0,0) = \frac{q}{a} \sum_{n=1}^{\infty} \left[-\frac{1}{2n} + \frac{1}{2n-1} \right] = \frac{q}{a} \sum_{n=1}^{\infty} -\frac{1}{2n(2n-1)} . \tag{46}$$

The series converges as $1/n^2$. Its sum is about 0.69, so

$$V(a,0,0) \simeq \frac{0.69q}{4\pi\epsilon_o a} . \tag{47}$$

Then

$$dV = \frac{-0.69q \; da}{4\pi\epsilon_o a^2} \tag{48}$$

or using $\Phi = \frac{qV}{2}$ we have

$$d\Phi = \frac{-0.69q^2 \; da}{8\pi\epsilon_o a^2} . \tag{49}$$

This has the same dependence on the distance a, but is smaller by a factor of 0.69. The result for a cylinder would presumably lie between that of the sphere and the two infinite planes.

BIBLIOGRAPHY

[1] P.G. Roll, R. Krotkov, and R.H. Dicke, Ann. Phys. (U.S.A.) 26:442 (1964).

[2] D. Paya, J.W.T. Dabbs, J.A. Harvey, and H. Horstmann, Bull. Am. Phys. Soc. 9 Ser. II, 173 (1964).

[3] R.V. Pound and J.L. Snider, Phys. Rev. Letters 13:539 (1964).

[4] P. Morrison and T. Gold, Essays on Gravity (New Boston, N.H.: Gravity Research Foundation, 1957) p. 45.

[5] P. Morrison, Am. J. Phys. 26:358 (1958).

[6] L.I. Schiff, Proc. Natl. Acad. Sci. 45:69 (1959).

[7] R.V. Eötvös, D. Pekár, and E. Fekete, Ann. Physik 68:11 (1922).

[8] M.L. Good, Phys. Rev. 121:311 (1961).

[9] J.H. Christianson, J.W. Cronin, V.L. Fitch, and R. Turlay, Phys. Rev. Letters 13:138 (1964).

[10] W.R. Smythe, Static and Dynamic Electricity (McGraw-Hill Book Co., Inc., New York, 1950) pp. 178-180.

[11] E. Jahnke and F. Emde, Tables of Functions with Formulae and Curves, 4th Ed., (Dover Publications, New York, 1945).

[12] C. Herring and M.H. Nichols, Revs. Mod. Phys. 21:185 (1949).

[13] J. Bardeen, Phys. Rev. 49:653 (1936).

[14] J.H. Parker, Jr., and R.W. Warren, Rev. of Sci. Inst. 33:948 (1962).

[15] L.D. Landau and E.M. Lifschitz, Quantum Mechanics Non-Relativistic Theory (Addison-Wesley Publishing Co., Inc., Reading, Mass., 1958) pp. 474-476.

[16] J.D. Jackson, Classical Electrodynamics (John Wiley and Sons, Inc., New York, 1962) p. 413.

[17] R.E. Honig and H.O. Hook, RCA Review XXI:360 (1960).

[18] R.C. Weast (ed.), Handbook of Chemistry and Physics 45th Edition, (The Chemical Rubber Co., 1964) p. E-33.

[19] C. Kittel, Elementary Statistical Physics (John Wiley and Sons, Inc., New York, 1958) p. 212.

[20] A.V. Gold, D.K.C. MacDonald, W.B. Pearson, I.M. Templeton, Phil. Mag. 5 Ser. 8, 765 (1960).

[21] H.M. Rosenberg, Low Temperature Solid State Physics (Oxford at the Clarendon Press, 1963) p. 276.

[22] G.K. White, Experimental Techniques in Low-Temperature Physics (Oxford at the Clarendon Press, 1961) p. 183.

[23] R.L. Powell and D.O. Coffin, "Thermal Conductivity of Solids at Low Temperatures", Advances in Cryogenic Engineering, Vol. 1, K.D. Timmerhaus, (ed.) (Plenum Press, Inc., New York, 1960) p. 262

[24] R.T. Swim, "Temperature Distribution in Liquid and Vapor Phases of Helium in Cylindrical Dewars", Advances in Cryogenic Engineering, Vol. 5, K.D. Timmerhaus, (ed.) (Plenum Press, Inc., New York, 1960) p. 498.

[25] F.W. Sears, An Introduction to Thermodynamics, the Kinetic Theory of Gases, and Statistical Mechanics (Addison-Wesley Publishing Co., Inc., Reading, Mass., 1953) p. 235, 2nd edition.

[26] W.M. Feist and G. Wade, Electronics (June 7, 1963) pp. 39-45.

[27] C.A. Meade, Jour. App. Phys. 32:646 (1961).

[28] J.W. Hall, II, Research, Development and Fabrication of Tunnel Cathodes, Final Report (General Electric Receiving Tube Department, Owensboro, Kentucky, 1964).

[29] R.E. Collins and L.W. Davies, <u>Solid-State Electronics</u>, Vol. 7, (Pergamon Press, Great Britain, 1964) pp. 445-453.

[30] Z.Bay, Rev. Sci. Inst. <u>12</u>:127 (1941).

[31] J.M. Lafferty, "The Hot-Cathode Magnetron Ionization Gauge with an Electron Multiplier Detector", <u>Vacuum Symposium Transactions 1962</u>, G.H. Bancroft (ed.) (The MacMillan Co., New York, 1962) p. 438.

[32] J.L. Pietenpol, Phys. Rev. Letters <u>7</u>:64 (1961).

[33] E.W. McDaniel, <u>Collision Phenomena in Ionized Gases</u> (John Wiley and Sons, Inc., New York, 1964) p. 413.

[34] E. Holøien and J. Midtdal, Proc. Phys. Soc. (London) <u>A68</u>:815 (1955).

[35] H.D. Hagstrum, Phys. Rev. <u>123</u>:758 (1961).

[36] W.H. Munse and N.A. Weil, ASTM Proc. <u>51</u>:996-1022 (1951).

[37] K.R. Spangenberg, <u>Vacuum Tubes</u> (McGraw-Hill Book Co., Inc., 1948) p. 348.

[38] W.K.H. Panofsky and M. Phillips, <u>Classical Electricity and Magnetism</u> (Addison-Wesley Publishing Co., Inc., Cambridge 42, Mass., 1955) p. 45.

[39] O.D. Kellogg, <u>Foundations of Potential Theory</u> (J. Springer, Berlin, 1929) p. 230.